https://doi.org/10.5194/egusphere-2026-4440
Preprint. Discussion started: 17 August 2026

Dust in the Inner Heliosphere

Arnaud Zaslavsky[1,★], Ingrid Mann[2,★], Russell A. Howard[3], Zoltan Sternovsky[4,5], Simon Anghel[6], Andreas Kvammen[2], David M. Malaspina[4,7], Nicole Meyer-Vernet[1], Filippo Pantellini[1], Arthur Péronne[8], Kristina Rackovic-Babic[9], Veerle J. Sterken[10,8], Jamey R. Szalay[11], Stuart D. Bale[12,13,14], Volker Bothmer[15,🎗], Craig E. DeForest[16], L. Claire Gasque[13], Ryo Ishimaru[17], Hiroshi Kimura[17], Milan Maksimovic[1], Michiko Morooka[18], Teresa Nieves-Chinchilla[19], Libor Nouzák[20], David Píša[21], Petr Pokorný[22,23], Nour E. Raouafi[3], Mitchell M. Shen[11], Austin Matheus Smith[4,5], and Guillermo Stenborg[3]

[1]LIRA, Observatoire de Paris, Université PSL, Sorbonne Université, Université Paris Cité, CY Cergy Paris Université, CNRS, 5 Place Jules Janssen, 92190 Meudon, France
[2]Department of Physics and Technology, The Arctic University of Norway, Postboks 6050 Langnes, 9037 Tromsø, Norway
[3]The Johns Hopkins University Applied Physics Laboratory, 11100 Johns Hopkins Road, Laurel, Maryland 20723, USA
[4]Laboratory for Atmospheric and Space Physics, University of Colorado at Boulder, Boulder, CO 80303, USA
[5]Smead Aerospace Engineering Sciences Department, University of Colorado at Boulder, Boulder, CO 80303, USA
[6]LTE, Observatoire de Paris, Université PSL, Sorbonne Université, Université de Lille, LNE, CNRS, 61 Avenue de l'Observatoire, 75014 Paris, France
[7]Astrophysical and Planetary Sciences, University of Colorado, Boulder, Boulder, CO 80303, USA
[8]Institute for Particle and Astroparticle Physics, ETH Zurich, Wolfgang-Pauli-strasse 27, 8093 Zürich, Switzerland
[9]LPC2E, CNRS, Université d'Orléans, CNES, 3A Avenue de la Recherche Scientifique, 45071 Orléans, France
[10]Institute of Physics, Laboratory of Astrophysics (LASTRO), Ecole Polytechnique Federale de Lausanne (EPFL), Observatoire de Sauverny, CH-1290 Versoix, Switzerland
[11]Department of Astrophysical Sciences, Princeton University, 4 Ivy Ln., Princeton, NJ 08540, USA
[12]Physics Department, University of California, Berkeley, Berkeley, CA 94720-7300, USA
[13]Space Sciences Laboratory, University of California, Berkeley, Berkeley, CA 94720-7450, USA
[14]The Blackett Laboratory, Imperial College London, London SW7 2AZ, UK
[15]Institute for Astrophysics and Geophysics, University of Göttingen, Friedrich-Hund-Pl.1, 37077 Göttingen, Germany
[16]Solar System Science and Exploration Division, Southwest Research Institute, Boulder, CO, 80302, USA
[17]Planetary Exploration Research Center (PERC), Chiba Institute of Technology, Tsudanuma 2-17-1, Narashino, Chiba 275-0016, Japan
[18]Swedish Institute of Space Physics, Uppsala, Box 537, SE-751 21 Uppsala, Sweden
[19]Heliophysics Science Division, NASA Goddard Space Flight Center, Greenbelt, MD 20771, USA
[20]Department of Surface and Plasma Science, Charles University, 180 00 Prague, Czech Republic
[21]Department of Space Physics, Institute of Atmospheric Physics of the Czech Academy of Sciences, 141 00 Prague, Czechia
[22]Astrophysics Science Division, NASA Goddard Space Flight Center, Greenbelt, MD 20771, USA
[23]Department of Physics, The Catholic University of America, Washington, DC 20064, USA
🎗deceased, 23 april 2026
★These authors contributed equally to this work.

Correspondence: Arnaud Zaslavsky (arnaud.zaslavsky@obspm.fr) and Ingrid Mann (ingrid.b.mann@uit.no)

Abstract. The inner heliosphere hosts a dynamically rich population of dust particles – the Zodiacal Dust Cloud – spanning sizes from nanometers to hundreds of micrometers and originating primarily from comets and asteroids. Over the past two decades, a generation of space missions has transformed our observational grasp of this environment. This review consolidates

https://doi.org/10.5194/egusphere-2026-4440
Preprint. Discussion started: 17 August 2026

the advances enabled by the Wind, STEREO, Parker Solar Probe, and Solar Orbiter space missions, which together observe from heliocentric distances of 1 au down to less than 0.05 au. Two complementary observational approaches are addressed in detail. The first is in-situ dust detection via radio and plasma wave instruments, which commonly measure characteristic voltage pulses resulting from hypervelocity dust impacts on spacecraft. We describe the underlying physics, signal interpretation, dust particle mass calibration and machine-learning classification methods for this technique, which constitutes the only in-situ dust measurement capability on current inner-heliosphere missions. The second approach is remote sensing of the Zodiacal Light and F-corona through white-light coronagraph and heliospheric imagers. The combination of these approaches has yielded a consistent picture of the radial brightness profile of the cloud, provided the first observational evidence for a dust depletion zone developing sunward of 35 solar radii and a dust-free zone interior to 5 solar radii. The in-situ measurements established flux densities of dust in hyperbolic trajectories (β-meteoroids) across multiple missions, revealed variable fluxes of nanodust, and revealed solar-cycle modulation of the interstellar dust flux. This review presents these results, discusses their implications, and outlines the prospects offered by near-future missions.

1 Introduction

Cosmic dust particles are a ubiquitous and dynamically rich component of the inner solar system. They span an enormous range of sizes – from nanometer-scale grains to hundred-micrometer fragments. Originating primarily from cometary activity and asteroidal collisions (Nesvorny et al., 2011; Mann et al., 2004), they are collectively forming the interplanetary or Zodiacal dust cloud. Their macroscopic manifestation, the Zodiacal Light, arises from the scattering of photospheric light by Zodiacal cloud particles and has been observed from Earth for centuries; it remains visible from the ground just after sunset or before sunrise, and can be monitored continuously from space. At small elongations from the Sun ($\lesssim 8°$), the Zodiacal light is called the Fraunhofer (F)-corona, which physically shares the same origin – scattering of solar light by dust – in contrast to the electron-scattered K-corona.

Continuous brightness observations from space have become possible in recent time. Detectors on spacecraft have measured local dust fluxes since the beginning of the space age. Measurements with dust impact detectors from spacecraft have also shown that interstellar dust particles, alongside interplanetary dust, travel through the interplanetary medium. For example, through electrical charging and electromagnetic forces, the dust particles are linked to heliospheric processes, and their study is part of the current space missions to the inner heliosphere. Studying dust in the inner heliosphere is an important subject for research on the planetary system and the heliosphere, because phenomena of dust dynamics, dust destruction, and interactions with the solar wind become especially apparent there. The composition of the dust fluxes and their variability moreover affect the lunar environment (Farrell et al., 2023) and the Earth's upper atmosphere (Plane et al., 2018) (and that of other planets). At the same time, the results obtained are often exemplary and help to improve our understanding of dust in the interstellar medium and in circumstellar systems.

Exploration of the dust inside 1 au has undergone an important renewal over the past two decades, driven by a generation of space missions designed to probe the near-Sun environment. Four spacecraft stand out in this context. The STEREO twin

https://doi.org/10.5194/egusphere-2026-4440
Preprint. Discussion started: 17 August 2026

probes, drifting ahead of and behind the Earth at ≈ 1 au, provided an extensive observational record for both in-situ antenna dust detection and remote-sensing heliospheric imaging. The Wind spacecraft, stationed at the Sun-Earth Lagrange point L1 since 2004, has accumulated an unrivaled continuous time series of dust impact data now spanning almost two full solar cycles. Most recently, Parker Solar Probe (PSP) and Solar Orbiter (SolO) spacecraft have carried the investigation inside 0.5 au, with PSP reaching perihelia as close as $9.86\,R_\odot$ from Sun center. Together, these missions have opened an entirely new observational window on the spatial distribution, dynamics, and variability of the dust in the inner heliosphere.

Two complementary observational strategies underpin the results reviewed here. The first is *in-situ dust detection via radio and plasma wave instruments*. Rather than dedicated impact detectors, these missions rely on the electric field sensors originally designed for wave measurements: hypervelocity dust impacts on spacecraft generate plasma clouds, that produce characteristic voltage pulses routinely measured by radio and plasma waves instruments. While first applied serendipitously to Saturn's rings by Voyager, this detection technique was extended to the interplanetary medium only with STEREO (Meyer-Vernet et al., 2009; Zaslavsky et al., 2012), before becoming the primary – and only – in-situ dust measurement capability on PSP and SolO. Because this method is less well known than conventional impact ionization detectors, Section 3 of this review is devoted to a thorough description of the underlying physics, the signal interpretation, and the associated calibration uncertainties. The second strategy is *remote sensing of the Zodiacal Light and F-corona* via white-light imagers on STEREO and on PSP, which provide spatially resolved brightness maps of the dust-scattered sunlight from ~ 1 au down to $\lesssim 15\,R_\odot$ (Howard et al., 2008; Vourlidas et al., 2016).

The combination of these two approaches has yielded a number of important advances that this review aims to consolidate. White-light observations through SECCHI and WISPR instruments have characterised the global structure of the Zodiacal cloud, including the symmetry plane of the Zodiacal cloud, its radial brightness gradient, and the super-elliptic shape of its brightness iso-contours. Most strikingly, WISPR observations with PSP have provided the first unambiguous evidence for a dust depletion zone (DDZ) developing gradually sunward of $\approx 35\,R_\odot$, leading to a largely dust-free zone (DFZ) interior to $\approx 5\,R_\odot$. At the same time, in-situ measurements from STEREO, Wind, PSP, and SolO have established consistent β-meteoroid flux densities, uncovered solar-cycle modulation of the interstellar dust flux, stream-like density enhancements, and systematic reductions in impact rates associated with coronal mass ejections (CMEs) and stream interaction regions (SIRs). Also, interplanetary nanodust were detected in-situ for the first time. This review deals with the in-situ measurements made with antennas, and we refer the reader to other reviews on dust instruments (Auer, 2001a), and measurements in the outer heliosphere with Galileo and Ulysses (Grün et al., 1992) and Cassini (Srama et al., 2004).

This review is organized as follows: Section 2 briefly describes the space missions and datasets considered in this review; Section 3 provides a detailed account of the radio-antenna detection method: the physics of impact ionisation and electric signal generation, the interpretation of dipole and monopole measurements, mass calibration, atypical signals including magnetic signatures and "single-hits" impulses, and the machine-learning classification techniques now routinely applied to large waveform databases. Section 4 presents the main observational results, organised by dust population: the large-scale structure of the Zodiacal cloud (4.2), constraints from in-situ measurements of dust in bound orbit and in hyperbolic orbit (i.e. β-meteoroids) (4.3), the dust depletion zone and interaction with solar wind structures (4.4, 4.5), nanodust dynamics and variability (4.6), and

https://doi.org/10.5194/egusphere-2026-4440
Preprint. Discussion started: 17 August 2026

interstellar dust (4.7); and finally, section 5 summarizes the key results, discusses the broader implications for debris disk and interstellar dust science, and outlines the prospects offered by ongoing and future missions.

2 Space Missions

This section provides a brief description of the space missions that have yielded the results on dust in the inner heliosphere which constitute the focus of this review.

2.1 Solar Orbiter, 2020–present

Solar Orbiter, launched on 10 February 2020, orbits the Sun with an elliptical orbit with perihelia around 0.3 au and aphelia around 1 au (Müller et al., 2019). It uses repeated encounters with Venus to raise its orbital inclination, eventually reaching $\sim 24^{\circ}$ out of the ecliptic plane in December 2026. This unique latitudinal tilt allows SolO to routinely sample regions above and below the ecliptic plane. Dust impacts have been recorded during the mission by the Radio and Plasma Waves (RPW) instrument – a complete description of which is given by (Maksimovic et al., 2020), designed to measure and analyze the electric field fluctuations from near-DC to 16 MHz and magnetic fluctuations from several Hz to 0.5 MHz. The electric sensors of RPW consist of three monopoles of length $L = 6.5$ m and radius $a = 1.5$ cm, mounted on 1 m rigid booms to separate them from the spacecraft body. They lie in the same plane and make angles of roughly 120° with each other. Remote observation of the zodiacal dust is performed by the heliospheric white light imager (SolOHI) (Howard et al., 2020).

2.2 Parker Solar Probe, 2018–present

The Parker Solar Probe is in a highly elliptical orbit around the Sun and has used seven Venus gravity assists to change its orbit and lower its perihelia after each flyby (Fox et al., 2016; Raouafi et al., 2023). PSP was launched on 12 August 2018; its first Venus gravity assist occurred on 3 October 2018, and it reached a perihelion of 0.16 au ($35.55\,R_{\odot}$) on 5 November 2018. It reached a perihelion of 0.044 au ($\approx 9.86\,R_{\odot}$ on 24 December 2024. The orbit plane is the same as that of Venus, which is similar to the symmetry plane of the Zodiacal cloud, although the ascending nodes are different. After nearly eight years of operations, all four instrument suites continue to operate nominally. Although PSP does not carry a dedicated dust detector, the signatures of dust impacts on the spacecraft are detected by the five electric field antennas of the FIELDS instrument suite (Bale et al., 2016; Malaspina et al., 2016; Pulupa et al., 2017). The four primary antennas consist of thin-walled niobium C-103 tubes mounted just behind the heat shield, each approximately 2 m in length and 1/8 inch in diameter. A simple fifth voltage probe is mounted on the magnetometer boom at the rear of the spacecraft. Some impact plasma clouds are also detected by the search coil magnetometer (SCM) (Malaspina et al., 2022). FIELDS' Radio Frequency Spectrometer (RFS) (Pulupa et al., 2017) also provides a proxy for dust impacts by counting the number of saturated waveforms during each Digital Signal Processor (DSP) cycle, which is also a metric of dust impacts. However, the RFS dust data have not yet been fully analyzed for scientific investigation. The Wide-field Imager for Parker Solar Probe (WISPR) provides white light remote-sensing observations of the

https://doi.org/10.5194/egusphere-2026-4440
Preprint. Discussion started: 17 August 2026

F-corona/zodiacal light through the scattering of sunlight by interplanetary dust particles along the lines-of-sight (Vourlidas et al., 2016).

2.3 STEREO, 2006–present

The Solar Terrestrial Relations Observatory (STEREO) mission (Kaiser et al., 2008) consists of two spacecraft, at ≈1 au, both drifting away from Earth at the rate of $22.5°$ per year, one drifting ahead of Earth (STEREO-A) and the other drifting behind Earth (STEREO-B). At the end of the 2 year prime mission, they were $90°$ apart. Having launched in 2006, they operated continuously for 8 years and were preparing in late 2014 for the superior conjunctions with the Sun in early 2015, when communications were lost with STEREO-B[1]. STEREO-A continues to operate well. The spacecraft are equipped with the STEREO/WAVES (or S/WAVES) radio instrument (Bougeret et al., 2008), consisting of three orthogonal electric antennas (of length 6 m and radius ~ 1.6 cm close to the cylindrical antenna base) (Bale et al., 2008) connected to an electronic analyzer, designed to provide observations in the radio frequency range (2.5 kHz–16 MHz), including a time-domain sampler (TDS) providing electric waveforms, which were used to detect and characterize dust impacts on the spacecraft. STEREO is also equipped with the Sun Earth Connection Coronal and Heliospheric Investigation (SECCHI) remote-sensing instrument suite (Howard et al., 2008), consisting of the Extreme Ultraviolet Imager (EUVI), two white-light coronagraphs (COR-1 and COR-2 with field-of-views of 1.4˘4 solar radii and 2˘15 solar radii, respectively), and two white-light heliospheric imagers (HI-1 and HI-2 with field-of-views covering elongation ranges of $4° - 24°$ and $18.7.0° - 88.7°$, respectively). The four white-light telescopes provide mapping of the zodiacal dust brightness distribution from Sun to Earth.

2.4 Wind, 1994–present

Wind is a spin stabilized spacecraft launched in November 1, 1994. After some orbits in the Earth's magnetosphere, Wind was placed at the Lagrange L1 point where it has stayed continuously since May 2004. Wind is equipped with the Wind/Waves electric field instrument (Bougeret et al., 1995), which has been able to record dust impacts on the spacecraft (Malaspina and Wilson, 2016). The instrument measures voltage between antenna arms, consisting in a long E_x dipole of original length $L = 100$ m tip-to-tip (which has been considerably shortened by several breakages due to dust impacts) and another shorter dipole E_y of length $L = 15$ m tip-to-tip. Both dipoles lie in the spacecraft's spin plane. Another E_z dipole (12 m tip-to-tip) lies along the spin axis of the spacecraft. The very long uninterrupted Wind data set makes it ideal to study long-term variability of the interplanetary and interstellar dust fluxes (Baalmann et al., 2024; Hervig et al., 2022).

3 In-situ dust detection by radio and plasma wave instruments

In this section, we review current knowledge on the generation of dust impact signatures in the radio domain, gathered from space observations and complementary laboratory experiments.

[1] A detailed description of the attempts to recover STEREO-B is given in https://stereo-ssc.nascom.nasa.gov/behind_status.shtml

https://doi.org/10.5194/egusphere-2026-4440
Preprint. Discussion started: 17 August 2026

The electric field sensors onboard Voyager 2 detected dust impacts on the spacecraft within Saturn's G ring (Aubier et al., 1983; Gurnett et al., 1983). This serendipitous observation marked the first use of radio and plasma wave instruments to infer dust fluxes. Similar pioneering measurements were subsequently performed in the dilute ring systems of Uranus (Meyer-Vernet et al., 1986a; Gurnett et al., 1987) and Neptune (Gurnett et al., 1991; Pedersen et al., 1991) by Voyager 2, as well as in cometary environments by other spacecraft (Scarf et al., 1986; Meyer-Vernet et al., 1986b; Oberc, 1999).

It took considerably longer for radio techniques to be applied to probe the zodiacal cloud, as its low dust density generally renders the associated power spectral signatures below the noise floor of radio instruments under most observational conditions. The first radio dust measurements in the interplanetary medium were performed by the STEREO mission, benefiting from the large sporadic impact rate of nano-dust (Meyer-Vernet et al., 2009) and then extended to larger grains (Zaslavsky et al., 2012), using the S/WAVES time domain sampler, which made it possible to isolate individual impacts. The technique has then been used with Wind (Malaspina et al., 2014), Cassini during its cruise phase to Jupiter (Schippers et al., 2014, 2015) and at Jupiter (Ye et al., 2016, 2018), MMS (Vaverka et al., 2019), MAVEN (Andersson et al., 2015; Ijaz et al., 2024), Juno (Ye et al., 2020) and it currently provides all the in-situ dust measurements onboard PSP (Szalay et al., 2020) and Solar Orbiter (Zaslavsky et al., 2021).

3.1 Voltage signatures of dust impacts in space: observations and interpretation

The detection capabilities of electric sensors depend on the receiver's characteristics, in particular, whether it is operated in monopole mode (when the receiver measures the voltage between an antenna and the spacecraft body) or dipole mode (when the receiver measures the voltage between two antennas). Figure 1 shows a few examples of measurements in monopole and dipole mode with Solar Orbiter/RPW.

As can be seen in Figure 1, the signals produced by dust impacts are recognizable as sharp pulses, with rise times typically of a few tens of μs and decay times typically of a few hundreds of μs (in conditions of interplanetary space at a fraction of an au). These pulses can reach amplitudes of a few hundred or thousands of mV, making them more intense than most plasma wave events recorded. Dust impacts will therefore be found en masse in plasma waveform databases selected on the basis of algorithms that favor large-amplitude signals.

3.1.1 Time evolution of a conductor's potential following a dust impact

To understand how the pulses observed in the electric field instrument data are generated, we first examine the temporal evolution of the potential of a conductor immersed in the interplanetary medium plasma and located close to a dust grain impact, whether the impact occurs on the conductor itself or on another spacecraft structure in its vicinity. This evolution proceeds in several stages, which we describe hereafter. More details can be found in (Zaslavsky, 2015; Meyer-Vernet et al., 2017; Mann et al., 2019; Shen et al., 2021a; Rackovic Babic et al., 2022; Kočiščák et al., 2024).

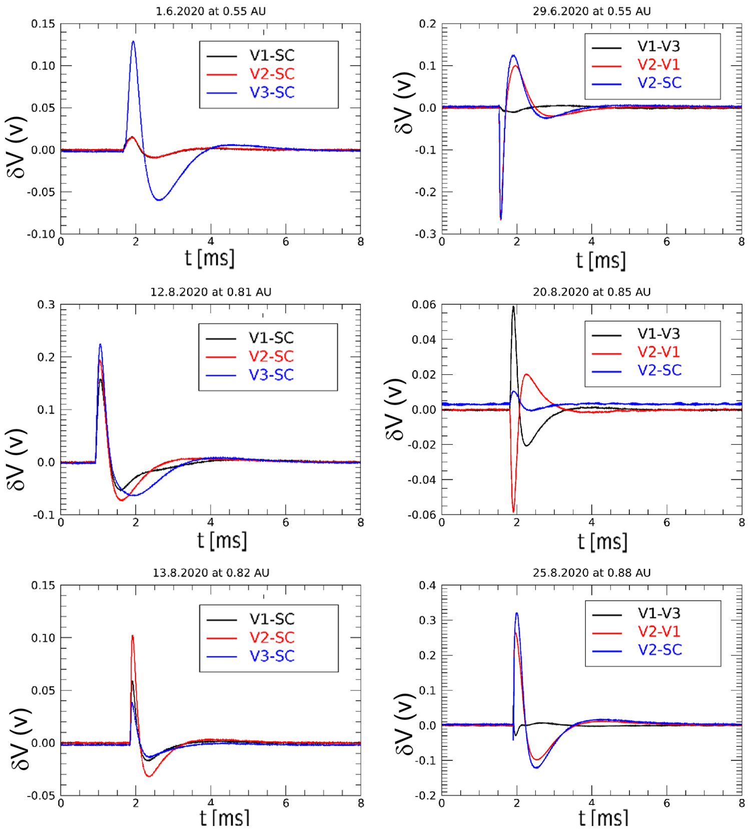

Figure 1. Examples of waveforms recorded by the Radio and Plasma Wave instrument onboard Solar Orbiter at several heliocentric distances. Left column: voltage measured by the three monopoles ($V1$ in black, $V2$ in red, $V3$ in blue), each referenced to the spacecraft potential. Right column: monopole $V2$ (blue) referenced to the spacecraft potential, together with two dipole measurements ($V1-V3$ in black, $V2-V1$ in red). Reproduced from Zaslavsky et al. (2021).

First, free electric charges (ions and electrons) are generated during dust impacts at speeds $\gtrsim 1$ km s^{-1} (a threshold generally exceeded in interplanetary space), which vaporize and ionize part of the target material as well as the dust grain itself (Drapatz and Michel, 1974).

This process is called impact ionisation, and the amount of charge generated scales with the mass m and relative speed v as $Q \sim \alpha m v^{\beta}$, where α and β depend strongly on the target and impactor materials (Collette et al., 2014). Values often used are $\alpha = 0.7$ and $\beta = 3.5$ (McBride and McDonnell, 1999), with Q in Coulombs, m in kg and v in km s^{-1}.

Just after impact ionisation, the charges are distributed in a small quasi-neutral cloud. Although there are large uncertainties regarding the temperature of this plasma just after impact, with conflicting measurements, one can assume a value on the order of a few eV (Hornung and Kissel, 1994; Ratcliff et al., 1997; Miyachi et al., 2008; Lee et al., 2012; Collette et al., 2014; Fletcher et al., 2015; Kočiščák et al., 2020). The cloud expansion is mostly collisionless, and occurs at approximately the ion thermal speed $c_s \sim 5-15$ km s^{-1}, driven by an internal electric field arising from charge separation at the boundary of the

https://doi.org/10.5194/egusphere-2026-4440
Preprint. Discussion started: 17 August 2026

cloud (Pantellini et al., 2012b). The cloud stays quasi-neutral until this electric field is overcome by the ambient electric field, determined by the conductor's potential and the photoelectron and ambient plasma Debye lengths – of the order of ~ 10 V m^{-1} near the spacecraft at 1 au (Meyer-Vernet et al., 2017). This happens when the plasma cloud is a few centimeters size, or after a few microseconds.

Afterwards, the ion and electron populations lose their electrostatic coupling and evolve essentially independently. The conductor will sense these charges and see its electric potential modified. The time evolution of this potential is determined by the dynamics of impact-ionisation charges and by the exchange of charges between the conductor and the surrounding solar wind plasma.

First, we examine the dynamical behavior of the charges generated by impact ionization. The electron thermal speed is of the order of 500 km s^{-1}, so their displacement over meter-scales typical of the spacecraft or antennas systems occurs on timescales $\sim 2\ \mu$s, shorter than the sampling time of most radio instruments. This fast motion sees electrons getting collected, or, for a fraction of them, escaping away. After a few microseconds, only a cloud of positive ions remains in the vicinity of the conductor. This cloud, of total charge $\sim Q$, influences the conductor so as to produce a change of its potential $\delta\varphi_{ions} \sim Q(1-r/R)/C$ (Meyer-Vernet et al., 2017) where R is the typical size of the conductor, r it distance to the ion cloud and C the conductor's capacitance.

We define ϵ as the fraction of electrons that escape. This fraction is smaller than 0.5 because, owing to their quasi-isotropic velocity distribution immediately following ionisation, half of the electrons are initially directed inward and are collected by the positively charged target (for sunlit surfaces in interplanetary space), while a fraction of those initially moving outward will subsequently return, depending on the conductor potential relative to the electron temperature. The collected fraction induces a change of potential $\delta\varphi_{col.} = -(1-\epsilon)Q/C$. Hence, a few μs after the impact, the conductor potential has increased by $\delta\varphi_{esc.} = \delta\varphi_{col.} + \delta\varphi_{ions} = \epsilon Q/C$: this manifests as a fast precursor, or "pre-shoot", the amplitude of which reveals the amount of escaping charge ϵQ (Rackovic Babic et al., 2022).

The electrostatic influence of the ion cloud on the conductor evolves with time under two effects: (i) its distance r to the conductor varies, and (ii) its charge is screened by the photo-electron sheath that surrounds any sunlit conductor in interplanetary space. Effect (i) occurs over a timescale $\sim 100\ \mu$s assuming a cloud expansion speed of ~ 10 km s^{-1} – although in the vicinity of an antenna, whose radius is typically of the order of a centimetre, transverse displacements of the order of a few tens of centimetres or even less can have a significant effect on the potential, and reduce this time scale to around 10 μs. Effect (ii) occurs over a timescale τ_{ph} depending on the density of the photoelectron sheath (or the plasma sheath in shadow), which depends on the distance to the Sun and amounts to a few tens μs at 1 au, increasing with distance to the Sun as $d^{2/3}$ and impact charge as $Q^{1/3}$ (Meyer-Vernet et al., 2017). Hence in general, one expects the electrostatic shielding effect to dominate the time evolution of the change in potential induced by the ion cloud $\delta\varphi_{ions}$, even though fast signature of the ion cloud dynamics close to antennas might also be seen. The decrease of $\delta\varphi_{ions}$ down to zero on a timescale τ_{ph} reduces the potential of the conductor down to a minimal value determined by the amount of electron charge collected $\sim \delta\varphi_{col.} = -(1-\epsilon)Q/C$. So, the amplitude of the pulse from the preshoot to the minimal value gives an estimate of the total charge collected, Q/C – at least if one can neglect the effect of charge exchange during the timescale τ_{ph}, as we discuss in the following.

https://doi.org/10.5194/egusphere-2026-4440
Preprint. Discussion started: 17 August 2026

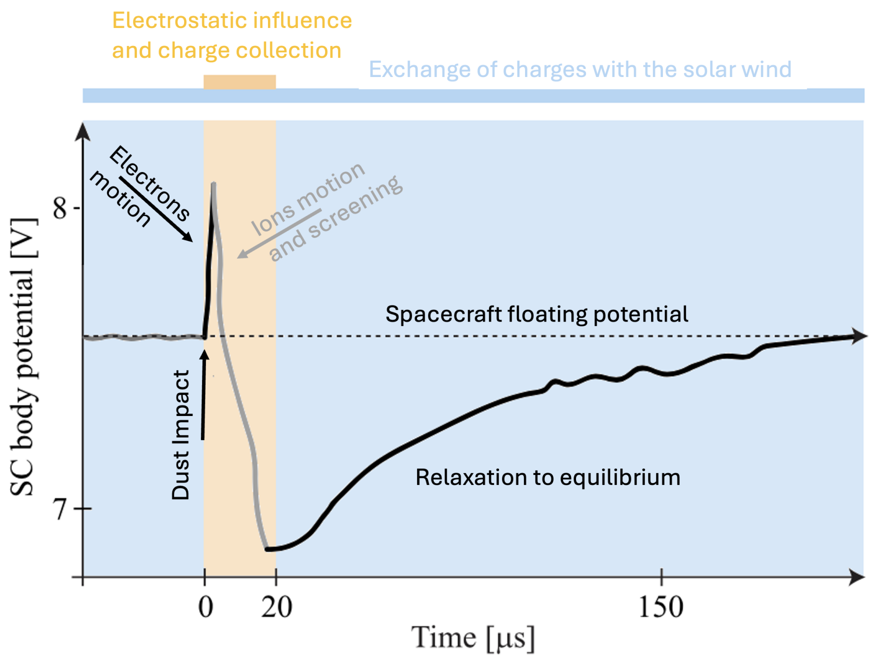

Figure 2. Schematic depiction of the variation of the potential of a spacecraft embedded in the interplanetary plasma at around 1 a.u., after a hypervelocity impact by a dust grain occurred. The dominant process shaping the signal in each phase is coded in color: orange for processes related to the impact charges dynamics, collection and screening; blue for charge exchange with the surrounding plasma. Adapted from Kočiščák (2024).

While evolving under the effect of the impact ionisation cloud dynamics, the potential of the conductor also evolves according to the exchange of charges with its environment. In the absence of dust impact, the equilibrium between the photoelectron escape current and the ambient plasma electron collection current drives the conductor's floating potential to a few times the photoelectron temperature, $\varphi_{eq} \sim 5-10$ V. The deviation from this equilibrium potential induced by the impact charges changes these currents so that the conductor's potential relaxes to its equilibrium value. This occurs on a timescale $\tau_{relax} \sim 200$ μs at 1 au for a collector surface $S = 10$ m^2 and typical solar wind plasma parameters. At 1 au, this time is much larger than the timescales of cloud dynamics. Hence, to a good approximation, the potential evolves first according to collection/influence effects, reaches a value $-(1-\epsilon)Q/C$, and then exponentially relaxes to equilibrium on a time τ_{relax}. However, at heliocentric distances $d \lesssim 0.4$ au, the solar wind density is sufficiently high to make the relaxation timescale of the order of (or smaller than) the typical rise time τ_{ph} of the pulse. In this case, the exchange of charges with the solar wind makes the potential relax faster than it changes under the effect of the impact charges; the overall amplitude of the pulse is then reduced by a factor $\sim \tau_{relax}/\tau_{ph}$ (Zaslavsky, 2015). Figure 2 illustrates the different stages of the variation of the potential discussed in this section, in the case where the relaxation time is much larger than the dynamics/screening times of the ion cloud.

https://doi.org/10.5194/egusphere-2026-4440
Preprint. Discussion started: 17 August 2026

3.1.2 Implementation on electric field instruments. Dipole and monopole configurations.

An electric field instrument measures the voltage difference between two conductors: either an antenna and the spacecraft (monopole mode) or between two antennas (dipole mode) – a difference that produced apparently conflicting results in early measurements (Meyer-Vernet et al., 1996). In both cases, the wiring of the receiver and the mechanical base of the antennas induce stray capacitance in the system, which decreases the measured voltage (Bale et al., 2008; Zouganelis et al., 2010). The transfer function accounting for this imperfect coupling, which generally depends on the frequency of the signal measured, is, in the range of interest for dust impacts, $\Gamma \simeq C_a/(C_a + C_{stray})$, with the antenna capacitance C_a calculated from the ambient plasma properties (Meyer-Vernet and Perche, 1989); Γ is of the order $1/2$ for most devices.

Since most impacts occur on the spacecraft body, which has a much larger surface than the antennas, the potential of the spacecraft body is most likely to vary – following the scenario presented in the previous section – than the antennas. As a consequence, the monopole configuration is usually more favorable to the detection of dust: the receiver measures $V_{monopole}(t) = \Gamma(\delta\varphi_{ant}(t) - \delta\varphi_{sc}(t)) \simeq -\Gamma\delta\varphi_{sc}(t)$, except when $\delta\varphi_{ant}$ is not negligible compared to $\delta\varphi_{sc}$ (see below). Thus, the pulse $V(t)$ recorded is proportional to the spacecraft potential variation, and makes it possible to determine the value of the total charge Q from the pulse amplitude.

In a dipole configuration, the spacecraft potential (the "common mode") is rejected from $V(t)$, which consists of the difference of potential between the two antenna booms. Since the antenna booms are usually rather far from the impact location and their surface is much smaller than that of the spacecraft, they do not collect much charge (O'Shea et al., 2017), and their variation in potential is essentially determined by the influence from the ion cloud, which is different from an antenna to another, depending on the impact location (Meyer-Vernet et al., 2014; Shen et al., 2021a). Without prior information on the impact location, estimating the total charge released is much more challenging for dipole measurements than for monopole measurements (Shen et al., 2023). As an order of magnitude, an impact relatively close to an antenna of length L_{ant} will induce a potential variation of amplitude $\delta\varphi_{ant} \sim Q/(4\pi\varepsilon_0 L_{ant})$ if the distance is smaller than the ambient Debye length. The efficiency of dipole measurements can then be inferred from two parameters: the ratio of the distance between the antenna bases to the antenna length, and the ratio $\eta = C/(4\pi\varepsilon_0 L_{ant})$(Meyer-Vernet et al., 2014), where C is the spacecraft capacitance. If both ratios are small compared to unity, all the antennas will measure roughly the same signal, which is much smaller than the voltage measured in monopole mode. In this case, the efficiency of dipole measurements is small, and $\delta\varphi_{ant}$ does not affect the monopole measurement. On the other hand, if the ratios are of the order of unity or larger, the impact position that will usually occur closer to a particular base will produce imbalances, roughly of the order of $V(t) \sim \Gamma\delta\varphi_{ant}$ – a value of the same order of magnitude as the signal measured in monopole mode. In this case, the dipole measurement is as effective as the monopole one, and the latter is affected by $\delta\varphi_{ant}$, making the evaluation of Q more difficult. For spacecraft like Solar Orbiter and Parker Solar Probe, the imbalances are of the order of the monopole signal itself – these imbalances have indeed been measured on these spacecraft by (Page et al., 2020; Kočiščák et al., 2024). On the other hand, spacecraft such as STEREO or Wind have rather poor dipole efficiencies (at least, concerning Wind, before one of its Ex dipole arm was cut, making it asymmetric).

https://doi.org/10.5194/egusphere-2026-4440
Preprint. Discussion started: 17 August 2026

3.1.3 Mass calibration

Finally, we discuss how to estimate the mass of the impacting dust from the measured signals. As we have seen, the pulse amplitude, in the best case of monopole measurements with $\eta \ll 1$, provides a good estimate of the total charge Q generated by impact ionization. Given the charge yield of the impacted material $Q = \alpha m v^{\beta}$, we can derive the mass of the particle only if we know the impact speed, which we cannot measure independently. Models for a grain's speed as a function of mass $v(m)$ derived from numerical simulations (e.g. (Czechowski and Mann, 2010; Poppe et al., 2011; Poppe and Lee, 2020; Mann and Czechowski, 2021)) can be used to determine an estimate of the size from a measured voltage pulse (see fig.6 of Zaslavsky et al. (2012) or fig.7 of Zaslavsky et al. (2021)). This approach entails significant uncertainties stemming from the neglected spread in impact velocities for a given mass, uncertainties in the charge yield, and the estimation of Q from the impact voltage. As a consequence, the mass of a particle cannot be reliably estimated from a single impact – but robust statistical estimates can be made on the impact voltages expected from different populations of interplanetary dust.

Nanometer grains, which can reach drift speeds of ~ 300 km s^{-1} at 1 au, generate impact charges of a few pC, and monopole pulses $\sim 2 - 10$ mV, for typical spacecraft capacitance $C_{sc} \sim 200$ pF and gain factor $\Gamma = 1/2$, except when the perturbation of the photoelectron sheath increases the signal (see Sec. 3.3.3). Grains in the 100 nm range, or β-meteoroids, have typical radial velocities ~ 80 km s^{-1} and will produce $\sim 10 - 100$ pC impact charges, and pulses $\sim 20 - 200$ mV – the latter population constitutes the broad majority of the impacts detected. Grains with micron size have roughly Keplerian impact speeds – as the spacecraft orbital speed – and the charge they produce will depend on the distance to the Sun and the spacecraft position on its orbit. At 1 au, it is typically $\gtrsim 500$ pC, producing voltage pulses $\gtrsim 1$ V. The latter will tend to saturate radio receivers, whose dynamic range is often limited to a few hundred mV.

3.2 Voltage signatures modeled and observed in laboratory experiments

Dust impacts on spacecraft release electric charge that produces transient voltage signals detectable by electric field antennas (Aubier et al., 1983; Gurnett et al., 1983, 1981). These signals arise from impact ionization, a process in which the high-speed impact of a dust particle (> 1 km s^{-1}) generates a rapidly expanding plasma cloud (Auer, 2001b). The properties of this impact plasma govern the observed antenna response and must therefore be understood to interpret dust-induced electric signals and infer basic particle parameters, such as mass. Direct experimental investigation of antenna-based dust detection became possible through laboratory simulations using a dust accelerator. Such experiments enable controlled characterization of impact plasmas, including charge generation yields for spacecraft-relevant materials, plasma composition, and the energy, velocity, and angular distributions of plasma particles. Laboratory studies employing scaled models of spacecraft–antenna systems have further clarified the physical mechanisms by which the expanding plasma cloud couples to antennas and produces measurable electric signals.

For completeness, we note that dedicated dust detectors and analyzers based on impact ionization have been developed and flown on several missions, e.g. (Auer, 2001b; Srama et al., 2004; Horányi et al., 2014; Simolka et al., 2024; Kempf et al., 2025; Horányi et al., 2025a). These instruments are highly sensitive and well calibrated in the laboratory, enabling

https://doi.org/10.5194/egusphere-2026-4440
Preprint. Discussion started: 17 August 2026

accurate determinations of particle mass, speed, and composition, whereas antenna-based detection benefits from the much larger spacecraft impact area and is therefore sensitive to relatively large, low-abundance particles.

3.2.1 Dust accelerator

The dust accelerator employed, and the results of which are discussed in the following, is operated at the University of Colorado at Boulder (Shu et al., 2012). The facility is an electrostatic accelerator with a design heritage tracing back to earlier systems (Friichtenicht, 1962; Mocker et al., 2011) and is capable of accelerating particles with diameters of $\sim 0.02 - 2\ \mu$m to velocities relevant to space applications (Figure 3). Each accelerated particle is characterized in flight in terms of its velocity and mass using two pickup-tube detectors installed along the beamline (Shu et al., 2012; Thomas et al., 2013). The accelerator can operate with conductive or electrically dissipative particles, whereas dielectric materials require the application of a thin conductive coating. Several techniques have been developed to deposit nanometer-scale polymer, platinum, or palladium coatings for this purpose (Hillier et al., 2009; Fielding et al., 2015). As a result, a broad range of dust samples – including minerals and organic materials – is now available for experimental studies (Hillier et al., 2009; Hillier et al., 2012; Hillier, 2018; Fielding et al., 2015; Eckart et al., 2023; Mikula et al., 2024). Iron dust is commonly used for fundamental impact studies where composition is not critical, owing to its reliable accelerator performance and its historical use in the calibration of spaceborne dust instruments.

3.2.2 Impact Ionization and Characteristics of Impact Plasmas

Impact ionization provides one of the most sensitive techniques for detecting and analyzing the composition of dust particles in space (Auer, 2001b). The transient, partially ionized plasma generated upon impact consists of ions, electrons, and neutrals. A number of models have been proposed to explain its observed characteristics, including plasma, shock-wave, and desorption-ionization models (Hornung and Michel, 1972; Drapatz and Michel, 1974; Knabe and Krueger, 1982; Kissel and Krueger, 1987; Hornung et al., 1996, ?). Despite these efforts, a first-principles understanding of impact ionization remains incomplete, as the properties of the impact-generated plasma are largely constrained by laboratory measurements rather than derived from fundamental theory.

For the detection of dust particles using antennas, the relevant parameters of the impact plasma include the charge yield, ion composition, energy (or velocity) distribution, and angular distribution. It is important to note that impact ionization is inherently non-deterministic, exhibiting substantial variability in the generated charge and other plasma characteristics even for nearly identical particles impacting the same material at the same velocity. Among these parameters, the impact charge is relatively well characterized, largely as a result of extensive laboratory calibration of spaceflight instruments. The impact-generated plasma contains approximately equal amounts of positive and negative charge carriers, which can be separated by modest electric fields (Auer, 2001b). The impact charge, or charge yield, is commonly described by a power-law relation, $Q_{\mathrm{IMP}} = \alpha m v^{\beta}$, where m and v denote the particle mass and velocity, respectively, and the empirically derived coefficients α and β depend primarily on the target material rather than on the projectile (e.g., (Horányi et al., 2014)). Over a broad velocity range, a single power law fails to capture the observed behavior, and the normalized charge yield Q_{IMP}/m exhibits a characteristic S-shaped dependence on impact velocity (Dietzel et al., 1972; Mocker et al., 2013; Kempf et al., 2025; Horányi

https://doi.org/10.5194/egusphere-2026-4440
Preprint. Discussion started: 17 August 2026

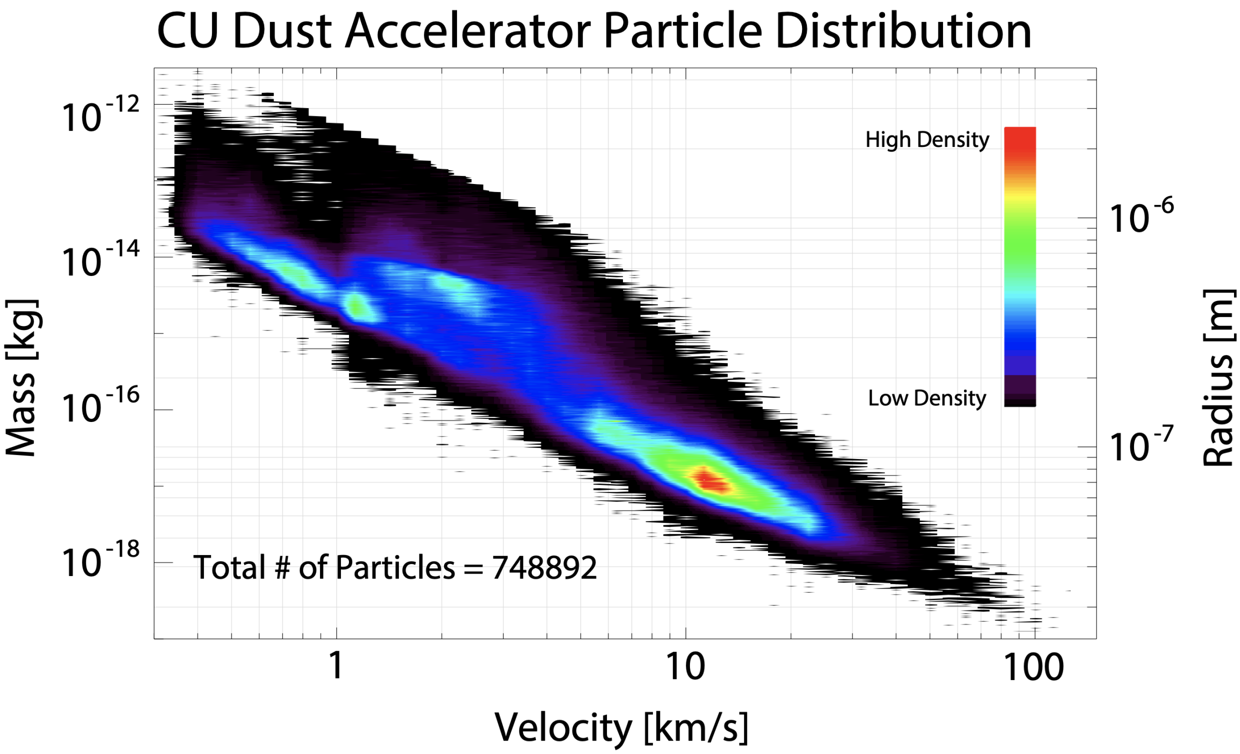

Figure 3. Typical mass–velocity distribution of iron particles produced by the accelerator (Shu et al., 2012). The color scale indicates the probability of occurrence for particles with the given parameters.

et al., 2025a). A recent review of charge yields for spacecraft-relevant materials is provided by (Collette et al., 2014). For fixed m and v, the uncertainty of the impact charge Q_{IMP} follows a log-normal distribution, with an error factor of approximately 2 for standard surfaces; for highly polished target surfaces, this factor decreases to about 1.6 (Horányi et al., 2025a). Surface cleanliness also influences charge yield, which generally decreases with increasing cleanliness. Also the density ratio of the dust particle versus impact surface plays a large role in impact ionization (Hornung and Drapatz, 1981; Hunziker et al., 2022).

Several laboratory investigations have examined the ion composition of impact plasmas, which reflects the chemical makeup of both the dust and target materials but varies strongly with impact velocity (Hillier et al., 2012; Hillier, 2018; Fiege et al., 2014; Goldsworthy et al., 2002; Goldsworthy et al., 2003; Mikula et al., 2024). At lower impact velocities ($\lesssim 5\ \mathrm{km\,s^{-1}}$), alkali metal ions such as $\mathrm{Na^+}$ and $\mathrm{K^+}$ dominate the spectra due to their low ionization energies, even when present only as minor contaminants (Auer and Sitte, 1968). At impact velocities of $\sim 10\ \mathrm{km\,s^{-1}}$, alkali ions remain prevalent, while additional species such as $\mathrm{H^+}$ and $\mathrm{C^+}$ (likely originating from surface contamination), as well as atomic or molecular ions derived from the dust and target materials, become prominent. At higher impact speeds ($\gtrsim 16\ \mathrm{km\,s^{-1}}$), the relative abundance of alkali ions decreases, whereas $\mathrm{H^+}$, $\mathrm{C^+}$, and ions representative of the dust composition increasingly dominate the spectra (Mocker

https://doi.org/10.5194/egusphere-2026-4440
Preprint. Discussion started: 17 August 2026

et al., 2013). At still higher velocities, extensive molecular fragmentation leads to a reduction in the average ion mass. Organic materials, if present, generate a broad distribution of ion masses arising from both fragmentation of the parent molecules and clustering processes within the impact plasma (Mikula et al., 2024). Composition measurements are often conducted using precious-metal targets. Among these, Au and Ir exhibit minimal ionization due to their high ionization energies (e.g., (Mikula et al., 2024)), whereas Ag and Rh targets contribute substantially to the total ion content of impact plasmas at velocities above $5-10\ \mathrm{km\,s^{-1}}$ (e.g., (Hillier et al., 2012; Fiege et al., 2014)). For impacts occurring on typical spacecraft surfaces, such materials are therefore expected to constitute a significant fraction of the ions produced. An example mass spectrum measured by the laboratory prototype of the Interstellar Dust Experiment (IDEX) instrument is shown in Figure 4.

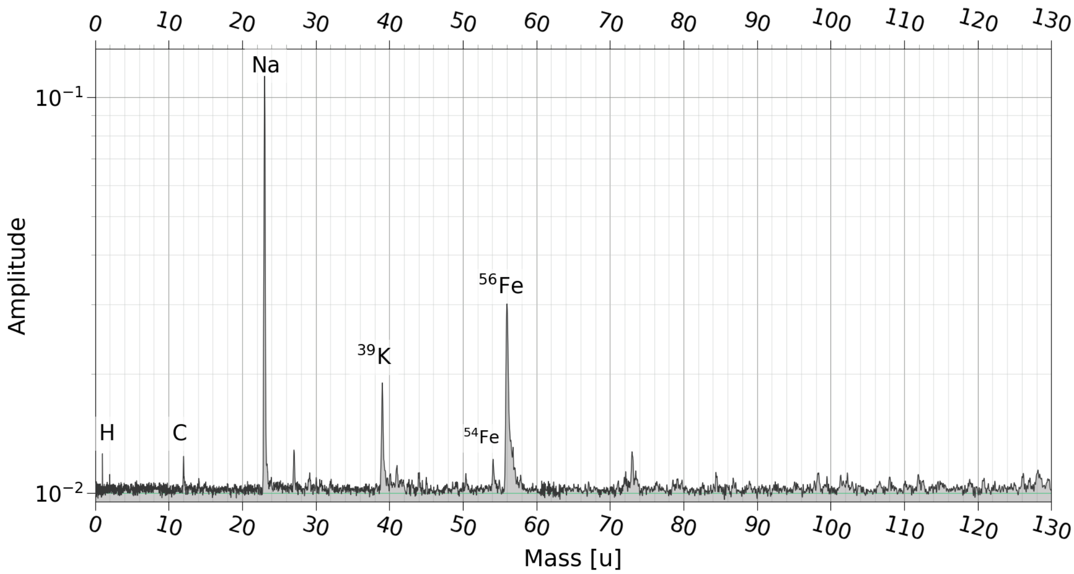

Figure 4. Time-of-Flight (ToF) mass spectrometry can be used to determine the composition of the impact plasma. The spectrum shown corresponds to an $11\ \mathrm{km/s}$ impact of iron dust onto a clean gold target surface. The abundant alkali ions, $\mathrm{Na^+}$ and $\mathrm{K^+}$, originate from minor contamination of the dust particles and/or the target material. Hydrogen and carbon ions are also commonly observed due to surface contamination. At this impact speed, the abundance of gold ions ($\mathrm{Au^+}$) is negligible and therefore not shown in the figure.

The energy and ion velocity distributions of impact plasmas have been characterized using optical diagnostics, linear time-of-flight (TOF) techniques, and measurements of ion expansion under near field-free conditions. Optical observations have been used to infer impact-plasma temperatures by modeling the emission as blackbody radiation. Reported temperatures typically range from $(2-6)\times10^3$ K, with temperature increasing with impact velocity (Eichhorn, 1975, 1976; Tsembelis et al., 2008; Collette et al., 2013). Some measurements indicate substantially higher temperatures, up to $(1-3.5)\times10^4$ K (Miyachi et al., 2008). The corresponding characteristic ion energies are approximately $0.2-0.5$ eV and $1-3$ eV, respectively.

In linear TOF measurements, the ion energy distribution is inferred from the widths of the mass spectral peaks. These measurements indicate relatively high ion energies. One study reported ion energies ranging from 10–70 eV, depending on the

https://doi.org/10.5194/egusphere-2026-4440
Preprint. Discussion started: 17 August 2026

ion species (Burchell et al., 1996); another found energies of 20–40 eV with only a weak dependence on dust impact velocity (Ratcliff et al., 1997); and a third study observed ion energy distributions spanning tens of eV for impact speeds $\leq 10\ \mathrm{km\ s^{-1}}$, increasing to hundreds of eV at higher impact velocities (Hillier et al., 2006).

Lee et al. (2012) investigated the free expansion of impact plasmas and determined a mean expansion speed of $20.8\ \mathrm{km s^{-1}}$, largely independent of dust particle mass or impact velocity. Collette et al. (2016), using a basic retarding field analyzer, measured the effective temperatures of both positive and negative ions in impact plasmas at speeds of 4, 10, and 20 $\mathrm{km s^{-1}}$. Their findings showed that positive ion temperatures increased from about 4 eV to 20 eV, with the latter observed at speeds exceeding $20\ \mathrm{km s^{-1}}$. Similar energy values were reported by Nouzák et al. (2018, 2020) in experiments using a scaled-down antenna model. Kočiščák et al. (2020) measured energy distributions for cations from olivine particles coated with polypyrrole, impacted at velocities between 2 and $18\ \mathrm{km s^{-1}}$. Their results indicated that cation energy remained around 7 eV with little dependence on dust impact speed. Meanwhile, negative charge carriers, likely consisting of free electrons and anions, exhibited energies between $1-10$ eV with non-monotonic variation based on impact velocity. Shen et al. (2021a, b) employed a physical model to interpret antenna signals, successfully fitting laboratory data and estimating an expansion velocity of approximately $10\ \mathrm{km s^{-1}}$ for cations in impact plasmas at dust impact speeds of $20\ \mathrm{km s^{-1}}$ or greater.

Experimental studies have also investigated the free expansion of impact-generated plasma under field-free conditions. Lee et al. (2012) reported a mean expansion speed of $20.8\ \mathrm{km s^{-1}}$, largely independent of dust mass or impact velocity (Lee et al., 2012). Shen et al. (2021a, b), on the other hand, estimated a lower expansion velocity of $\sim 10\ \mathrm{km s^{-1}}$ for cations produced at dust impact speeds $\gtrsim 20\ \mathrm{km s^{-1}}$ (Shen et al., 2021b, a). Studies employing retarding field analyzers have measured effective ion temperatures in impact plasmas. Collette et al. (2016) found that cation temperatures increase with impact speed, from ~ 4 eV at low velocities to ~ 20 eV above $20\ \mathrm{km s^{-1}}$, while negative charge carriers exhibit lower energies of 1–10 eV. Similar ion energies were reported in antenna-based experiments (Nouzák et al., 2018, 2020). Measurements using olivine particles coated with polypyrrole indicate that cation energies remain near ~ 7 eV with weak dependence on impact velocity over 2–18 $\mathrm{km s^{-1}}$ (Kočiščák et al., 2020).

A recent and particularly relevant study by Nouzák et al. (2025) measured the temporal and spatial distributions of ions emerging from impact plasmas using a large-area delay-line detector. The resulting velocity distributions were broad, extending to $\sim 10\ \mathrm{km s^{-1}}$ for low-speed impacts (2–5 $\mathrm{km s^{-1}}$) and exceeding $50\ \mathrm{km s^{-1}}$ for impact speeds above $\sim 10\ \mathrm{km s^{-1}}$. By separating contributions from the dominant ion species in the plasma ($\mathrm{Fe^+}$, $\mathrm{Na^+}$, $\mathrm{C^+}$, and $\mathrm{H^+}$), the authors showed that the translational energy of the expanding ions typically lies in the range 3–8 eV, with an additional thermal component of ~ 1 eV that exhibits little dependence on impact speed or ion species. The wide velocity range is therefore attributed to different ion species expanding with approximately the same kinetic energy. An example velocity distribution for impacts is shown in Figure 5.

Nouzák *et al.* (Nouzák et al., 2025) also measured the angular distribution of the expanding ions and found it to follow a cosine power-law distribution, $\cos^n \theta$, with $n = 1$. Their measurements were, however, limited to angles $\theta = 13°$–$45°$ relative to the surface normal. Other investigations have reported cosine distributions ranging from $n = 0$ (isotropic emission) (Hillier et al., 2006) to $n = 2$–3 (Ratcliff and Allahdadi, 1996). Measurements by Abramov *et al.* investigated the angular distribution

https://doi.org/10.5194/egusphere-2026-4440
Preprint. Discussion started: 17 August 2026

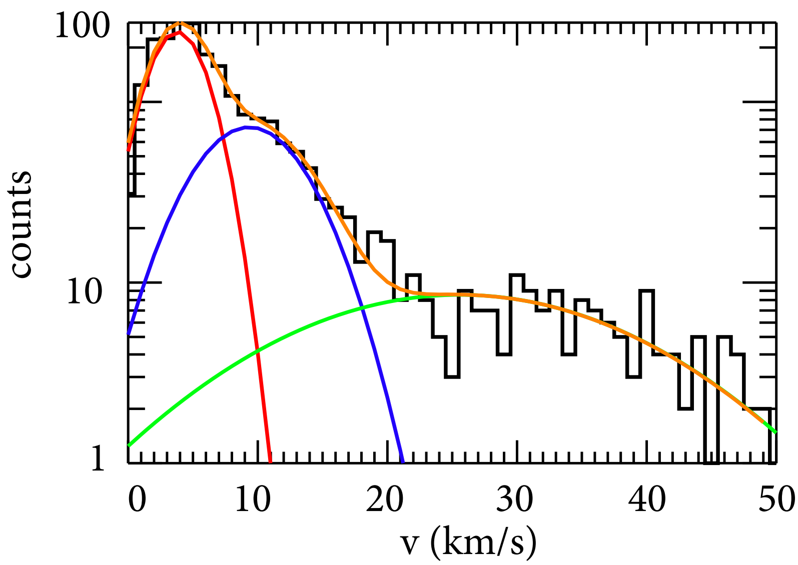

Figure 5. Average cation velocity distribution (black) from plasmas produced by iron dust impacts in a velocity range of 10–15 $\mathrm{km\,s^{-1}}$. The measured distribution can be reconstructed as a sum (orange) of contributions from three major ion species present in the impact plasma (Fe^{+} (red), C^{+} (blue), and H^{+} (green)). Data accepted from Nouzák et al. (2025), see text for details.

at lower impact speeds, between 1 and 11 $\mathrm{km\,s^{-1}}$ (Abramov et al., 1991). They observed peak emission at angles between 16°–36°, and the reduced ion occurrence near the surface normal was attributed to ion shielding by residual dust fragments.

3.2.3 Physical processes of antenna signal generation

Direct simulation of antenna signals using dust accelerators has also led to the development of first-principles physical models that complement those described in Sec. 3.1.1. Early models assumed that antenna signals arise primarily from the direct collection of a significant fraction of the impact-generated charge (Gurnett et al., 1983, 1987). A theoretical analysis by Oberc (1999) identified three mechanisms responsible for voltage generation: charging of the antenna, charging of the spacecraft, and detection of the electric field associated with charge separation in the expanding impact plasma. This work emphasized the strong dependence of the antenna response on the impact location, particularly for dipole configurations. Zaslavsky (2015) later introduced the floating-potential perturbation model, in which both the spacecraft and antenna recollect portions of the impact plasma, and the observed waveform is governed by their differing discharge time constants. Meyer-Vernet et al. (2017) highlighted key aspects of signal generation, noting that electrons in the impact plasma rapidly become isotropically distributed and that the expanding plasma induces charging on both the spacecraft and antennas, with the plasma expansion dynamics also contributing to the observed signal waveforms.

Laboratory simulations of the underlying physical processes began with a simple configuration consisting of an impact plate and a single antenna. Measurements by Collette et al. (2015) identified three relevant mechanisms: spacecraft charging,

https://doi.org/10.5194/egusphere-2026-4440
Preprint. Discussion started: 17 August 2026

antenna charging, and induced charging. They further showed that antenna charging is significant only for impacts occurring very close to the antenna base, a conclusion later supported by numerical modeling, which confirmed that this mechanism is of secondary importance (O'Shea et al., 2017). Subsequent laboratory measurements were performed using a scaled-down model of the Cassini spacecraft and the Radio and Plasma Wave Science (RPWS) instrument, operated in both monopole and dipole configurations (Nouzák et al., 2018, 2020). The measured waveforms showed good qualitative agreement with in-situ measurements and illustrated how key waveform characteristics depend on the spacecraft bias voltage. The experiments further demonstrated that antennas operated in dipole mode are largely insensitive to dust impacts on the spacecraft body (cf. section 3.1.2), and that the ambient magnetic field influences electron recollection from the impact plasma through gyro-motion effects.

These laboratory measurements collectively led to the development of a first-principles electrostatic model of antenna signal generation reported by Shen et al. (2021b, a), which was recently extended by Smith et al. (2025) to incorporate a more realistic description of impact-plasma expansion. A simplified laboratory configuration, consisting of a spherical target spacecraft and four coplanar antennas, was developed to validate the model and refine key parameters. For a full description of the electrostatic model, the reader is referred to Refs. (Shen et al., 2021a; Smith et al., 2025); only its key elements are summarized here.

The model rests on four fundamental components, the first of which concerns the energetics of the impact plasma. The total impact charge, Q_{IMP}, is composed of equal populations of free electrons and cations. These charge carriers separate from one another over spatial scales small compared to the spacecraft's size. Owing to their high thermal velocities, electron dynamics occur on timescales that are often not temporally resolved by measurements. Instead, a fraction of the electrons, κQ_{IMP}, is recollected by the spacecraft body, while the remaining fraction, $(1-\kappa)Q_{\mathrm{IMP}}$, escapes rapidly. Model fits to laboratory measurements indicate $\kappa \approx 0.5$. This result is interpreted physically as evidence that the electrons have an approximately isotropic velocity distribution, with roughly half propagating toward the spacecraft and subsequently being recollected. The cation dynamics are modeled following the work of Nouzák et al. (2025), assuming an initial cosine angular distribution and three distinct ion populations with characteristic velocities of 4, 14, and 36 $\mathrm{km\,s^{-1}}$. These populations correspond to light, intermediate-mass, and heavy ions present in the impact-generated plasma (see also Figure 5). The recent update to the electrostatic model demonstrated that incorporating physically realistic cation dynamics enables good agreement between the model and the measurements (Smith et al., 2025).

The second component of the model concerns the calculation of induced charging on each independent element due to the expanding plasma cloud. A numerical solver is used to determine the fraction of charge at location $\boldsymbol{r}$ that is induced on the spacecraft and on each antenna. This fraction is described by the geometry function $g_x(\boldsymbol{r})$ (with values between $0-1$), where x denotes the spacecraft or a given antenna, and is evaluated throughout the relevant vicinity of the system. The induced charge on any element at a given time during the plume expansion is calculated as $\int \rho_i(\mathbf{r},t) g_x(\mathbf{r}) \mathrm{d}^3\mathbf{r}$, where $\rho_i(\mathbf{r},t)$ is the charge density distribution of the plasma cloud.

The third component of the model employs the capacitance matrix, $[\mathbf{b}]$, of the spacecraft-antenna system to compute the transient voltages induced by the impact plasma on each independent element via the relation $[\boldsymbol{\delta V}(t)] = [\mathbf{b}]^{-1}[\boldsymbol{\delta Q}(t)]$. Reference (Shen et al., 2021a) presents a detailed methodology for constructing the capacitance matrix based on the system geometry and physical dimensions of the spacecraft and antennas, supplemented by calibration measurements that account for the effects of the electronics, cabling, and related components. In this formulation, $\delta Q(t)$ represents the time-dependent charge on each component and includes contributions from the initially recollected electrons, the induced charge associated with the expanding plasma cloud, and the cumulative charging and discharging of the elements through interconnected resistors and through charge collection from the ambient plasma environment.

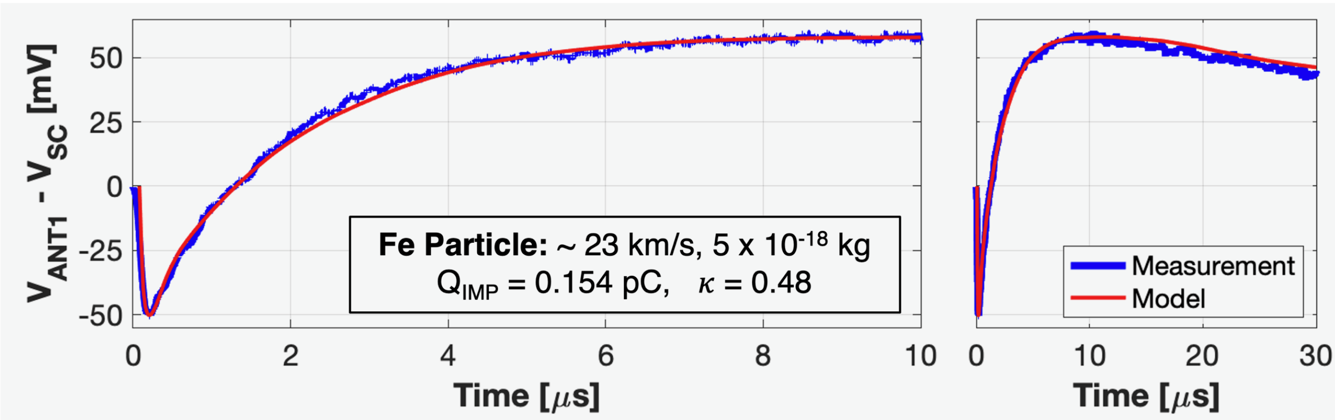

Figure 6. Laboratory measurements (blue) fitted with the updated electrostatic model (red). The figure shows the early-stage evolution of the antenna signal following a dust impact at $t = 0$. For comparison, see Figure 2. From (Smith et al., 2025), © AAS. Reproduced with permission.

The final component of the model involves solving for $\delta V(t)$ to obtain the temporal evolution of the voltages on the spacecraft and antennas. This is accomplished by numerically tracking the dynamical evolution of the impact plasma cloud using appropriately chosen time steps. The model is based solely on first principles and has been shown to provide excellent agreement with accelerator-based measurements (Smith et al., 2025). It was further demonstrated that incorporating the experimentally determined velocity and angular distributions from Nouzák et al. (2025) yields excellent fits independent of the impact location relative to the antennas.

Figure 6 shows the early-time evolution of the antenna signal following a dust impact and the good agreement with the model. The initial negative-going excursion arises from rapid electron escape, leaving the spacecraft temporarily positively charged. The subsequent increase in antenna potential results from the induced charging associated with the dynamically expanding plasma cloud. The scientific value of a first-principles model lies in its ability to fit the data with higher fidelity and to extract key physical parameters, such as the impact charge. In addition, detailed modeling of antenna signals enables localization of the dust impact position on the spacecraft and provides constraints on the particle's orbital parameters, thereby aiding in the identification of the dust source or origin.

https://doi.org/10.5194/egusphere-2026-4440
Preprint. Discussion started: 17 August 2026

3.3 Atypical signals

In this section, we review various dust impact signatures observed with electric field instruments, but which are not fully described by the charge collection and electrostatic influence effects as described in sections 3.1 and 3.2.

3.3.1 Magnetic signatures of dust impacts

It happens that electric signals associated with dust hits on PSP or SolO are accompanied by a high-frequency magnetic signal detected by the search-coil magnetometers (SCM) (Malaspina et al., 2022; Rackovic Babic et al., 2022; Dudok de Wit et al., 2022). Recent studies suggested that this signal may originates either from the initial escape current of free electrons within the impact-generated cloud (Rackovic Babic et al., 2022) or from an ionic current associated to the expansion of the ion cloud produced after an impact (Malaspina et al., 2022).

These magnetic signals usually occur simultaneously with the electric field antenna dust impact signals, and are characterized by timescales that can be very short ($< 10\ \mu$s) for signals of electron current origin, or much larger in the case of plasma cloud expansion (Figure 7). Both PSP and SO have 3-axis SCMs, but only one axis on each includes a double band X-antenna capable of capturing the highest-frequency magnetic signals, covering 10 kHz to 500 kHz on SO and 10 kHz to 1 MHz on PSP (Jannet et al., 2021).

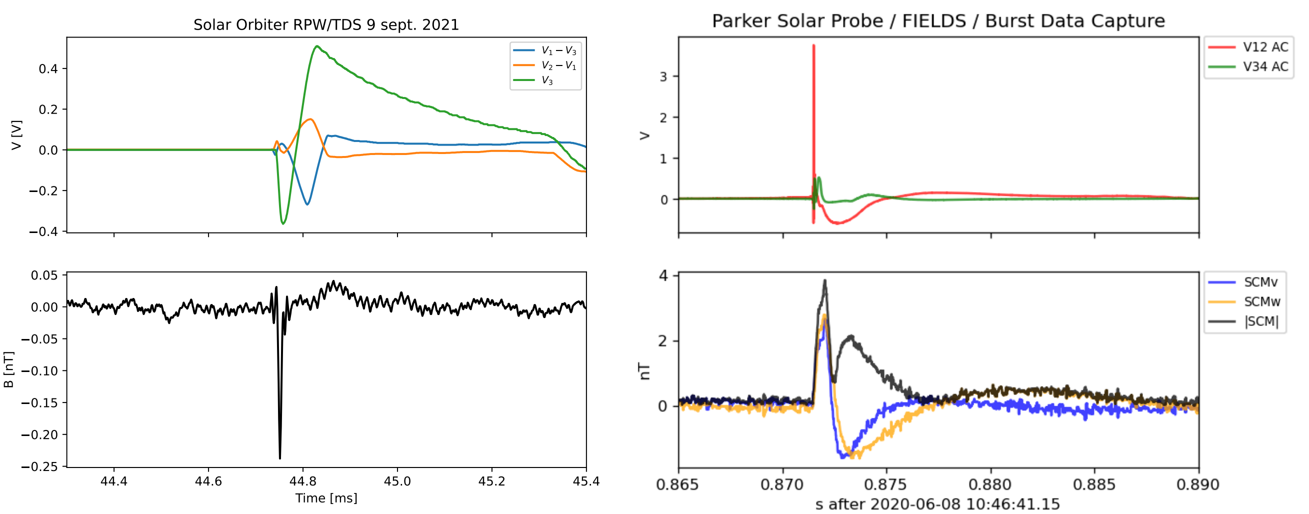

Figure 7. Example of dust impacts with magnetic signatures captured by SolO RPW/TDS (left panel) and from PSP/FIELDS (right panel), illustrating dust impact events. The top panels display the voltages, while the bottom panels show the SCM data. Voltages variations present characteristic signatures of dust impacts, while bottom panels clearly show corresponding signals in the magnetic field.

Both the SolO and PSP probes have detected events with remarkable similarities. The vast majority of these events exhibit large-amplitude voltage-channel signals – often saturating the SolO RPW instrument. This suggests that particularly large and/or fast dust grains impacts generate these signals. On SolO, a large proportion of the magnetic pulses coincide with the onset of the voltage pre-shoot associated to the electron escape, suggesting that the magnetic pulses may originate from initial electron escape currents within the plasma cloud formed after the impact (Rackovic Babic et al., 2022). On PSP, small timing differences between the peak of the electric field response and the SCM response to a dust impact, combined with the $\sim$ 6-m separation between the electric field antennas in the plane of the heat shield and the boom-mounted SCM, enable estimates of the impact plasma cloud expansion velocity. An analysis of ~ 60 events yielded a typical expansion velocity of ~ 15 km/s, consistent with a magnetic signature primarily driven by the ion cloud expansion velocity (Malaspina et al., 2022).

A more detailed analysis of the magnetic signals, along with a better understanding of the relationship between the magnitudes of the electrical and magnetic responses, is needed to resolve the extent to which plasma cloud electron and ion dynamics contribute to the formation of the magnetic field signature. Detailed analysis of these events can also yield new insights into the properties of large, fast-moving dust grains, an area that remains largely unexplored when using electric field instruments for dust studies. Furthermore, comparing signatures between SO and PSP may elucidate the role of spacecraft geometry in interpreting dust impacts. For example, a strong correlation between the electric and magnetic signal magnitudes is observed in PSP data from antenna V5, which is located near the SCM. This indicates that dust impacts in the vicinity of the search coil lead to a stronger coupling between electrical and magnetic signatures(Dudok de Wit et al., 2022).

3.3.2 Long duration events

While most dust-impact electric signals have a characteristic duration of a few microseconds to milliseconds, longer-duration waveforms – lasting from seconds up to several minutes – are occasionally observed both in the inner heliosphere and in the Earth's magnetosphere. These signals are attributed to impacts by relatively large (> 10 μm) grains, whose hypervelocity collisions with the spacecraft generate an extended debris cloud of micron-sized fragments. This cloud undergoes surface charging in the ambient solar wind, producing a long-duration electrical potential perturbation in the vicinity of the spacecraft as well as streaks in the white-light imager caused by sunlight reflected from the debris. Similar streak events associated with dust impact voltage perturbations were observed by STEREO (St. Cyr et al., 2009).

On PSP, such signals are usually associated with impact-produced debris captured by the white-light imager, magnetic field perturbations as discussed in Sec. 3.3.1, as well as impact-driven plasma waves (Malaspina et al., 2022). Fitting the observed electric signal to a theoretical debris-cloud model yields total released charges of $\sim 10^{-10}$ C during such events and debris-cloud radial expansion speed of ~ 8 cm/s. The occurrence rate of these events showed a radial evolution peaking at a distance of 40–50 $R_\odot$ (~ 0.2 au) from the Sun.

Long-duration signals have also been observed by the Solar Orbiter's low-frequency receiver (LFR) as presented in Fig. 8. Compared to PSP, the SolO detections occur at larger heliocentric distances and at rates roughly an order of magnitude higher, due in part to the different operational modes used by the SolO/RPW and PSP/FIELDS instruments. While many of the long-duration signals were associated with the spacecraft debris for PSP, no such evidence of large fragments has been observed for SolO so far. Finally, note that Earth-orbiting spacecraft occasionally record long-duration signals with timescales of around 10 seconds, consistent with impacts by millimetre-sized particles (Vaverka et al., 2018). The presence of these long-duration

https://doi.org/10.5194/egusphere-2026-4440
Preprint. Discussion started: 17 August 2026

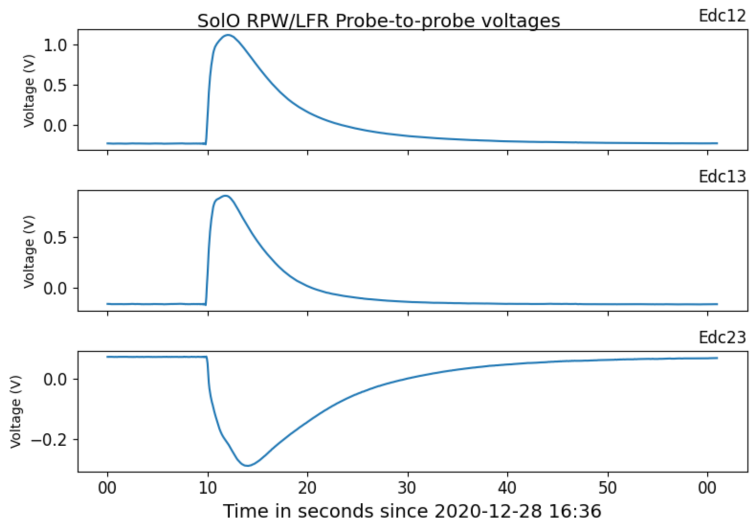

Figure 8. An example of a long-duration signal (∼a minute) observed by the SolO Low frequency receiver in the continuous waveform data sampled at 256 samples/s.

signals highlights how grain size, impact speed, and the plasma environment shape the morphology of dust-impact electrical signatures in a highly nonlinear regime.

3.3.3 Single hits and photo-electron sheath perturbation

As discussed in Sec. 3.1, typical voltage pulses recorded after dust impacts on independent antennas are simultaneous, with essentially the same peak amplitude and recovery phase. In these events, only considering the most frequent situation of a positive spacecraft potential (with respect to the surrounding plasma), the voltage pulses are primarily due to the charging of the spacecraft body through the recollection of electrons from the plasma cloud generated by a $\lesssim \mu$m dust impact on the spacecraft body itself. The case of single hits, first observed on the STEREO spacecraft (Zaslavsky et al., 2012), and later on Solar Orbiter (Kočiščák et al., 2024), is different: the voltage pulse is much stronger on one antenna with respect to the others so that charge recollection by the spacecraft body cannot be an adequate explanation. On typical single hits observed by STEREO/WAVES, a small signal – most of the time below the noise level – on two out of three antennas is interpreted as being due to charge collection after the impact of a small dust particle, in the nanometer rather than in the μm range, whereas the large signal is produced by an amplification mechanism that is not fully elucidated. The flux of dust particles decreases with increasing size (Meyer-Vernet et al., 2009; Mann, 2010), it is not surprising that triple hits are generally outnumbered by single hits (Zaslavsky et al., 2012; O'Shea et al., 2017) when the latter are present.

The origin of these single hits has been debated, and Kellogg (2017); Kellogg et al. (2018) have advocated that they may be the result of some spacecraft internal noise. But a physical model for the amplification of these signals has also been the subject of extensive works, that we cover in the following. As a first step, using data from STEREO A and B, Zaslavsky et al.

https://doi.org/10.5194/egusphere-2026-4440
Preprint. Discussion started: 17 August 2026

(2012) have shown that the signal on the antenna with the strong signal scales remarkably well with the portion of the antenna located inside the impact-generated plasma cloud at the time of its maximum expansion. The conclusion one may draw is that the potential of the one antenna, which finds itself partly inside the plasma cloud (the other two being unfavorably placed), is modified either because it collects some of the cloud's charge or because it is exposed to the cloud's electrostatic field. Due to its small cross-section, the collection efficiency of a boom antenna is believed not to exceed 1% of the cloud's charge (O'Shea et al., 2017), possibly reaching 5% with a favorable set-up and no photo-electrons as in some laboratory experiments (Collette et al., 2015).

For a $10^{-20}\,\mathrm{kg}$ nanodust grain that impacts the spacecraft at $300\,\mathrm{km/s}$, the charge released in the expanding cloud is of the order of $Q = 3\times10^{-12}\,\mathrm{C}$ (Meyer-Vernet et al., 2009; Pantellini et al., 2012b). As a reference, on one of the three boom antennas on STEREO, with a capacitance $C \approx 60\,\mathrm{pF}$, the voltage pulse would peak at a negligibly small amplitude of $\sim 0.01\,Q/C = 0.5\,\mathrm{mV}$ only, to be compared to the typical pulse amplitudes of the order $10^2\,\mathrm{mV}$ (Zaslavsky et al., 2012). Variations of the antenna's potential due to its partial exposure to the cloud's field have not been observed in laboratory experiments (O'Shea et al., 2017).

A more plausible scenario evoked to explain the occurrence of a large signal on only one of the three antennas on STEREO rests on the hypothesis that the electrostatic field of the expanding plasma cloud is sufficiently intense to efficiently interrupt the photo-electron return current to a nearby antenna (Pantellini et al., 2012b, 2013). Photo-electrons, emitted by the antenna at a temperature of $T_{\mathrm{ph}} = 2.5\,\mathrm{eV}$ have to overcome a potential well of the order of $10\,\mathrm{V}$ to escape to infinity. This implies that most of them cannot escape, and simulations indeed show that 9 out of 10 emitted electrons return to the antenna. A thermal photo electron of energy $1.5T_{\mathrm{ph}} = 3.75\,\mathrm{eV}$ reaches a maximum radial distance of $7.8\,\mathrm{cm}$ (i.e. ~ 7 times the antenna radius) before returning to the antenna.

Sample trajectories of photo-electrons emitted at different energies E_0 and angles θ with respect to the radial direction are shown in Figure 9. If unperturbed, the emitted electrons return to the antenna on sub μs time scales. However, even a small energy kick δE given to the particle near the apex of its trajectory may increase its angular momentum sufficiently to make the particle miss the antenna surface on its next flyby. In the examples of Figure 9, a small energy kick $\delta E = 0.01\,\mathrm{eV}$ prevents the particles from returning to the antenna. Hence, even a small perturbation of the cloud's electrostatic field can prevent a significant fraction of photoelectrons from returning to the antenna, inducing a transitory accumulation of positive charge. Such a perturbation is easily provided by a plasma cloud generated by a nanodust impact on the spacecraft body, where voltages of the order $0.01\,\mathrm{V}$ are still expected for clouds having expanded to a radius of the order $1\,\mathrm{m}$ (Pantellini et al., 2013). Now, if during a time interval τ a significant fraction of photo-electrons are prevented from returning to a portion of the length l of an antenna of radius a, its charge must rise by $\delta Q \sim j_{\mathrm{ph}} 2al\tau$, where j_{ph} is the photoemission current emitted by the antenna. On STEREO, the charging time is of the order $\tau = 40\,\mu\mathrm{s}$. Given an antenna radius $a = 1.15\,\mathrm{cm}$, $l = 0.5\,\mathrm{m}$ and a photoemission current $j_{\mathrm{ph}} = 40\,\mu\mathrm{A/m^2}$ (a rather conservative value at STEREO), one finds that the antenna's charge must increase by $\delta Q \sim 1.84\,10^{-11}\,\mathrm{C}$. Given an antenna capacitance $C \approx 60\,\mathrm{pF}$, one obtains a voltage pulse $\delta Q/C = 300\,\mathrm{mV}$, which is large enough to account for the observed single-hit voltages, which are generally in the range 10 to $10^2\,\mathrm{mV}$. It has been argued that the charging time τ, could be of the order of the inverse plasma frequency of the electron cloud, i.e. the

https://doi.org/10.5194/egusphere-2026-4440
Preprint. Discussion started: 17 August 2026

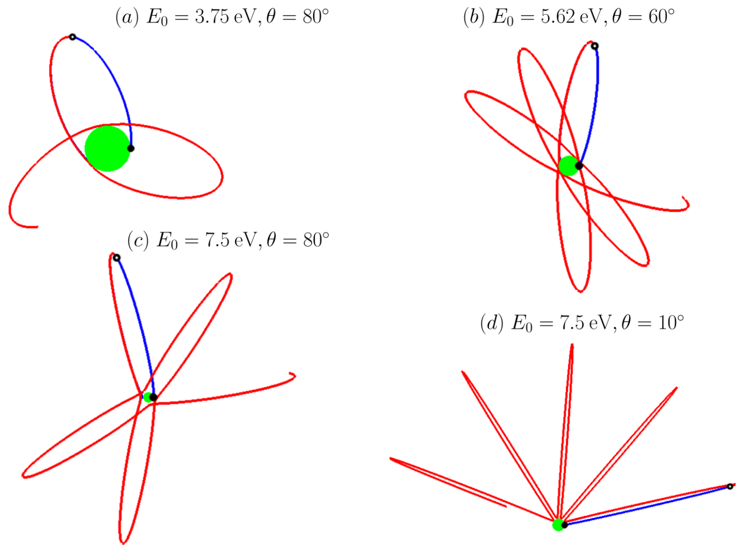

Figure 9. Trajectories of selected photo-electrons emitted at different energies E_0 and angles θ with respect to the radial direction in the typical electrostatic field of a cylindrical antenna. A small energy kick $\delta E = 0.01\,\mathrm{eV}$ at the indicated location prevents the electrons from falling back onto the antenna. No velocity component parallel to the antenna axis is given to the particles, which move in a plane perpendicular to the antenna axis. The green disc of radius 1.15 cm represents the antenna cross-section.

cloud's restoring time (Pantellini et al., 2012b, 2013). However, as shown by Kellogg (2017), emitted photo-electrons miss the antenna as long as the potential around the antenna is nonaxisymmetric. Now, even after redistribution of the photo-electrons, the surrounding field is not axisymmetric during the time $\sim r_{\mathrm{max}}/v_{\mathrm{p}}$ of the cloud's expansion. Hence, for a maximum cloud extension $r_{\mathrm{max}} = 0.5\,\mathrm{m}$ at the time of its merging with the surrounding plasma and a typical energy of $2\,\mathrm{eV}$ for the protons in the ejecta, the expected charging time is of the order $(2\mathrm{eV}/m_{\mathrm{p}})^{1/2} = 36\,\mu\mathrm{s}$, in good compliance with the measurements.

The above scenario appears to be plausible for the most common single-hits observed on STEREO, where the antenna potential goes positive with respect to the spacecraft body (see e.g. Figure 1a in O'Shea et al. (2017)). It has also been advanced as a plausible explanation for the imbalanced single or double hits observed by the RPW instrument aboard Solar Orbiter (Kočiščák et al., 2024).

We finish by mentioning the existence of single-hits for which the antenna potential goes negative (see e.g. Figure 1b in O'Shea et al. (2017)), and for which the above single-hit is clearly inappropriate. They constitute around 7% of the total number of single hits measured on STEREO. A likely scenario is a direct hit on the antenna, followed by recollection of the electrons in the ejecta onto the antenna itself, inducing a potential drop. On STEREO, the impact cross-section for a dust particle hitting one of the three antennas perpendicularly to its axis is $2al = 0.138\,\mathrm{m}^2$. This is the largest possible collecting surface for a single antenna, which one may use as a rough estimate of the cumulative cross-section of the three antennas. On STEREO, the observed number of negative to positive spikes is effectively of the order of the ratio of the exposed surfaces of

https://doi.org/10.5194/egusphere-2026-4440
Preprint. Discussion started: 17 August 2026

the antennas to the exposed surface of the spacecraft body (of the order $\sim \mathrm{m}^2$). However, whether negative potential spikes observed on a single antenna are due to direct dust impacts on its body remains an open question.

3.4 Automated detection and machine-learning classification of dust impacts

In practice, the scientific output of antenna-based dust measurements relies not only on the observational capabilities of the receiver system, but also on the procedure used to identify relevant signals in large waveform databases. The purpose of the detection software is to categorize recorded waveforms into classes that are useful for the intended analysis, here focusing on dust impacts. As discussed in Section 3.1.1, the observed dust impact waveform is dependent on spacecraft charging and the local plasma environment. At the same time, electromagnetic wave activity (notably solitary-wave-like structures (Vaverka et al., 2018) and nonlinearly steepened plasma waves) may induce resembling electric field signatures, complicating the separation of dust impacts from the plural of other signal shapes recorded by radio and plasma-wave receivers (Kvammen et al., 2023).

Dust candidates have traditionally been identified using rule-based procedures. Most missions select short-duration high-rate waveform data onboard for telemetry back to Earth using a set of simple criteria (e.g. Wind/Waves, STEREO/WAVES, Solar Orbiter, and Parker Solar Probe/FIELDS (Meyer-Vernet et al., 2009; Malaspina and Wilson, 2016; Bale et al., 2016)), and report the maximum measured electric field amplitudes at a low cadence (Bougeret et al., 2008; Maksimovic et al., 2020; Malaspina et al., 2023; Chadda et al., 2024)). In either data set type, identification of dust impacts is typically carried out in subsequent ground-based analysis. For Solar Orbiter/RPW, an onboard classification step is additionally used to pre-select waveform snapshots for downlink (Soucek et al., 2021).

Recent work on Solar Orbiter/RPW demonstrates that supervised machine learning methods are suitable for classifying waveform snapshots into physically meaningful categories with higher reliability than rule-based onboard logic (Kvammen et al., 2023). In particular, convolutional neural network classifiers trained on expert-labeled waveforms substantially outperform the onboard algorithm, improving the dust detection precision from about 75% to ∼94% (Kvammen et al., 2023), reducing contamination by dust-like plasma-wave transients and yielding waveform catalogs better suited for statistical dust distribution studies (Kočiščák et al., 2023).

4 Observational results

This section presents the main observational advances on dust in the inner heliosphere delivered by the spacecraft described in Section 2, covering brightness observations and in-situ antenna measurements. Results are organised by dust population and physical process: the large-scale structure of the Zodiacal cloud and its brightness distribution (Section 4.2), constraints on the bound and unbound (β) meteoroid populations from in-situ measurements (Section 4.3), dust depletion near the Sun (Section 4.4), interaction with solar wind structures (Section 4.5), nanodust (Section 4.6), and interstellar dust (Section 4.7).

Before addressing spacecraft results, Section 4.1 establishes the necessary context. It summarises the state of knowledge from near-Earth observations, introduces the reference interplanetary dust flux model, and defines the terminology for the main dust populations (bound dust, β-meteoroids, nanodust, interstellar dust) that is used throughout the remainder of the paper

https://doi.org/10.5194/egusphere-2026-4440
Preprint. Discussion started: 17 August 2026

4.1 Zodiacal dust mass distribution, meteoroid fluxes and populations

This section exposes our understanding of dust and meteoroid fluxes near Earth, where the mass and size distribution are known over a broad range. The mass distribution is crucial for identifying particle sizes responsible for observed brightness and dominant fluxes in in-situ measurements, and it also affects the dust cloud's collisional evolution.

4.1.1 Mass distribution near Earth

The interplanetary dust cloud forms as fragments of asteroids and comets undergo collisional evolution, forming a size distribution in which the number density increases steeply towards smaller sizes, typically described by a power law. By combining different observational constraints from meteors, lunar micro-craters, and in-situ measurements, an empirical mass distribution – the interplanetary dust flux model – was derived by Grün et al. (1985). It is characterized by a combination of three power laws across different mass regimes, and has long served as the reference model for the meteoroid environment near 1 au.

Making robust flux estimates remains however challenging: different techniques (zodiacal-light photometry, satellite and spaceborne dust detectors, radar observations, and accumulations of cosmic spherules in ice cores and sediments) yield total cosmic dust influxes to Earth that vary by more than an order of magnitude from each other. Deviations from the interplanetary dust flux model were for instance found with the impact crater analysis of the Long Duration Exposure Facility (LDEF) (Love and Brownlee, 1993). Recent atmospheric and geochemical studies suggest a global input of order a few tens of tonnes per day, but with substantial systematic uncertainty (Plane et al., 2018; Carrillo-Sanchez et al., 2016; Carrillo-Sánchez et al., 2020; Hervig et al., 2022). This illustrates that the absolute normalisation of the flux remains poorly constrained, even if the overall shape of the size distribution is reasonably well established.

Despite uncertainties, the Grün interplanetary dust flux model (Grün et al., 1985) remains a baseline for studying interplanetary dust: The latest spacecraft risk assessment models, such as NASA's MEM3.1 ((Moorhead et al., 2026)) and the ESA IMEM2 model ((Soja et al., 2019)) for the inner Solar System, account for distinct source populations as well as orbital and size-frequency distributions while still capturing the general characteristics of the interplanetary flux model. This general characteristic implies that sub-micron and nanometer-sized grains dominate in-situ flux measurements due to their higher number densities. It also implies that the grains in the 1–100 μm size range (approximately 10^{-11} g to 10^{-5} g) generate the main geometric cross-section of dust and hence determine the brightness of the Zodiacal light (Nesvorny et al., 2011; Pokorný et al., 2024). Although the zodiacal light represents only a specific size range of the interplanetary dust cloud, which may change with distance from the Sun, it is nevertheless often referred to as the zodiacal cloud, see 4.2 for further discussion.

4.1.2 Meteoroid flux from Earth-based observations

An important complementary perspective on the near-Earth flux comes from meteor and bolide observations in Earth's atmosphere, which sample particles from the sub-millimetre to multi-metre regime. High-power meteor radars (Weryk, 2014; Janches et al., 2015), combined with specular and head-echo systems, monitor sporadic and shower meteoroids with masses of

https://doi.org/10.5194/egusphere-2026-4440
Preprint. Discussion started: 17 August 2026

roughly 10^{-9}–10^{-3} kg, providing continuous measurements of fluxes, radiant distributions, and temporal variability on diurnal to solar-cycle timescales.

Multi-station video meteor networks (Jenniskens et al., 2011; Vida et al., 2020) – including CAMS (Jenniskens et al., 2011), SonotaCo (SonotaCo, 2009), EDMOND (Koseki, 2019), FRIPON (Colas et al., 2020), DFN (Devillepoix et al., 2020), MOROI (Nedelcu et al., 2018) and the Global Meteor Network (GMN) (Vida et al., 2020) – constrain the flux and orbital distribution of millimetre- to centimetre-sized meteoroids, corresponding approximately to masses of 10^{-7}–10^{-2} kg, with high astrometric and photometric precision. GMN, which now deploys hundreds of low-cost CMOS cameras worldwide, provides long-term global monitoring of radiants, fluxes, and size distributions through an open-source pipeline (Vida et al., 2020; Vida et al., 2022).

For larger meteoroids, satellite and ground-based bolide observations, complemented by infrasound and seismic detections, constrain the flux of decimetre- to multi-metre objects. Brown et al. (2002) showed that 1–10 m objects follow a cumulative power law that smoothly extends the near-Earth object distribution, anchoring the high-mass tail. Subsequent multi-sensor analyses have refined entry frequencies and detection thresholds (Ens et al., 2012), and well-observed events allow optical impact-energy measurements to provide the best constraints on decimetre-scale impactors (Anghel et al., 2021). Across techniques, advances in CCD/CMOS sensors and machine-learning–based event detection (Galindo and Lorena, 2018; Gural, 2020; Anghel et al., 2023) have substantially improved data fidelity, and recent cross-method analyses show that the next improvements would come from applying novel machine learning to model the physical properties of such impacts (Anghel, 2026).

Figure 10 shows the radiant distribution measured by these video networks, colour-coded by geocentric velocity. The high-velocity radiants clustered trace retrograde Halley-type and long-period cometary populations, while the lower-velocity populations concentrated along the ecliptic reflect prograde, low-inclination orbits typical of Jupiter-family comet and asteroidal parent bodies (Wiegert et al., 2009; Nesvorný et al., 2010). The latter supposedly being the same dynamical reservoirs that feed the bound meteoroid population probed in-situ by PSP and SolO (see Sect. 4.1.3).

These Earth-based observations confirm that the meteoroid flux exhibits genuine temporal variability, driven by meteor showers, sporadic source variations, and changes in parent small-body populations. Establishing a quantitative link between fluxes inferred from spacecraft measurements in the inner heliosphere and those from meteor, bolide, and cosmic-dust influx observations therefore remains a key step towards a unified description of the Zodiacal dust and meteoroid environment across the entire mass range.

4.1.3 Forces and Trajectories: Distinguishing Dust Populations

Interplanetary dust grains are mainly influenced by solar gravitation, solar radiation pressure, and the Lorentz force (Morfill and Grün, 1979; Leinert et al., 1978; Burns et al., 1979). As gravitation and radiation pressure both scale as $1/r^2$, with distance r from the Sun, their ratio β is independent of heliocentric distance (Burns et al., 1979). The β depends on the light scattering properties of the grain, and with this on properties like composition, density, size, shape (Wilck and Mann, 1996; Kimura and Mann, 1998b; Kolokolova et al., 2006). Grains who are pushed on hyperbolic orbits by the outward directed radiation pressure

https://doi.org/10.5194/egusphere-2026-4440
Preprint. Discussion started: 17 August 2026

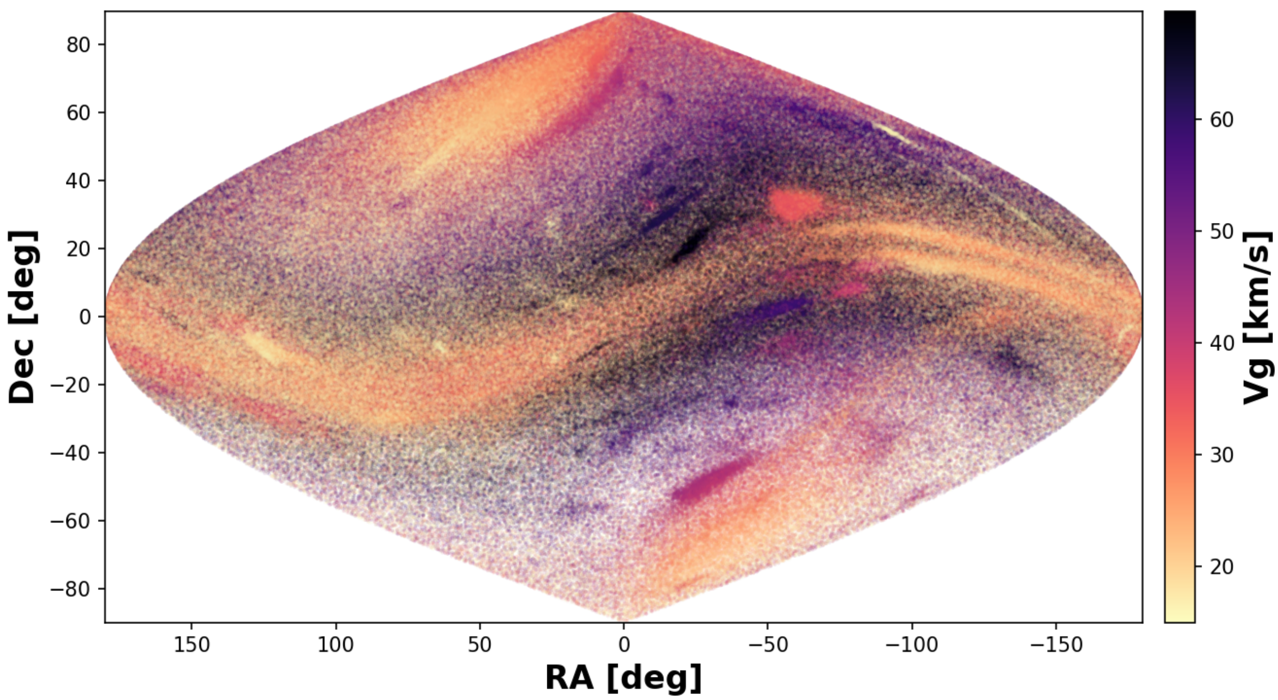

Figure 10. Radiants of measured meteoroid impacts onto Earth plotted in equatorial coordinates. Each point shows the apparent radiant of a meteor in right ascension and declination, projected using a sinusoidal (equal–area) projection and coloured by its geocentric velocity ν_{G} (colour bar on the right). The map combines multi-station orbits from all networks over the period 2007–2024 (data from the IAU Meteor Data Center video database; Porubcan and Jopek, 2015) and reveals the established meteor showers and sporadic background sources sampled by the global video networks. The background data are available on the International Astronomical Union – Meteor Data Center[2]

force are often denoted as β-meteoroids(Berg and Grün, 1973); their typical size range is around ~ 100's nm. The Lorentz force depends on the charge and the motion of a grain relative to the interplanetary magnetic field (Morfill and Grün, 1979). The total surface charge of a grain in the interplanetary medium depends on the composition and over most sizes considered here increases linearly with the size of the grains (Kimura and Mann, 1998; Mann et al., 2014). In result, the charge to mass ratio scales with size s like $1/s^2$, so the Lorentz force has a strong effect on nanodust – i.e. grains of sizes around 10 nm or less. Depending on which of the forces has a major effect one can note characteristics in the fluxes distinguishing dust in bound orbits, β-meteoroids and nanodust.

Bound dust particles for which ($\beta \ll 1$) follow Keplerian elliptical orbits. The bound orbits lose orbital angular momentum due to Poynting-Robertson (e.g. Burns et al., 1979) and solar wind drags (Minato et al., 2004); they approach the Sun over thousands to millions of years or shorter (Burns et al., 1979). Zodiacal light is predominantly produced by these gravitationally bound particles. Note that some works use the terminology "α-meteoroids" to refer to the entire dynamical class of gravitationally bound dust grains (e.g. Szalay et al., 2021; Malaspina et al., 2022; Zaslavsky et al., 2021; Szalay et al., 2024; Szalay et al.,

https://doi.org/10.5194/egusphere-2026-4440
Preprint. Discussion started: 17 August 2026

2025) – although this terminology was historically introduced to refer to a specific category of bound grains on very eccentric orbits (cf. Sommer (2023) for a detailed discussion). This use has the advantage of unambiguously defining α-meteoroids on intrinsic dynamical properties, and allows for simple grouping between α (bound) and β (unbound) meteoroids. Therefore, in this review, α-meteoroids (when used for instance in Section 4.3), corresponds to "dust on bound orbits".

Dust in hyperbolic orbits, i.e. β-meteoroidsexist in the heliosphere in considerable amounts, even though for most interplanetary grains gravitational force exceeds radiation pressure. They form as a result of the collisional fragmentation. When collisions between large grains produce smaller fragments, those have the specific kinetic energy of the initial grain but less potential energy than before the collision, since they are subject to stronger repelling radiation pressure force. Hence, depending on their initial speed the orbits of grains with ($0.5 \leq \beta \leq 1$) can become hyperbolic.

Nanodust, i.e. grains with sizes of about 10 nm, are strongly affected by the Lorentz force. The dynamics of nanodust in the interplanetary magnetic field result in complex trajectories or pickup-ion-like entrainment in the solar wind (Morfill et al., 1986; Czechowski and Mann, 2010; Schwadron and Gloeckler, 2007; Poppe and Lee, 2020, 2022). The effects of electromagnetic forces, also notably change the orbital planes of the nanodust with respect to the one of their parent bodies. It is worth noting that the effect of gravitation and radiation pressure keeps the orbital plane unchanged, implying that dust in bound orbits share a similar three-dimensional distribution to their parent objects, which leads to the Zodiacal cloud being concentrated to the ecliptic.

One can show that grains in circular orbits that move to the Sun due to the Poynting - Robertson drag would form a cloud with number density increasing closer to the Sun, proportional to the solar distance raised to the power of -1 for circular orbits (Leinert et al., 1976) and an exponent close to 1 is indeed consistent with Zodiacal light observations. This is however not the full picture because most of the bound dust present at 1 au experiences at least one collision before reaching the vicinity of the Sun where sublimation becomes effective (e.g. Mann et al., 2004; Mann and Czechowski, 2005). Model calculations of the collision evolution have shown that in order to describe the dust cloud with the mass distribution from the interplanetary dust flux model at 1 au ((Grün et al., 1985)) and the Zodiacal cloud model increase with distance raised to the power of -1 (Leinert et al., 1976) is only possible by assuming additional dust production, e.g. from meteoroids inside 1 au (Ishimoto and Mann, 1998).

While its is helpful to distinguish these three components of the interplanetary dust cloud, they are overlapping and conditions may be different locally and for individual grains. A fourth, but distinct component comprises the interstellar dust grains that stream into the heliosphere from the direction of the Sun's motion toward the galactic apex.

4.2 Zodiacal cloud structure derived from brightness observations

The Zodiacal light brightness arises from sunlight scattering and thermal emission by dust particles; most observations of the dust cloud inside Earth orbit are in visible wavelengths. The Zodiacal light extends from close to the Sun into the solar corona and to 1 au and beyond (Stenborg et al., 2022, 2024; Leinert et al., 1981; Kimura and Mann, 1998a). The white light corona consists of dust-scattered light (F-corona) and Thomson scattering by electrons (K-corona); the components are separated using polarization models using the fact that Thomson scattering varies strongly by polarization (Koutchmy and Lamy, 1985;

https://doi.org/10.5194/egusphere-2026-4440
Preprint. Discussion started: 17 August 2026

Hayes et al., 2001). A further ambiguity (aside from the F - and K - corona separation) arises from the fact that the observations provide integrated brightness along the line of sight, which is influenced by the number density and the scattering properties of grains along the line of sight (Mann et al., 2004).

From space, the structure of the Zodiacal cloud inside 1 au (Figure 11) has been studied extensively from instruments onboard five missions - the Skylab White Light Coronagraph (1973–1974) (Ise and Cagle, 1974; MacQueen et al., 1974), the Helios Zodiacal Light Photometer (1974–1984) (Porsche, 1981; Leinert et al., 1981), the Clementine Star Tracker Camera (1994) (Nozette et al., 1994; Hahn et al., 2002), the STEREO Sun Earth Connection Coronal and Heliospheric Imager (SECCHI) (2007–present) (Kaiser et al., 2008; Howard et al., 2008) and the Wide Field Imager for the Solar Probe (WISPR) (Vourlidas et al., 2016) on board the Parker Solar Probe.

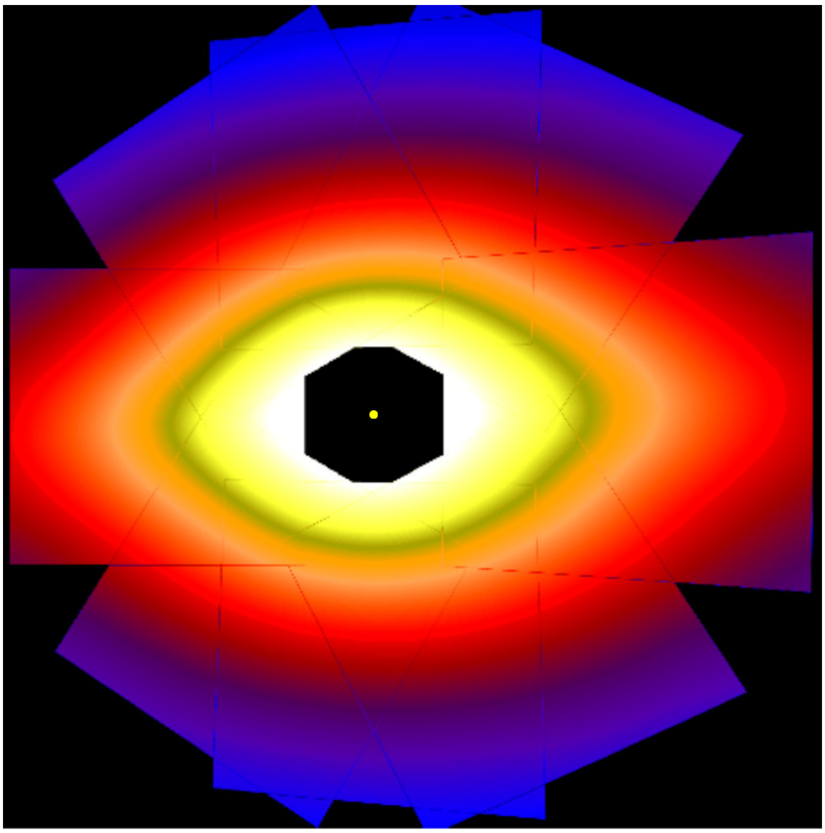

Figure 11. The Zodiacal Light from 0.07–0.39 au ($15-84\,R_\odot$). Constructed using 8 images from the STEREO-A SECCHI-HI1 instrument taken during a 360° calibration roll. The position and size of the Sun are represented by the yellow circle in the center. The color differences reveal a decrease in intensity within the super-elliptical intensity structure of the Zodiacal Light. The boundaries of the images can be seen as dark lines due to the motion of the spacecraft in its orbit around the Sun, and thus viewing the scene from a slightly different point in space. Reproduced from Stenborg et al. (2018), © AAS. Reproduced with permission.

https://doi.org/10.5194/egusphere-2026-4440
Preprint. Discussion started: 17 August 2026

Before the launch of Parker Solar Probe, only the Helios missions enabled studies of the Zodiacal light with optical measurements at distances inside 1 au. The Helios Zodiacal Light Photometer, ZLP, consisted of three photometers, which scanned the sky at ecliptic latitudes of 16°, 31°, and 90°. The photometers on the two spacecraft thus scanned different hemispheres and reached a minimum distance to the Sun of about 0.09 au (or 20 $R_\odot$) (Leinert et al., 1980). They showed that the Zodiacal light had a plane of symmetry located at an inclination of 3.0° and an ascending node of 87° in ecliptic longitude. Photometry of the Zodiacal light was quite stable for observer locations between 0.3 and 1.0 au (Leinert et al., 1981; Leinert and Blanck, 1982; Leinert et al., 1982) with the intensity on the symmetry axis as a function of heliocentric distance following I(R) $\approx R^{-2.3\pm0.05}$. The upper and lower limits were the deviations they found for large and small elongations, respectively, from the Sun.

At 1 au, the Clementine observations (Hahn et al., 2002) provided a number of interesting results for the short mission lifetime. The Clementine star tracker camera had a field of view of $29.3°$ x $44.5°$. The CCD detector was a 2D array of 384 x 576 pixels, giving a plate scale of $0.0756°/\mathrm{pixel}$ The surface brightness was similar to that of the Helios mission, $\approx R^{-2.45\pm0.05}$, a little steeper than that of Helios. They also found asymmetries in both east-west and north-south directions on the order of $\approx 10\%$.

With STEREO starting in 2006, images from SECCHI-HI1 (Howard et al., 2008; Eyles et al., 2009) were used to perform a detailed study of the Zodiacal light inside 1 au; Figure 11 reveals the Zodiacal light pattern at 0.07–0.39 au distance from the Sun. The results were reported in a series of papers (Stenborg and Howard, 2017b, a; Stenborg et al., 2018; Stauffer et al., 2018). The nearly 6 years of SECCHI data confirmed models from Helios of the surface of symmetry, only adding a decimal point. The inclination was $\approx 3.7°$, and the ecliptic longitude of the ascending node was $\approx 83°$. However, further inward at about $11° - 14°$ both the inclination and the ascending node, respectively, start to evolve to $6°$ and $\approx 57°$ at $5°$, the inner limit of the HI1 FOV. In addition, the center of symmetry was shifted to $\approx 0.5\,R_\odot$ to the side of the hemisphere containing Jupiter.

The slope of the radial gradient of the axis of symmetry found by SECCHI-HI1 is -2.315 for the entire range of elongations, $5° - 24°$, with a standard deviation of 0.002 (Stenborg et al., 2018). The Helios data had indicated that the slope increased toward the Sun, and SECCHI-HI1 showed the same effect - for three increasing elongation regions, $5° - 14°$, $9° - 18°$, and $14° - 24°$, the slopes were -2.41, -2.31, and -2.18 (Stenborg et al., 2018). As also seen in the Helios data, the intensity profiles are symmetric about the ascending node. The SECCHI-HI1 data showed (Stenborg et al., 2018; Stauffer et al., 2018) that the shape of the Zodiacal light contours (defined by the flattening index (Koutchmy and Lamy, 1985)) could be well described by a super-ellipse function with exponents ranging from about 1.53–1.64 and then 2 close to the Sun (Saito et al., 1977). The flattening of the Zodiacal light in the north and south hemispheres exhibited a periodicity (Stauffer et al., 2018) and showed that the Zodiacal light intensities in the north and south were asymmetric when the observer was at the maximum north and south inclinations of the ecliptic plane compared to when they were at the ascending and descending nodes.

With Parker Solar Probe, WISPR observations from distances down to 0.336 au found brightness profiles that matched those from earlier missions (Howard et al., 2019), whereas, for observer distances below that point, they showed a dependence on observer position. Parker orbits 10–16 all had the same orbital parameters, including the perihelion distance: the range of heliocentric distances was 0.25 au down to 0.0617 au ($\approx 53.78 - 13.28\,R_\odot$) and the range of heliocentric longitudes was $20° - 270°$. Figure 12 shows the evolution of the Symmetry Axis (SA) determined for all of the data for the seven perihelion

https://doi.org/10.5194/egusphere-2026-4440
Preprint. Discussion started: 17 August 2026

passes for two Lines of Sight (LOS) (Stenborg et al., 2024). The LOS are $54.7°$ for the left plot and $100.8°$ for the right one. Plotted along with the SA location are the orbits of Venus and Jupiter. Note that for both plots, the SA is close to the JOP for the inbound part of the orbit, but the outbound SA separates from the JOP and for the LOS closer to the Sun clearly approaches the VOP. The SA are very dependent on the observer position. It was suggested that these variations are probably due to a combination of the barycenter location, the gravitational effects of Jupiter, and the inclination variation of PSP's orbit (Stenborg et al., 2024).

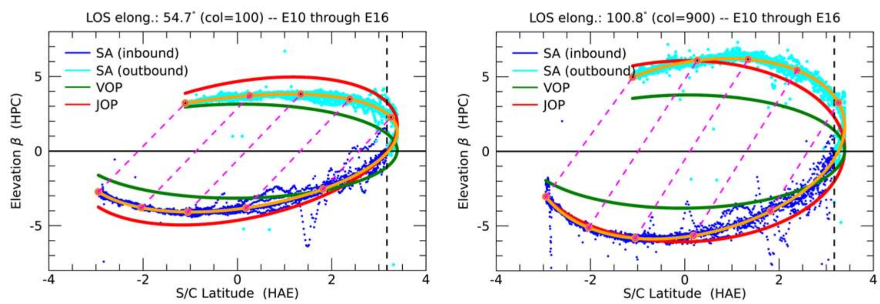

Figure 12. Elevation of various features in the HPC system as a function of spacecraft helioecliptic latitude (HAE) for two selected Lines of Sight (LOS) in WISPR-O ($54.7°$ and $100.8°$). The four features are the measurements of the symmetry axis (SA) inbound (in blue) and outbound (in light blue), and the projections of the Jupiter and Venus orbits (JOP in red and VOP in green, respectively). The orange line delineates a fifth-degree polynomial fit to the measurements of the location of the SA at the corresponding LOS. The black line at 0° elevation delineates the projection of the solar equator. The dashed pink lines in the bottom right panel connect locations in the inbound and outbound segments at equal heliocentric distances (namely, at [0.25, 0.15, 0.11, 0.085, 0.068] au). The encounters start at the lower left and proceed counterclockwise around the plots. The odd excursions in the SA are due to planets or dust streaks in the images throughout an encounter.

From an analysis of the east-west asymmetry of the zodiacal light brightness, Stenborg and Howard (2017a) found that the center of the Zodiacal cloud in the SECCHI-HI1 analyses from 2007–2014 was shifted away from Sun center to $\approx 0.5\,R_\odot$ in the direction of Jupiter. At that time the barycenter varied between $0.8-1\,R_\odot$ in comparison to its location from 2021 to 2023 during orbital encounters E10 to E16 of the Parker Solar Probe mission, when the barycenter was located at $2.0\,R_\odot$ from the Sun center. Also, the inbound segment of the encounters was on the opposite side of the Sun to the barycenter and the outbound segment was on the same side of the Sun as the barycenter (Stenborg et al., 2024). The left panel of Figure 13 gives the relative brightnesses of the two segments in each orbit. The radial profiles have been divided into four segments of different distance ranges: $30-50\,R_\odot$, $50-70\,R_\odot$, $70-90\,R_\odot$ and $90-105\,R_\odot$, with solid lines being inbound and dashed lines being outbound. The inbound segments, indicated by the solid lines, show a $2-3\%$ increase over the normalized median brightness for each perihelion pass, while the outbound segments, dashed lines, are, initially, $2-3\%$ dimmer for the first 3 passes. But then the median brightness decreases with a steady rate, which was shown to be consistent with the motion of Jupiter away from the barycenter (Stenborg et al., 2024), illustrating the significant effects the planets have on the zodiacal dust cloud.

https://doi.org/10.5194/egusphere-2026-4440
Preprint. Discussion started: 17 August 2026

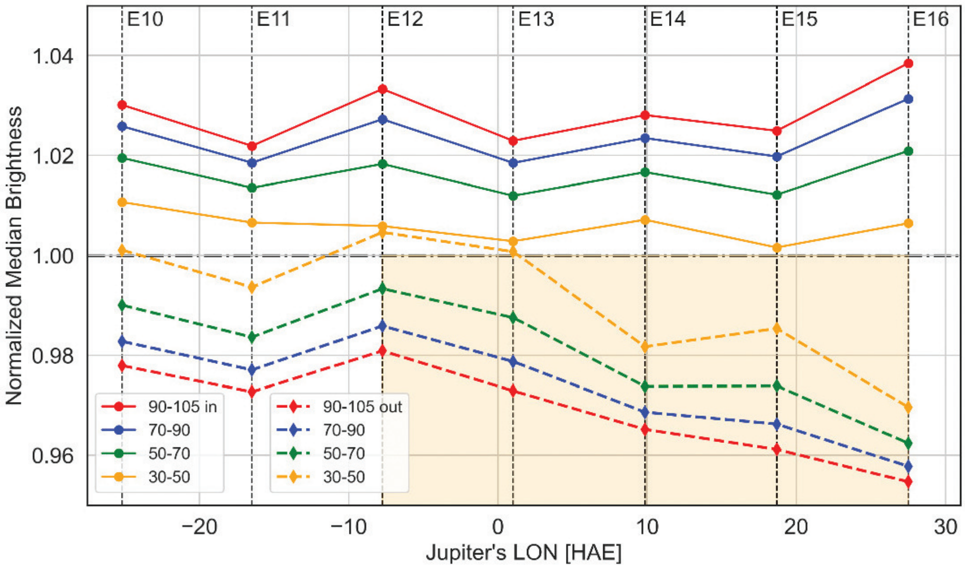

Figure 13. Normalized median brightness per encounter and segment in selected elongation distance ranges (as specified in the inset labels). The colored circles (diamonds) depict the median brightness values in the inbound (outbound) segment of the PSP encounters. The brightness trend in the different elongation distance ranges, for the inbound and outbound segments, are delineated with the colored solid and dashed lines, respectively. Reproduced from Stenborg et al. (2024), © AAS. Reproduced with permission.

4.3 Constraints from in-situ observations

The previous section discussed the dust cloud structure inferred from remote sensing, and in particular from the analysis of white light images. A complementary view is reached from in-situ detection of interplanetary dust by using dedicated dust detectors or electric field instruments, which measure signals when a hyper-velocity impact occurs on a spacecraft (see Sec. 3 of this review for a detailed description of such measurements).

Four spacecraft have probed the inner zodiacal dust cloud in the past 20 years (STEREO, Wind, Solar Orbiter, and Parker Solar Probe) and observed the Zodiacal cloud by detecting dust impacts with antenna measurements.

In this section, we focus on in-situ measurements of dust in bound orbits and β-meteoroids performed by these spacecraft – in-situ measurements of nano-sized grains and of dust of interstellar origin are covered in the forthcoming sections 4.6 and 4.7 of this review.

4.3.1 β-meteoroids

The β-meteoroid population was previously characterized with the few sparse flux estimates obtained from the data of the in-situ dust analyzers aboard Pioneers 8 & 9 (Berg and Grün, 1973; Grün et al., 1985) and Ulysses (Wehry and Mann, 1999). While those observations were performed with dedicated dust instrumentation, they had limited statistics due to the smaller

https://doi.org/10.5194/egusphere-2026-4440
Preprint. Discussion started: 17 August 2026

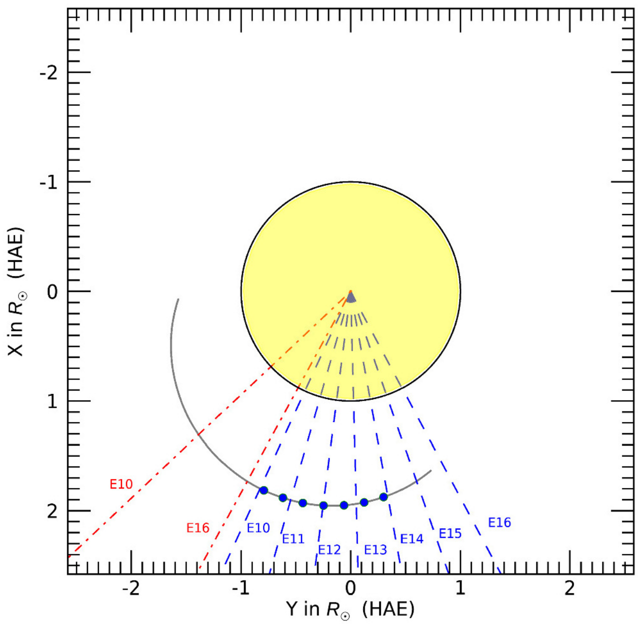

Figure 14. Positions of the solar system barycenter, Jupiter, and Saturn during the 10-day Parker solar encounters, E10–E16. The Sun is the yellow circle. The positions of the barycenter are indicated by the blue dots, about $1\,R_\odot$ from the solar limb. The blue and red dashed lines indicate the direction toward the positions of Jupiter and Saturn, respectively. Reproduced from Stenborg et al. (2024), © AAS. Reproduced with permission.

effective areas on these instruments compared to antenna-based measurements. In the past 20 years, β-meteoroids fluxes have been measured by various spacecraft at and within 1 au from the Sun via antenna measurements, which, while more challenging to interpret than dedicated dust observations, leverage the large effective area of the spacecraft to enable improved count rates and associated statistical uncertainties.

These results, summarized in Figure15, demonstrate good overall agreement with the Grün interplanetary dust flux model (Grün et al., 1985).

At 1 au, an analysis of STEREO/WAVES data over the period 2007–2011 provided a flux of $1-6\times10^{-5}$ m^{-2}s^{-1} for grains in the 100–300 nm range (10^{-17} to 5×10^{-16} kg) (Zaslavsky et al., 2012); a β-meteoroids flux of 4.3×10^{-5} m^{-2}s^{-1} was also obtained as a by-product an interstellar dust flux evaluation by S/WAVES (Belheouane et al., 2012). A subsequent study by Malaspina et al. (2015), extending the analysis to 2014 and taking into account later measurements of impact ionization charge yield on STEREO cover provided a similar value of $3-7\times10^{-5}$ m^{-2}s^{-1} for particles with mass $\gtrsim 8\times10^{-18}$ kg. At 1 au, Wind/WAVES reported an interplanetary flux of $2.7\pm1.4\times10^{-5}$ m^{-2}s^{-1} for grains roughly $0.3-1$ μm (not only β-meteoroids , but with a dominant contribution from them) in size (Malaspina et al., 2014).

https://doi.org/10.5194/egusphere-2026-4440
Preprint. Discussion started: 17 August 2026

The eccentric orbits of SolO and PSP made it possible to scan the β-meteoroids flux densities radial distance to the Sun within 1 au, showing in both cases radial profiles approximately following $1/v_\beta r^2$, consistent with flux conservation where grains having an approximately constant radial velocity v_β outside a few 10's of solar radii (Szalay et al., 2020; Mann and Czechowski, 2020; Malaspina et al., 2020; Zaslavsky et al., 2021). The flux density measured by the RPW instrument aboard SolO was first estimated at $8\times10^{-5}\mathrm{m}^{-2}\mathrm{s}^{-1}$ for particles about $\gtrsim 100$ nm (Zaslavsky et al., 2021), before being refined by a Bayesian modeling to $1.1\pm0.2\times10^{-4}\ \ \mathrm{m}^{-2}\mathrm{s}^{-1}$ (Kočiščák et al., 2023). The flux measured by the FIELDS instrument aboard PSP, interpolated 1 au, was estimated at $4-8\times10^{-5}\ \mathrm{m}^{-2}\mathrm{s}^{-1}$ (Szalay et al., 2021) during the first two years of the mission, consistent with analyses of further three years of measurements (Kočiščák et al., 2024). Overall, SolO measures higher fluxes than the other spacecraft, with comparisons to PSP under similar orbital conditions showing a systematic factor of 2–3 difference (Kočiščák et al., 2024). This is likely because SolO detects smaller dust, with its RPW instrument's voltage pulse (3.1) lower bound threshold of ~ 3 mV set about 10 times lower than that of STEREO or PSP. The PSP threshold is set high to exclude frequently high amplitude plasma waves observed closer to the Sun (Malaspina et al., 2023).

Additional constraints on β-meteoroids have recently been obtained using a dedicated dust detector. Preliminary results from the ASTERISC 3U CubeSat mission (Ishimaru et al., under review) provide measurements of β-meteoroids near 1 AU. The spacecraft carries a deployable polyimide-film dust detector instrumented with piezoelectric transducer sensors that detect elastic waves generated by impacts of dust particles. Impact signal amplitudes provide estimates of impact momentum, which are consistent with an origin through collisional fragmentation of larger parent bodies. Assuming production interior to Earth's orbit, the inferred particle masses and the observed flux are broadly consistent, within uncertainties, with those derived from Parker Solar Probe observations.

The difference in the impact rates on SolO when the spacecraft was going in the sunward and anti-sunward directions enabled a direct determination of the radial velocity of the β-meteoroids in a range of distance to the Sun of 0.5–1 au, which yielded a value of 63 ± 7 km s^{-1} (Zaslavsky et al., 2021; Kočiščák et al., 2023) – cf. Figure 16, consistent with grains having a ratio of radiation pressure to gravitational forces $\beta\simeq0.6$, and created by fragmentation of larger grains between 0.05 and 0.1 au.

Solar Orbiter also provided estimations of the β-meteoroids cumulative flux power-law index between 0.3 and 1 au. This was made through two methods: either by making power-law fittings of the distributions of the measured impact voltages, or by assuming cumulative fluxes of the form $F(m>m_0)=F_0(m/m_0)^{-\delta}$, and fitting the impact rates along the eccentric orbits of these spacecraft. The two methods provided a consistent value of $\delta\simeq0.3-0.4$ (Zaslavsky et al., 2021).

4.3.2 Dust in bound orbits

For most of PSP's and SolO's orbits so far, bound dust – or α-meteoroids as they are broadly referred to in SolO and PSP litterature – is not the main contributor to impact rates but must be considered to explain variations, and becomes more important especially near PSP's perihelia: under the assumption that the bound orbits dust population is entirely on circular prograde orbits, the impact rate on PSP is nearly completely due to bound dust during a few days period after perihelion (Szalay et al., 2024), as illustrated by Figure 17. This feature was used to determine the power exponent of the cumulative flux of dust on circular orbits at 0.1–0.25 au from the Sun. By fitting of the voltage distributions observed during the α-dominated intervals, a

https://doi.org/10.5194/egusphere-2026-4440
Preprint. Discussion started: 17 August 2026

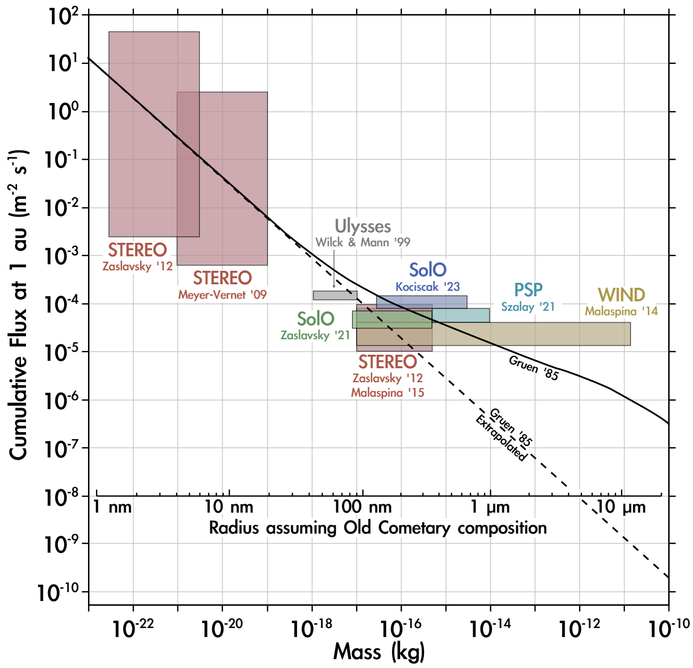

Figure 15. Comparison of measurements of β-meteoroids fluxes with different spacecraft. PSP and SolO fluxes are rescaled to 1 au. Wind measurements not only include β-meteoroids . Two crosses at small masses indicate STEREO measurements of nanodust. The interplanetary dust flux model of Grün et al. (1985) is represented as a solid black line, and its interpolation as a power law represented by a dashed line.

power-law exponent $\delta = 1.1 \pm 0.3$ was obtained for dust of size $\sim 0.6 - 1.4$ μm within 0.25 au, and $\delta = 1.3 \pm 0.2$ at distances smaller than 0.15 au (Szalay et al., 2024) – an interesting result which implies that close to the Sun, the mass of the dust cloud is mainly contained in small fragments (rather than in large ones when $\delta < 1$, as is usually observed). Using another method, i.e., fitting the impact rate curves along the trajectory of PSP and assuming a composite model of α and β-meteoroids, a smaller power exponent was found, $\delta \sim 0.15 - 0.4$, for the bound dust population between 0.15 and 0.5 au (Kočiščák et al., 2024). This apparent inconsistency may be due to an evolution of δ with distance from the Sun, and to slightly different assumptions on the bound dust dynamics.

PSP results between 0.15 and 0.5 au also made it possible to infer the number density radial slope for dust in bound orbits, assuming $n(r) \propto r^{-\gamma}$. The study gave $-2 < \gamma < -1$ (Kočiščák et al., 2024), consistent with expected values for bound dust (Ishimoto and Mann, 1998), and more specifically with the value of $\gamma = 1.3$ reported from Helios and PSP measurements of the zodiacal light (Leinert et al., 1981; Stenborg et al., 2021), and cf. Section 4.2. Additionally, multiple telescopes on the PSP ISOIS instrument were punctured by dust impacts. Using the location and pointing of these punctures, a data-model comparison was performed to independently estimate the density of dust in bound orbits in the inner solar system, consistent with the FIELDS-based constraints (Shen et al., 2025).

https://doi.org/10.5194/egusphere-2026-4440
Preprint. Discussion started: 17 August 2026

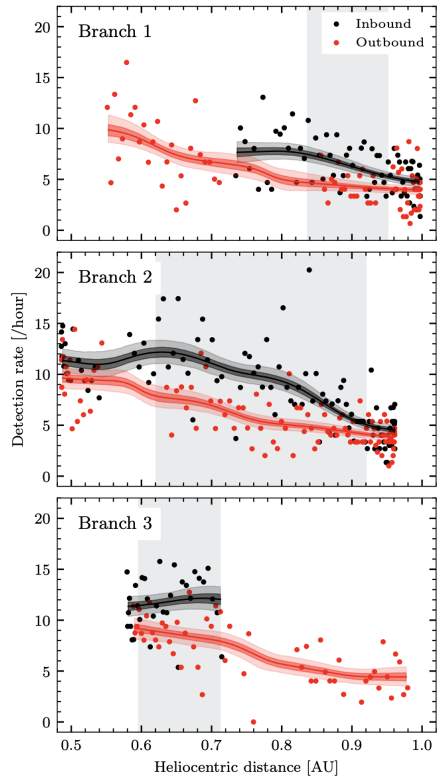

Figure 16. Dust detection rate observed by SolO RPW/TDS between June 29, 2020 and November 27, 2021 in the inbound (grey) and outbound (red) parts of the trajectory, with branches being separated by Venus gravity assists on December 26, 2020 and August 8, 2021. The lines are the results of non- parametric fitting. The differences in outbound and inbound impact rates arise from the non-zero radial velocity of the measured dust population. Reproduced from Kočiščák et al. (2023)

We finally mention the systematic decrease or "dip" in the dust impact rate onto PSP that was observed around nearly every close perihelion of the spacecraft (Szalay et al., 2021; Malaspina et al., 2023; Kočiščák et al., 2024), which can be seen on panel (a) of Figure 17. It can be attributed to the velocity alignment of PSP velocity vector with the prograde bound dust; a model assuming that the α-meteoroids population all have circular orbits indeed predicts the observation of a dip which can be well fitted to the data (Szalay et al., 2021). On the other hand, it was shown that including a spread in the eccentricities or inclinations of the grains' orbits reduces or even completely smears this dip (Kočiščák et al., 2024). Other explanations are needed to explain this decrease in the impact rate. Possibilities include a decrease in PSP's detection efficiency within 0.15 au or a physical decrease in the dust density, may be linked to the dust depletion zone observed in white light (Stenborg et al., 2021).

https://doi.org/10.5194/egusphere-2026-4440
Preprint. Discussion started: 17 August 2026

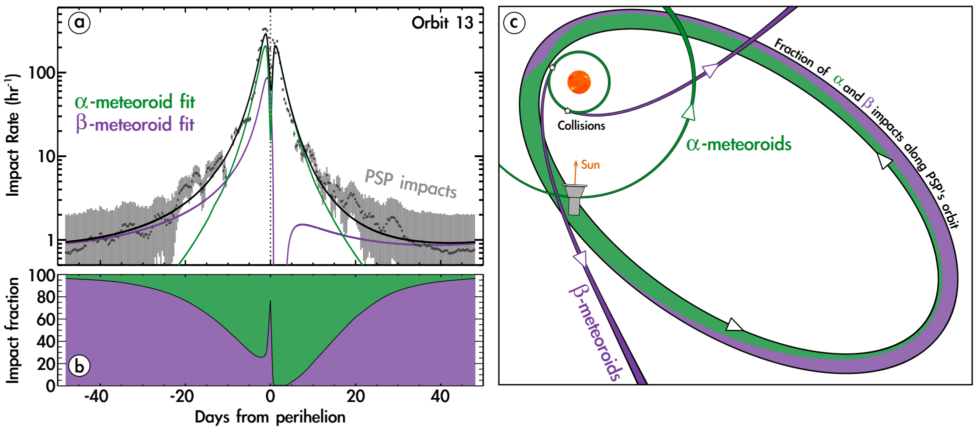

Figure 17. (a) Impact rate from PSP/FIELDS, representative of encounters 10–16, along with modeled abundances of bound dust and β-meteoroids, from a 2 compenent best fit to the data (Szalay et al., 2021). (b) Fractional contribution of bound dust and β-meteoroids to total modeled impact rate. (c) Same information as panel (b) shown in the ecliptic J2000 x-y plane with example circular and hyperbolic orbits. Adapted from Szalay et al. (2024), © AAS. Reproduced with permission.

4.3.3 Variability, streams and collisional evolution

The values of the fluxes presented in the previous paragraph are averaged over long time periods – months, or even years or decades in the case of STEREO and Wind. But the impact rates present variations on relatively small timescales, which overcome by far variations due to counting statistics. Typically, PSP observes a $\sim 50\%$ variability in dust densities (Malaspina et al., 2020; Szalay et al., 2025; Malaspina et al., 2025) on the timescale of its ~ 100-day orbits, corresponding to structures of size $\sim 10^5$ km. This variability exists in both the bound and unbound (β-meteoroids) populations, suggesting that the zodiacal cloud is internally structured on these small spatial scales (Szalay et al., 2025). These spatial fluctuations propagate to the very near-Sun environment via PR drag and may directly drive variability in the production of inner source pickup ions (Szalay et al., 2026a), providing a signature of the near-Sun dust environment that could be measured remotely from in-situ particle instruments (Schwadron and Gloeckler, 2007).

An example of such an enhancement in the β-meteoroids flux was found in a post-perihelion period after PSP's orbits 4 and 5 (Szalay et al., 2021; Pusack et al., 2021), at a location where PSP crosses Phaethon's orbit. Phaeton – the parent body of the Geminids meteoroid stream, which dust trail was also imaged by PSP's WISPR imager (Battams et al., 2020), had an estimated mass loss of $6 - 40$ kg s^{-1}, sufficient to produce the β-stream fluxes (impact rates of $0.1 - 30$ hr^{-1}) observed by PSP (Szalay et al., 2021). Furthermore, the location of the Geminids stream observed by WISPR (Battams et al., 2020; Battams et al., 2022) allowed for model comparisons on the formation of this stream (Battams et al., 2025), and revealed the Geminids may have been produced from a catastrophic breakup of its parent body (Cukier and Szalay, 2023).

Just as Phaethon, every airless body releases grains that populate the vicinity of its orbit, either due to cometary activity (Whipple, 1951), disruption (Knight et al., 2010), or to a lesser extent, impact ejection from zodiacal cloud impacts (Szalay

https://doi.org/10.5194/egusphere-2026-4440
Preprint. Discussion started: 17 August 2026

and Horányi, 2016). The more than 10^4 airless bodies that orbit the inner solar system and their associated dust trails could be at the origin of the observed dust variability and internal meteoroid and β-meteoroids streams observed in-situ. The remote observation of such streams is a complicated task, since a 50% density variation would only manifest as a $\sim 3\%$ variation in line-of-sight integrated brightness (Szalay et al., 2025), but a few in-situ stream detections have been documented for Helios (Krüger et al., 2020), Ulysses (Krüger et al., 2024), and Parker Solar Probe (Malaspina et al., 2025). Therefore, it can be anticipated that numerous meteoroid streams intersect the zodiacal cloud, which can erode the very local density distribution due to collisions (Steel and Elford, 1986).

Collisions are currently understood to be an important process eroding the zodiacal cloud, expelling ~100's kg/s (Szalay et al., 2021) to 10 tons/s (Grün et al., 1985) from the heliosphere via β-meteoroids. The high velocity collisions also generate considerable amounts of free molecules and atoms that are quickly dissociated and ionised by solar UV and deflected in the solar wind contributing to the inner source pick up ions in the solar wind (Mann and Czechowski, 2005; Schwadron and Gloeckler, 2007). The β-meteoroids fluxes values presented in this review have provided a bit lower estimates, ~100's kg/s for fluxes around $5 \times 10^{-5}\mathrm{m}^{-2}\mathrm{s}^{-1}$ of particles $\sim 10^{-17}$ kg – at least considering that the mass flux is dominated by smaller particles. However, the amount of mass loss by emission of β-meteoroids depends on the exponent of the β-meteoroids flux as a function of its mass, which is currently not very well constrained, and may also indicate a different collision rate than previous estimated (Pokorný et al., 2024). For values of $\delta < 1$, for instance assuming $\delta \sim 0.4$ (Zaslavsky et al., 2021) and a maximum mass of a β-meteoroid to be 10^{-15} kg, one finds a value of the mass loss rate 2.6 tons/s, more compatible with Grün et al. (1985). Anyhow, it must be noted that these numbers characterize only the collisional loss due to production of β-meteoroids , and, for this reason, constitute a lower bound on the actual collisional mass loss rate (Szalay et al., 2021).

4.4 Dust near the Sun: sublimation and dust free zone

The prediction (Russell, 1929) that there should be a transition from a space filled with dust to a dust free region around any star has generated many attempts to find it experimentally and theoretically. If the dust particles were SiO_2, then it was estimated (Over, 1958) they would be sublimated at $\approx 4\,R_\odot$. A summary was made by Mann et al. (2004) of the results of reported analyses of the sublimation distance of various species, as well as identifying other possible mechanisms for dust depletion. There were 28 reports from 1971–1992 of using IR emission to reveal the sublimation zones, but the results were evenly divided between detection and non-detection ((Mann et al., 2004) and references therein).

With the first orbit of Parker, WISPR-I observed a slight decrease in the brightness of the SA starting at $\approx 19\,R_\odot$ when the spacecraft was at 0.238 au and at an elongation of about 20° (Howard et al., 2019). The brightness continued to decrease steadily as the spacecraft approached perihelion at 0.166 (Stenborg et al., 2021). At the perihelion distance, the decrease extended to the inner limit of the field-of-view at $10\,R_\odot$. The brightness decrease was simulated with Raytrace (Thernisien, 2011) which performs forward modeling of brightness created by the distribution of the line-of-sight dust distribution. The density model used, was a simple linear decrease with radius from $19\,R_\odot$ down to $3\,R_\odot$. The result of that model is shown in Figure 18, where the blue line is the model results and the blue dots are the observations. Figure 9 of Stenborg et al. (2021)

https://doi.org/10.5194/egusphere-2026-4440
Preprint. Discussion started: 17 August 2026

shows the excellent agreement between the observations and the modeling. The impact of the dust depletion results in a slight change in the slope.

Later, using WISPR-O data for orbits 10–16, a nearly circumsolar sublimation zone was found by Stenborg et al. (2024), as shown in Figure 19, starting at $\approx 35\,R_\odot$ and increasing in brightness to a 4% peak at $25\,R_\odot$. The peak was followed by a smooth decrease in total brightness down to about $10\,R_\odot$. The variations in the curves below that point are due to K-corona structures, which become significant below $\approx 10\,R_\odot$. The Figure 19 shows all the data for the 7 orbital perihelia for both inbound and outbound segments. The range of longitudes being crossed during the 10-day period is $\approx 270°$, and there is no departure from the overall trend. The increased width of the blue profile for the outbound segment is due to the gravitational effect from Jupiter, as discussed in Figure 13.

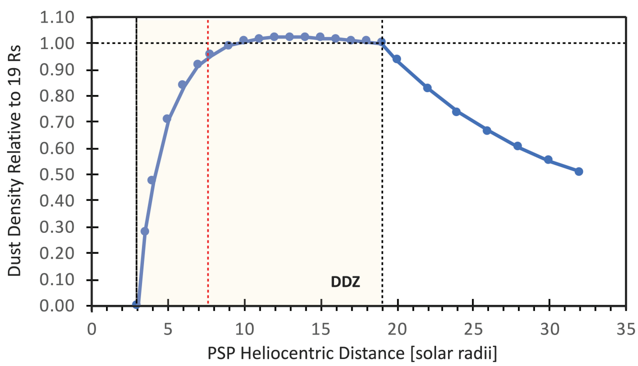

Figure 18. Forward modeling of the brightness of the dust depletion model inside $32R_\odot$. Shown is the ratio of the modeled brightness relative to the brightness at $19R_\odot$, the beginning of the dust depletion zone (DDZ label) assuming a linear dust density decease from $19R_\odot$ down to $3R_\odot$. The dashed, vertical line gives the innermost radial distance observed by the WISPR-I. Credit: Stenborg et al. (2021), reproduced with permission © ESO.

The implication of the brightness decrease is that the dust is being depleted continuously beginning at $25\,R_\odot$ in this dust depletion zone and is completely gone by $\approx 5\,R_\odot$, where the dust free zone begins. (Howard et al., 2019)), (Stenborg et al., 2021), and (Stenborg et al., 2022) all performed empirical calculations using the same dust depletion model that reduced the dust density by a linear factor from 1 at $19\,R_\odot$ down to 0 at $\approx 5\,R_\odot$ from the density at $19\,R_\odot$. The calculations could reproduce the radial brightness profile. The inner limit of $5\,R_\odot$ is not very firm and may depend on solar activity. They also noted that the dust sublimation ring was not seen in WISPR-I simply because the increase was followed by a decrease, which together obscured by the LOS integration, driving the start of the depletion region closer to the Sun, from $25\,R_\odot$ down to $19\,R_\odot$.

The very extended dust depletion region of $\approx 30\,R_\odot$ had been suggested earlier (Mann et al., 2004). Superimposed on that decline is an increase in the brightness for the first $10\,R_\odot$, consistent with the ideas of brightness enhancement caused by the sublimation process (e.g. Peterson, 1963; Kobayashi et al., 2009, and references therein).

https://doi.org/10.5194/egusphere-2026-4440
Preprint. Discussion started: 17 August 2026

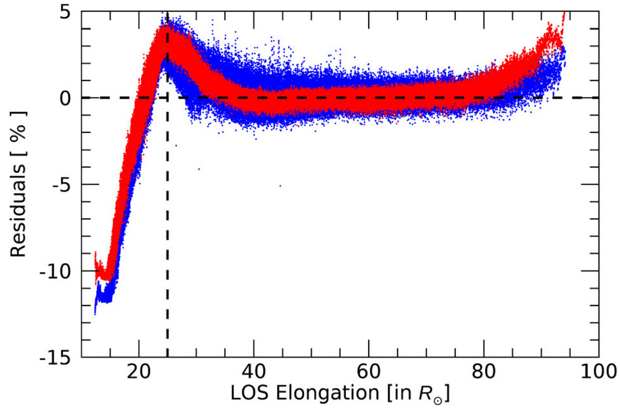

Figure 19. Ratio of the Observed to Background Modeled Brightness from Parker/WISPR-O. The red and blue dots show the 5σ filtered data from encounters 10–16 for the inbound and outbound segments, respectively, divided by the fifth percentile background model for each segment. The uptick at $\leq 10\,R_\odot$ is due to the presence of K-corona structures. Reproduced from Stenborg et al. (2024), © AAS. Reproduced with permission.

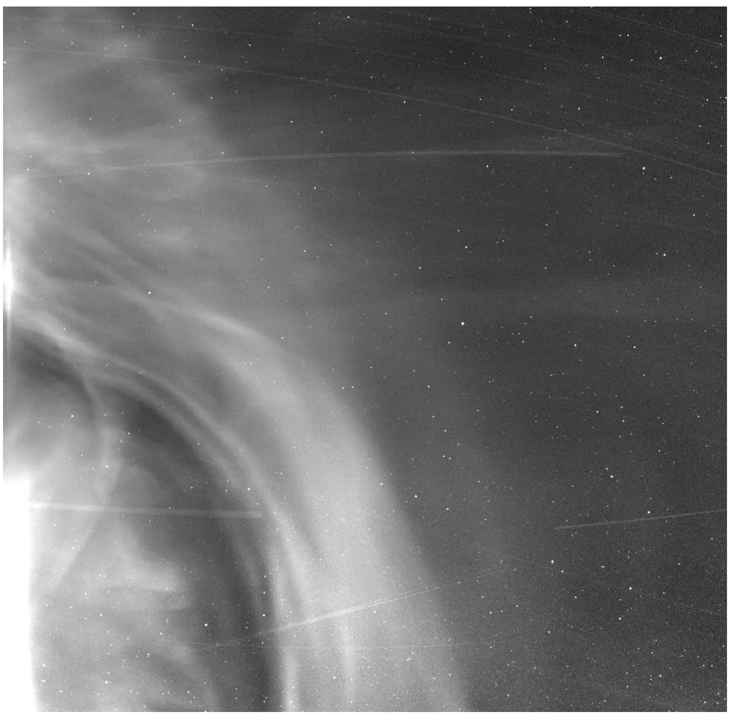

Figure 20. Image of the CME front as it was passing through the FOV of WISPR-Inner on 2022 Sep 9. It was a very complex, fast, and massive CME.

https://doi.org/10.5194/egusphere-2026-4440
Preprint. Discussion started: 17 August 2026

4.5 Interaction with solar wind structures

The influence of the solar wind in the interplanetary medium is evident in brightness observations of comet: the observation of a comet ion tail disruption led (Biermann, 1957), and reference therein, to suggest that there is a corpuscular stream of particles from the Sun. The tail was extending radially away from the comet nucleus, and observed disruption event was suggestive of plasma flowing radially and a magnetic field reconnecting with the ion tail. Many such disruption events of the plasma tail have been noted since (see review by (Voelzke, 2005)).

The influence of transient structures in the solar wind on dust particles has not often been observed in brightness measurements to date. Interactions of Coronal Mass Ejections (CMEs) with the dust tails of comets C/2006 P1 (McNaught) and comet C/2002 V1 (NEAT) have been reported in unpublished works (Lisse et al., 2003; Jones et al., 2004, 2008). In those observations, the tail is somewhat distorted. More recent brightness observations possibly show the influence of CME on the entire inner zodiacal cloud.

The Parker/WISPR instrument has observed the loss of dust behind a very fast and massive CME on 5 Sep 2022 (Stenborg et al., 2023; Paouris et al., 2023) during the orbit 13 perihelion. The first image of the CME is shown in Figure 20. The brightness evolution as the CME event is continuing outward is shown in three panels of Figure 21, with time proceeding left to right. The three panels, left to right, show the post-CME flow with energetic particles hitting the detector, the complete absence of electron scattering, and reduced dust scattering, leaving a clear view of the stars, and finally, the spacecraft is proceeding toward the boundary of the CME, depleting and viewing the undisturbed corona in the distance.

Figure 21. Evolution of the corona behind the 2024 Sep 05 CME. Time proceeds left to right. In the left panel, there is still a post-CME structure, which is virtually completely gone in the middle panel. In the third panel, the spacecraft is approaching the far boundary of the volume that the CME traveled through, as the brightness of the normal corona is starting to reappear. The explanation is that the CME swept up both the dust and electrons in its transit through the corona.

Dust depletion was identified when the radial brightness profile was lower than the F-corona model brightness profile. This is illustrated in Figure 22. The top panel shows the variations of the baseline brightness profiles from orbits 10 to 13, for heliocentric distances from 10 $R_\odot$ to 15 $R_\odot$.

https://doi.org/10.5194/egusphere-2026-4440
Preprint. Discussion started: 17 August 2026

The variation from orbit to orbit is due to the variation of the K-corona. The amount of dust along the LOS is greatly reduced by the location of Parker being close to the Sun, eliminating the dust from 1 au from the LOS. In addition, the reduction of dust in the Dust- Depletion Zone makes the contribution of the K-corona more significant.

The differences are quantitatively revealed in the lower panel of Figure 22, which gives the ratios for the same four orbits to the F-corona brightness model. The ratios give ranges from nearly 10% greater than the F model to about 2% lower than the model, indicating that the 5 Sep CME event in orbit 13, somehow swept out (or sputtered?) dust grains, in addition to the electrons. CMEs have been known to sweep up electrons, (e.g. Howard et al., 1985), but no evidence has been noted for sweeping up dust particles.

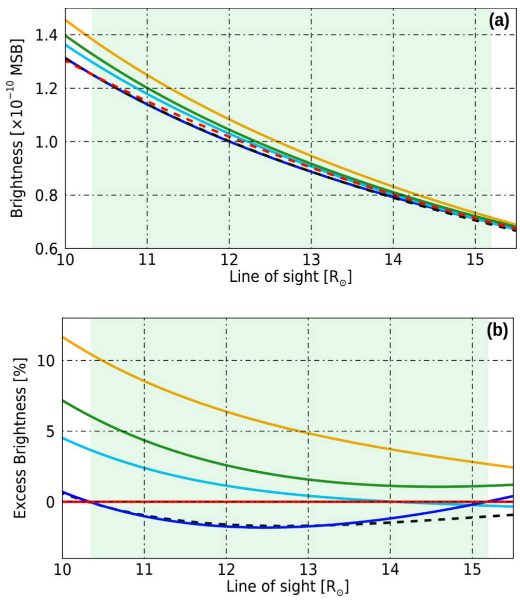

Figure 22. Coronal height evolution of the baseline brightness level for E10 (orange), E11 (light blue), E12 (green), E13 (dark blue), Background for E10 to E13 (dashed black line), and the baseline of the modeled F-corona (dashed red line). Note that the background model E10 to E13 is overlaid with the E13 from 10 $R_\odot$ up to about 14 $R_\odot$. The x-axis is restricted to the heights where the E13 brightness drops below the model F-corona to allow for a direct comparison among the sets. (b) The same data as in (1) plotted as percentage excess ratios. The color code is the same as in panel (a). The E13 minimum brightness is about 2% lower than the modeled F-corona baseline level in the 11 to 14 $R_\odot$ range. Reproduced from Stenborg et al. (2023), © AAS. Reproduced with permission.

Previously, Ragot and Kahler (2003) had reported on the possibility of a CME reducing the dust density in the volume it traversed through. But the mechanism proposed by these authors – scattering to higher latitude orbits by the action of the strong transient magnetic field of the CME on dust smaller than around 3 μm is efficient much closer to the Sun (at $4-5$ $R_\odot$) than these observations and would have moved the dust to higher or lower latitudes instead of just having removed the dust as it appears on the white light images.

https://doi.org/10.5194/egusphere-2026-4440
Preprint. Discussion started: 17 August 2026

Temporary dust flux reductions related to CMEs have also been reported, based on the Wind/WAVES and STEREO/WAVES data. Péronne (2024) – based on the original study by St Cyr et al. (2017) and reductions previously found in dust fluxes correlated with Corotating Interaction Regions (CIRs) (Baalmann et al., 2024) – reported that the dust impact rate detected by Wind/WAVES had decreased on average by 16% for the 401 CMEs listed by Nieves-Chinchilla et al. (2018). Stream Interaction Regions (SIRs) showed a similar pattern: the dust impact rate decreased by on average 21% over 480 SIRs (Baalmann et al., 2024), and 19% for the 867 SIRs (Péronne, 2024) listed by Jian et al. (2006); Jian (2021); Hajra and Sunny (2022). These results are illustrated in Figure 23 (top, from (Péronne, 2024), and bottom adapted from (Baalmann et al., 2024) in (Péronne, 2024)). The decrease in the dust impact rate is, on average, most intense during the CME or SIR events that have a high magnetic field intensity (Péronne, 2024).

https://doi.org/10.5194/egusphere-2026-4440
Preprint. Discussion started: 17 August 2026

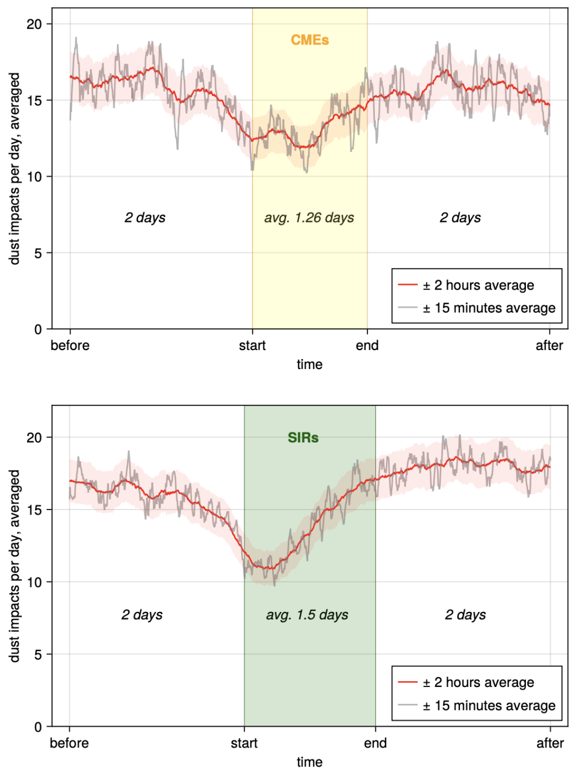

Figure 23. Average number of dust impacts per day, calculated from the dust impacts summed over all CMEs (top panel, from (Péronne, 2024)) and over all SIRs (bottom panel, from (Péronne, 2024), adapted from (Baalmann et al., 2024)), over an interval of ± 2 hours (red curve) or ± 15 minutes (gray curve). The period before the events (interval [before, start] on the time axis) and the one after the events (interval [end,after]) both have a length of two days. The highlighted period ([start,end], yellow for CMEs and green for SIRs) represents the typical duration of the events. Because different CMEs or SIRs vary in duration, they were rescaled before the superposition. The shaded red area represents a 95% statistical interval of confidence for the number of dust impacts per day. The top panel shows a clear decrease in the number of dust impacts per day during the CMEs, and the bottom panel shows a clear decrease for SIRs that appears shifted towards the beginning of the events.

Baalmann et al. (2024) discovered a Solar rotation signature in the Wind/WAVES dust database and found the decrease in the dust impact rates for CIRs to be most likely responsible for the observed Solar rotation signature (see also Section 4.7.3).

Similarly to Baalmann et al. (2024) on Wind, Chadda et al. (2024) highlighted a Solar rotation signature in the STEREO dust database. They carried out numerical simulations that suggested that the origin of such a signature could be due to the switches of polarity in the general structure of the interplanetary magnetic field (and, unlike (Baalmann et al., 2024), does not require a disruption by CIRs).

The effect of interplanetary transients was also studied using STEREO/WAVES by Le Chat et al. (2015), with a particular focus on nanodust grains of size around 20 nm, cf. next section. They found that the nanodust fluxes were higher on average

https://doi.org/10.5194/egusphere-2026-4440
Preprint. Discussion started: 17 August 2026

within SIRs events (~ 1.8 m^{-2} s^{-1}) and within CMEs (~ 2 m^{-2} s^{-1}) than on average during the whole mission (~ 1.2 m^{-2} s^{-1}): a trend opposite to the results for larger dust. The authors acknowledged that the physical process at the origin of these measurements was not understood, but proposed that nanodust previously accelerated to speeds close to the solar wind speed could get trapped in the CMEs magnetic field (a mechanism also considered by Ragot and Kahler (2003)).

Finally, it must be emphasized that these results, based on the analysis of voltage signals detected by Wind and STEREO, suffer from some limitation: first, the lower detection limit of Wind/WAVES for dust grains is probably higher ($\sim 100-300$ nm) than the maximum size ($\sim 10-30$ nm) of the dust strongly affected by CME and SIR magnetic fields at 1 au. On the other hand, the background plasma parameters, to which the dust impact detection technique is quite sensitive, are very different during the transients than in the unperturbed solar wind. Therefore, it is conceivable that the increase/decrease of dust fluxes observed are related to systematic changes in the detection thresholds during these events. Still, until now, all the possible instrumental biases verified in Baalmann et al. (2024), Le Chat et al. (2015), and Péronne (2024) have been ruled out, and the question remains open.

4.6 Nanodust

Nanodust, produced by collisional break-up of larger particles, lies at the lower end of the mass distribution of small bodies in the solar system. A nanodust grain, of size between 1 and 100 nm (from the norm ISO TS27687), which contains typically a few tens to a few 10^7 atoms or small molecules (if compact), lies at the frontier between macro-molecules and bulk matter. Its size can be smaller than many basic physical scales and ensures a large size-to-volume ratio, yielding a number of peculiar properties (Mann et al., 2014; Meyer-Vernet et al., 2015).

These properties enabled nanodust to be inferred in the interstellar medium a long time ago via a variety of phenomena (Li and Mann, 2012), which cannot be observed in the solar system because of the small integrated depth. We are only aware of one attempt to infer the existence of nanograins in the inner heliosphere from brightness observations: Polarisation measurements made during the 21 June 2001 solar eclipse were interpreted in terms of silicon nanoparticles in the solar corona (Habbal et al., 2003). However, the presence of silicon so close to the Sun was ruled out based on the condensation sequence of meteoric material (Mann and Murad, 2005). Even though these observations did not provide a clear indication of the existence of nanoparticles, they motivated further studies that found evidence that nanodust in the heliosphere can reach high velocities (Mann et al., 2007; Czechowski and Mann, 2010). And high velocities lead to high fluxes that can be readily detected *in situ*. In the absence of dedicated instruments (see O'Brien et al. (2014) for a concept), nanodust in the interplanetary medium has thus been observed only recently, with antenna measurements and other instruments that were not designed for that purpose. Notable exceptions are the detections of nanodust with dust experiments who discovered dust streams at Jupiter (Grün et al., 1993) and Saturn (Kempf et al., 2005), and the detection of nanodust during the fast flyby at comet Halley (Utterback and Kissel, 1990)).

https://doi.org/10.5194/egusphere-2026-4440
Preprint. Discussion started: 17 August 2026

4.6.1 What nanodust properties enable its detection in the interplanetary medium?

Most dust detections by spacecraft rely on impact ionization; successful detection therefore depends on the generation of a sufficient number of free charges during the impact. This makes the detection of nanograins challenging. But the impacts of low-mass particles can still generate sufficient amounts free charges when the impact speed is high, that is the particles are fast – and their detection can rely on amplification mechanisms around a specific antenna, as discussed in Section 3.3.3. The charge-to-mass ratio q/m of the dust grains increases with decreasing size so that the smallest ones are more affected by the solar wind magnetic field. The dynamics of the nanoparticles resembles more those of heavy ions, and their trajectories, while not identical, are similar to the pick-up process undergone by ions in the solar wind (Czechowski and Mann, 2010).

Indeed, the electric charge of a dust grain is proportional to its radius, except in very cold media of large Landau radius (Mann et al., 2014), yielding $q/m \propto r^{-2}$. The Lorentz force pushes the grains out of their orbital planes and when their gyroradii ($\propto m/q$) are much smaller than the scale of variation of the magnetic field $\mathbf{B}$, their motion has a component that gyrates around the frozen-in field lines moving with solar wind velocity $\mathbf{V}$ so that they move roughly at the $\mathbf{E} \times \mathbf{B}$ drift speed

$$\mathbf{v_D} \simeq \frac{\mathbf{E} \times \mathbf{B}}{B^2} \quad (1)$$

$$\text{where} \quad \mathbf{E} \simeq -\mathbf{V} \times \mathbf{B} \quad (2)$$

which exceeds 300 km/s farther than 1 au, plus a smaller vertical drift $v_\theta \propto m$ (Northrop, 1963). Nanoparticles can be trapped in the vicinity of the Sun, roughly inside 0.2 au and because the trapping critically depends on initial dust orbits, solar wind, magnetic field and magnetic field conditions (Czechowski and Mann, 2012; Czechowski and Mann, 2021; Stamm et al., 2019), trapped nanograins are possibly released intermittently.

Fast dust grains impacting a spacecraft vaporize and ionize part of the target and of the grain itself, generating a charge roughly proportional to their mass and to the relative speed to the power $\beta \sim 3-5$ (Section 3). Therefore, even though an impacting nano particle generates an electric signal somewhat smaller than does a beta meteoroid (of mass 10^3 times higher and speed roughly five times smaller), the large nanodust flux can generate a very large power spectral density. These properties enabled nanodust to be detected by the wave instruments inboard STEREO and Cassini.

An indirect detection of the nanodust grains was also proposed based on pick-up ions in the solar wind. The charge exchange processes of solar wind impacting dust grains are suggested to lead to the formation of low charge state ions in the interplanetary medium which contributes to the inner source pick-up ions (Wimmer-Schweingruber and Bochsler, 2003; Schwadron et al., 2000). Due to their large surface area the nanodust grains were suggested being the best candidate for producing the inner source pick up ions (Szalay et al., 2021).

4.6.2 Nanodust measurements by STEREO and Cassini

The capability of wave instruments to detect nanodust was shown for the first time when Cassini/RPWS detected high-speed nanodust streams ejected from Jupiter's magnetosphere, simultaneously with conventional dust detectors (Meyer-Vernet et al., 2009), setting the stage for nanodust detections in the interplanetary medium. The first measurements of nanodust accelerated

https://doi.org/10.5194/egusphere-2026-4440
Preprint. Discussion started: 17 August 2026

by the solar wind were performed at 1 au by STEREO/WAVES (Meyer-Vernet et al., 2009), and were later extended using the time domain sampler, which could isolate individual impacts (Zaslavsky et al., 2012). Cassini/RPWS confirmed and extended these detections to greater heliospheric distances (Schippers et al., 2014, 2015), and confirmed the speed given by Eq.(1) (Meyer-Vernet et al., 2017). The interplanetary nanodust fluxes measured by STEREO/WAVES are presented on fig.15.

These measurements were fostered by two instrumental properties, whose ignorance caused unfounded criticisms (Kellogg et al., 2018). Cassini had a very large spacecraft surface area (larger by one order of magnitude than STEREO), ensuring a large impact rate, and its waveform detection was very sensitive (Gurnett et al., 2004). On the other hand, since its aim was planetary exploration, it had only rare occasions to detect dust in the interplanetary medium, when the instrument was episodically turned on during its cruise phase with a large enough integration constant (Schippers et al., 2015). For its part, the STEREO detection was facilitated by the large radius and the position of the forward antennas, a part of which was lying along and close to a plane face of the spacecraft (Bougeret et al., 2008); thus the ion cloud produced by the impact could perturb the photoelectron sheath of these antennas (Pantellini et al., 2012a, 2013), increasing considerably the signal (cf. Section 3.3.3).

Figure 24 shows the cumulative flux at 10 nm (10^{-20} kg) deduced from Cassini/RPWS measurements during its cruise phase to Jupiter by the high frequency receiver in monopole mode. These observations (Schippers et al., 2014, 2015) are compatible with a power law decrease close to d^{-2} outwards of 1 au, consistent with numerical simulations of nanodust dynamics (Belheouane, 2014). The value at 1 au is consistent with the survey of five years of STEREO/WAVES data (2007–2011) by Le Chat et al. (2013), with the STEREO value lying near the low bound of Cassini results.

Could nanodust be detected by other spacecraft? The nano dust impact signal was too small to be measurable by the dipoles of Wind/WAVES (Meyer-Vernet et al., 2014), which had too thin antennas (Bougeret et al., 1995) for the perturbation of the photoelectron sheath to play a role (Pantellini et al., 2012a). Nanodust will be difficult to measure on PSP and SO because inward of 0.3 au, the drift speed (Eq.(1)) may not be large enough to produce a detectable dust impact charge, except in the presence of solar wind perturbations (Section 4.6.4).

4.6.3 Nanodust flux long-term variability

The nanodust flux near the ecliptic, where most spacecraft orbit, is critically determined by the heliospheric magnetic field, which reverses roughly every 11 years. When the solar radial magnetic field in the northern hemisphere is ingoing, the solar wind electric field (Eq.(2)) points towards the heliospheric current sheet (HCS), driving the posively charged grains towards it ((Meyer-Vernet, 2007) – pages 291–308 and 352–356). In this focusing geometry, nanodust is driven near the ecliptic when the HCS is weakly tilted. In contrast, a defocusing electric field drives nanodust away from the equator, except for the smallest particles ($\leq$ 10 nm), which have a slower vertical drift v_θ (Juhász and Horányi, 2013; Poppe and Lee, 2022). Furthermore, the HCS guides nanodust through the inner heliosphere via "current sheet surfing" (Czechowski and Mann, 2012). Figure 25 shows that both STEREO and Cassini nanodust observations took place in focusing conditions (Meyer-Vernet, 2025). Those of STEREO (2007–2011) stopped when the HCS tilt angle increased too much (Poppe and Lee, 2022), which suggests that STEREO detected large nanodust ($\geq$ 10nm), which has a large vertical drift. On the contrary, the occurrence of Cassini/RPWS nanodust observations near solar activity maximum, when the HCS was highly tilted most of the time, suggests that it measured

https://doi.org/10.5194/egusphere-2026-4440
Preprint. Discussion started: 17 August 2026

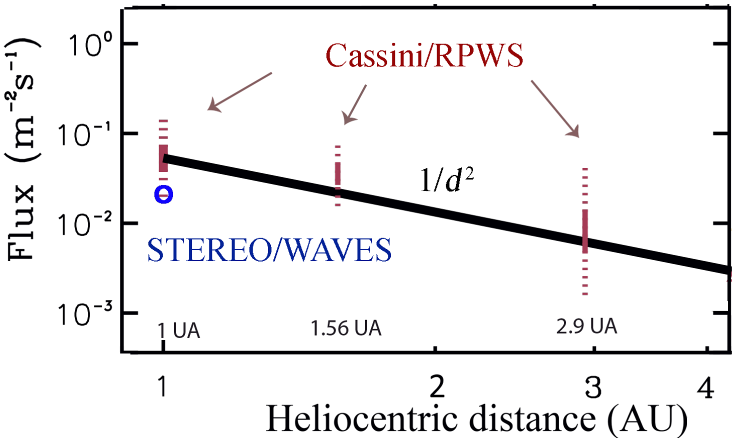

Figure 24. Nanodust flux measured by Cassini as a function of heliocentric distance d (Schippers et al., 2014, 2015) (red bars = mean $\pm 1\sigma$; dotted bars = mean $\pm 3\sigma$) superimposed to the peak of the flux distribution measured on STEREO from 2007 to 2011 (Le Chat et al., 2013) (blue circle) and to a variation as d^{-2}.

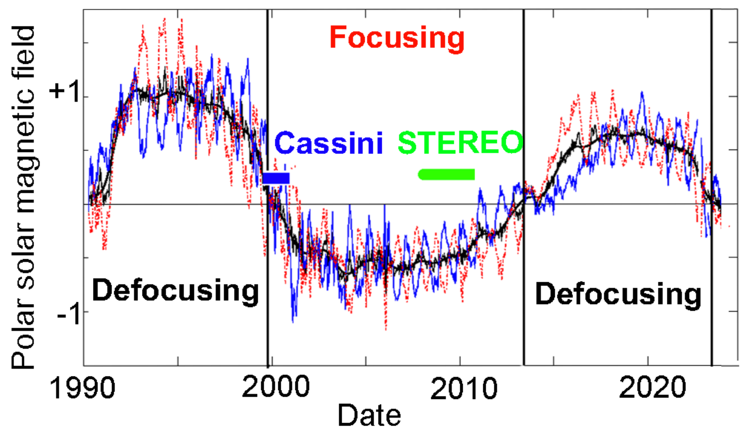

Figure 25. Polar solar magnetic strength (in Gauss) from the solar Wilcox Observatory (+ North: solid blue, - South: dashed red, average: medium solid, smoothed average: heavy solid). Negative (positive) north magnetic field produces a focusing (defocusing) electric field for positive charges. Both STEREO and Cassini nanodust observations took place during a focusing configuration. Adapted from Meyer-Vernet (2025).

particles somewhat smaller than 10 nm (Meyer-Vernet, 2025) which are weakly affected by the vertical drift. Since the flux increases with decreasing size, this might explain why STEREO measurements lie at the lower bound of the Cassini ones (Figure 24).

https://doi.org/10.5194/egusphere-2026-4440
Preprint. Discussion started: 17 August 2026

4.6.4 Nanodust short-term variability

The nanodust flux measured by STEREO and Cassini was highly variable, with bursts of high count rate separated by periods of very low rate. This high variability is caused by the variable production rate, transient magnetic field changes, and complex dynamics in the presence of the HCS (Czechowski and Mann, 2012; Juhász and Horányi, 2013; Poppe and Lee, 2022). The variable production rate was confirmed by PSP (Szalay et al., 2021), whereas Cassini observations (Meyer-Vernet et al., 2017) showed that nanodust follows closely the fluctuations of the solar wind velocity component perpendicular to the magnetic field (Eq.(1)), as predicted by dynamics.

Effects of solar wind transients on the nanodust flux were also identified with S/WAVES, discussed in Section 4.5.

4.7 Interstellar dust

Observational evidence that Interstellar Dust (ISD) grains traverse the heliosphere began to emerge in the 1970s, from dust flux variations measured from spacecraft near 1 au (Bertaux and Blamont, 1976). This was confirmed in 1993 with measurements of the dust detector aboard the Ulysses space probe (Grün et al., 1993).

The basic picture explaining the ISD flow is that the grains come from the interstellar medium that the Sun is currently traversing. The interaction of the interstellar medium plasma and the solar wind leads to the formation of the heliosphere. This interaction deflects most ionized components of the interstellar medium gas and smaller grains while the interstellar neutral gas and more massive dust grains stream into the heliosphere (Frisch et al., 1999).

With Ulysses, notably, ISD and neutral interstellar helium were observed from the same direction and on the same spacecraft. In the frame of the Sun they have velocities of approximately 26 $\mathrm{km\,s^{-1}}$ (Grün et al., 1994; Witte, 2004; Frisch et al., 1999). This corresponds to the Sun's velocity relative to the local interstellar cloud. While the ISD in the heliosphere is also consistent with brightness observations (Grün et al., 1993; May, 2008; Rowan-Robinson and May, 2013), it is more apparent in the in situ measurements. Ulysses detected ISD grains with diameters ranging from 0.05 μm to not much more than 1 μm (Krüger et al., 2015; Baalmann et al., 2024), which typically contribute little to the observed brightness (cf. 4.1). Finally it was in favor of the Ulysses ISD discovery that the interplanetary dust flux is decreasing at larger distance from the Sun and above and below the ecliptic, all regions which Ulysses traversed (Grün et al., 1997).

ISD grains are also observed in the inner heliosphere by the current space missions that are at the focus of this review, and a view of the principal forces acting on the ISD helps to place these observations into broader context. The mass of ISD measured with Ulysses ranges from 10^{-19} to 10^{-11} kg (Baalmann et al., 2024). The predominant forces on dust particles in this range of mass are solar gravitation, solar radiation pressure, and the Lorentz force. Their relative importance varies depending on the dust properties and surrounding plasma and magnetic field conditions; most importantly they change with mass, respectively size. For the ISD grains approaching the heliosphere, one can distinguish some processes that approximately dominate in different mass ranges (Mann and Kimura, 2000): The smallest grains ($\approx m < 10^{-18}$ kg) do not enter the heliosphere because they are deflected at the heliopause. The ISD that enter the heliosphere are deflected in the solar magnetic field, this deflection is most apparent for ISD with masses, $m < \ 10^{-17}\ kg$. The effects of radiation pressure force are most important for particles

https://doi.org/10.5194/egusphere-2026-4440
Preprint. Discussion started: 17 August 2026

with masses ($10^{-17}\ kg < m < 10^{-16}$ kg) and finally gravitational focusing by the Sun affects the flow of even larger ISD ($m > 10^{-15}$ kg). The antenna measurements in the inner heliosphere have enabled observations of the ISD flow over many years now and the measurements still continue. Below we present these results after examining ISD filtering at the heliospheric boundary and its modulation within the heliosphere.

4.7.1 Interstellar dust at the boundaries of the heliosphere

The dust grains in the interstellar medium carry a surface charge that is small, but sufficient so that the smallest grains are strongly deflected at the heliopause (Kimura and Mann, 1998). The deflection and entry conditions that lead to the "filtering" of the ISD flow were investigated in several works considering the dust flows traversing the heliosheath, which is characterized by the encounter of the solar wind and interstellar medium plasmas; these studies illustrate the effects like charge fluctuation, dust properties and local features (Linde and Gombosi, 2000; Czechowski and Mann, 2003a, b; Slavin et al., 2012; Sterken et al., 2015; Alexashov et al., 2016; Godenko and Izmodenov, 2024). An interesting finding was that in spite of the deflection force, the wavy structure of the heliospheric current sheet that separates regions of opposite magnetic field direction can facilitate the passing of tiny ISD because they quickly pass regions of different field polarity (Czechowski and Mann, 2003b; Godenko and Izmodenov, 2024; Baalmann et al., 2025). Recently, a method was developed to infer the filtering in the heliosheath from experimental data (Baalmann et al., 2025): this was applied on the Ulysses data and is a promising approach for future dust measurements with trajectory information. Measurements of the flux of ISD of different spacecraft at 1 AU can help unravel the permeability of the outer heliosphere for ISD. However, obtaining the full picture of the ISD processes at the edges of the heliosphere requires a dedicated dust instrument on an Interstellar Probe (e.g., Sterken et al., 2023).

4.7.2 Interstellar dust measurements with electric-field instruments, and long-term variability observations

The Ulysses ISD dataset contains 16 years of dust impact data over 1.5 solar cycles (Krüger et al., 2015) that have been analyzed concerning their mass distribution, flow direction, and variability, and have been compared to ISD dynamics modeling (Strub et al., 2015; Sterken et al., 2015).

Since then, electric field measurements of ISD were developed, and enabled long-term coverage of the interstellar flux. The principle of ISD measurements with radio and plasma waves instruments is intrinsically statistical: one usually cannot differentiate if a single impact is from interstellar or solar system origin. This principle is based on the identification of the orbital modulation produced in the impact rate onto the spacecraft because of the variation of ISD velocity vector in the frame of the spacecraft along its orbit. When the spacecraft moves "into the stream", relative velocity is high and consequently so is the impact rate; whereas the relative velocity, and impact rates, are low when the s/c moves together with the ISD stream (cf. Figure 26, panel b). A refinement of this effect comes from the variation of the detection threshold on the orbit: at higher impact speeds, a voltage pulse of given amplitude will be produced by a smaller grain than at smaller impact speeds – this effect amplifying the observed modulation. The large surface area of collection enabled by the electric field measurements make this statistical approach very effective in determining ISD fluxes.

https://doi.org/10.5194/egusphere-2026-4440
Preprint. Discussion started: 17 August 2026

The first observation of this orbital modulation was done by Zaslavsky et al. (2012) with S/WAVES data, benefiting from the large ISD flux at the launch of STEREO mission, which occurred in magnetic focusing configuration and solar minimum. Fitting the impact rate on STEREO gave a value of the ISD flux at 1 a.u. of $\approx 8.10^{-5}$ m^{-2}.s^{-1}, and of the latitude of the dust inflow – the latter value of $\approx 258°$ aligning well with the known direction of neutral hydrogen inflow, and confirming the interstellar origin of the dust. This initial study was refined by Belheouane et al. (2012), confirming the value of the flux, and identifying rather important time variations in the direction of the ISD inflow – with minimum about 250° and maximum at almost 280° on the 2007-2011 period.

The identification of the ISD orbital modulation was then carried on Wind/WAVES data by Malaspina et al. (2014). The derived ISD flux was smaller than on STEREO – consistent with the idea that Wind/WAVES dipole detects overall larger dusts than S/WAVES monopoles, cf. Section 3. The ISD flux was also found to be very variable in direction, with noted variations of about 25° between march 2008 and march 2009.

The Wind and STEREO dust impact data cover up to almost a full Hale cycle of observations ($<$ 22 years) of ISD impacts. Databases have been constructed and are open for use (e.g., Malaspina et al., 2016). The extended time span and differing vantage points (with respect to the ISD flow) of these missions enable the investigation of how the ISD flux evolves and how it is modulated by solar activity (Hervig et al., 2022; Baalmann et al., 2024).

Observations from the Wind spacecraft from 2005 to 2023 reveal long-term variations in the ISD flux at 1 au, as can be seen on the left panel of Figure 26. On this figure, superimposed on the orbital modulation of the impact rate discussed above, is the solar-cycle-driven trend: a gradual increase in ISD flux during the focusing phase up to ca. 2010, followed by a steady decline during the subsequent defocusing phase. Instrumental effects, such as reduced sampling from 2011 and outages in 2013–2014, temporarily impacted sensitivity, but do not obscure the overall trend that is in line with theoretical expectations and numerical models of ISD modulation by solar activity (Morfill and Grün, 1979; Landgraf, 2000; Sterken et al., 2012; Strub et al., 2019).

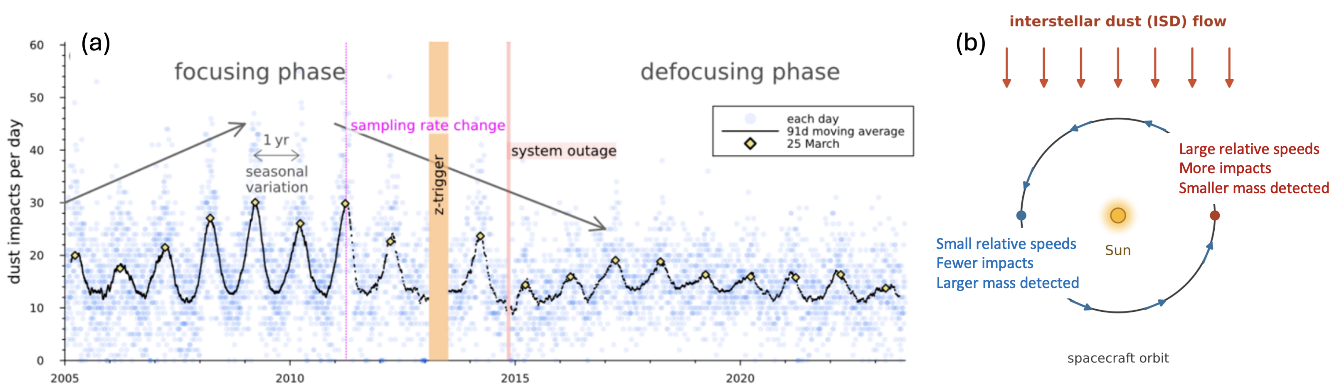

Figure 26. (a) Dust impacts per day observed by Wind at L1 (2005–2023). Blue points represent daily counts; the black curve shows a 91-day moving average. Annual peaks occur near 25 March (yellow diamonds). The long-term trend reflects solar cycle modulation, with instrumental effects marked in pink, orange, and red (reproduced from Baalmann et al. (2024)). (b) Geometry of the orbital modulation produced in the impact rates by the interstellar flow.

https://doi.org/10.5194/egusphere-2026-4440
Preprint. Discussion started: 17 August 2026

Long term monitoring from the STEREO A spacecraft at 1 au (Rackovic Babic, 2022) and at distance from Earth during the period 2007–2022 reveal a consistent ISD signal, corresponding to a focusing phase of the solar magnetic cycle on the period 2007-2012. After 2012, a gradual decrease in ISD detections is observed, reflecting the onset of a defocusing phase associated with magnetic field polarity reversal. STEREO B provided data until late 2014, after which contact was lost. Despite differences in viewing geometry and data availability between the two spacecraft, the overall modulation pattern caused by heliospheric magnetic conditions over solar-cycle timescales remains evident.

Long term monitoring showed differences in the longitude of the interstellar flux upstream direction derived from the impact data of different spacecraft and at different times (Belheouane et al., 2012; Malaspina et al., 2014; Rackovic Babic, 2022). The values derived from the antenna measurements range between 244 and nearly 280 degree. For the first years of Ulysses measurements, the ISD upstream direction was found to be around 259^o ecliptic longitude and 8^o latitude and coincided with the neutral interstellar helium flow (Frisch et al., 1998; Landgraf, 2000). Flow directions vary: there is for instance, an unexplained change in latitude in dust flow direction from Ulysses data (Strub et al., 2015), which most likely is attributed to the Lorentz force (Sterken et al., 2015) by comparing computer simulations with the data.

We note that no clear identification of ISD modulation has been made with SolO and PSP to date (July 2026). Factors explaining this are the important β-meteoroids impact rates on these spacecraft, their elliptical orbits which makes this impact rate vary with distance, and, probably more critically, the fact that they were both launched in magnetic defocusing configuration, where the modulation on STEREO or Wind is hardly distinguishable (see Figure 26). It is possible that ISD orbital modulation will be identified on these spacecraft at the next favorable solar magnetic configuration (around 2029).

4.7.3 Interstellar dust short-term variability

In the short term, the measured dust impact rates are (on average) reduced during CIRs, causing a solar rotation frequency in the impact data by Wind (Baalmann et al., 2024) (note that Wilson et al. (2023) reports on a solar rotation frequency in the spacecraft charging data). The exact mechanism of the reduction in measured flux is yet to be understood and it is possible that also some outgoing interplanetary dust (e.g., β-meteoroids) is subject to this modulation. The solar rotation frequency in the dust impact data has been confirmed by the measurements from the STEREO antenna (Chadda et al., 2024), where modeling pointed rather in the direction of a modulation in the dust impact rate due to the motion of interstellar dust through the heliosphere's alternating magnetic field polarity during the solar minimum of focusing phase. However, case studies in Baalmann et al. (2024) of the sector structure of the Heliospheric Current Sheet showed no correlation with these frequencies.

4.7.4 Interstellar dust measurements in the heliosphere in relation to interstellar conditions

In-situ spacecraft measurements of interstellar dust (ISD) complement astronomical observations because they yield direct measurements of individual grain sizes and masses instead of only ensemble-averaged properties inferred from remote observations. Ulysses' detection of ISD include larger grains than those predicted by many of the models based on astronomical data notably the often used model to explain interstellar extinction (Frisch et al., 1999; Draine, 1994). Knowledge of the ISD

https://doi.org/10.5194/egusphere-2026-4440
Preprint. Discussion started: 17 August 2026

allowed the first sample collection from spacecraft with Stardust (Westphal et al., 2014) and led to some elemental composition results from the Cassini dust detector (Altobelli et al., 2016). The in-situ ISD flow also allowed estimation of the dust-to-gas mass ratio in the interstellar medium surrounding the heliosphere (Frisch et al., 1999; Krüger et al., 2015), which affects interpretation of the polarization properties of the interstellar medium (Hiltner, 1949; Angarita et al., 2023), itself a probe of the interstellar magnetic field (Andersson et al., 2015). While the dust-to-gas ratio is important for astrophysics studies, such estimates are affected by uncertainties in the selection of ISD and in deriving the dust mass from the instrument data (Baalmann et al., 2025). Aside from the experimental uncertainty there arises the question to what part of the interstellar medium the dust is characteristic. For this it is helpful to have a view of the local interstellar medium.

The grains detected are identified as ISD based on their velocity and direction that can be explained with grains that are dynamically coupled to the local interstellar medium. On the other hand, the length of the friction coupling, which scales linearly with size, is approximately 300 parsecs for a micrometre grain under warm interstellar cloud conditions near the heliosphere (Mann et al., 2000). This 300 pc length is of the order of the size of the Local Bubble (O'Neill et al., 2024) in which the Sun resides. The Sun is more locally in a complex of warm interstellar clouds that extends 15 pc (Zucker et al., 2025). These local conditions have also been used to investigate the properties of the ISD that enters the heliosphere (Kimura et al., 2003b, a). The local interstellar medium clouds have different velocities (Redfield and Linsky, 2008), they are possibly overlapping and mixing (Swaczyna et al., 2022) and possibly better described as one cloud that is subject to disturbances (Linsky et al., 2022; Linsky and Redfield, 2023). Because of the coupling scale it is quite possible that the ISD flow in the heliosphere is made up by grains of these different clouds or from a heterogenous cloud. Another factor is that the interstellar medium is locally perturbed by the presence of the heliosphere (Slavin et al., 2012) and grain flows are part of this. Given this background, the differences in the ISD flow directions that were found in the observations (cf. Section 4.7.2) and the changes in direction seen with by Ulysses, STEREO and Wind may also reflect interplanetary medium conditions, as shown in Sterken et al. (2015) for the latitudinal shift in dust flow direction ca. 2005-2006.

5 Summary of recent advances and perspectives

The combination of new brightness observations and in-situ measurements, and the combined measurements of Wind, STEREO, PSP and SOlO has yielded a number of important advances that this review aimed to consolidate. The progress in the in-situ studies was made possible by using radio and plasma wave instruments as dust detectors, and are summarized in Section 5.1. Progress with the whitelight observations is summarized in Section 5.2. We discuss the implications of these measurements for other astrophysical environments in Section 5.3 and end with the near-term space missions and future perspectives for the study of the Zodiacal cloud, in Section 5.4.

5.1 Radio and plasma wave instruments as dust detectors

An important methodological advance reviewed here is the maturation and use of radio and plasma wave instruments as dust flux monitors in the inner heliosphere. The technique covers the full projected surface of the spacecraft body and antenna

https://doi.org/10.5194/egusphere-2026-4440
Preprint. Discussion started: 17 August 2026

system, providing an effective collecting area that can exceed that of conventional dust instruments by several orders of magnitude. This geometrical advantage enables statistically robust flux measurements even at the low dust number densities of the interplanetary medium. Over the past twenty years, the technique has been applied to an expanding fleet of spacecraft operating at a wide range of heliocentric distances – and in particular to STEREO and Wind near 1 au, and most recently Parker Solar Probe (PSP) and Solar Orbiter (SolO) inside 0.5 au – yielding the most extended in-situ record of inner-heliosphere dust fluxes to date.

Recent modeling advances and dedicated laboratory hypervelocity impact experiments have substantially refined waveform interpretation and dust-mass calibration (Sections 3.1.1 and 3.2). The first-principles electrostatic model (Shen et al., 2021a; Smith et al., 2025) is currently being applied to specific spacecraft (e.g., STEREO) to demonstrate that the individual waveforms from the three antennas can be accurately reproduced by the model using refined impact-charge values. In addition, variations among the three signals reveal the location of the impact on the spacecraft, which further constrains the orbital elements and thus the origin of the dust particle. Automated detection pipelines and machine-learning classifiers (Section 3.4) have made it practicable to process the large waveform archives now routinely accumulated by PSP and SolO. Nevertheless, open questions remain: the charge-yield calibration still relies on laboratory measurements performed under conditions that do not fully replicate the interplanetary environment, and the interpretation of signals in complex multi-antenna configurations continues to evolve and will require further modeling efforts or satellites with cross-calibration capabilities between impact ionization dust detectors and plasma wave antennas.

5.2 Main observational results

White-light observations through STEREO/SECCHI and PSP/WISPR instruments have characterised the global structure of the Zodiacal cloud. Photometric analyses have established the symmetry plane, radial brightness profile ($I \propto r^{-2.3}$ (Stenborg et al., 2018)), and iso-contour morphology of the inner Zodiacal cloud (Stenborg et al., 2018; Stauffer et al., 2018), and have provided the first observational evidence for a dust depletion zone developing sunward of $\approx 35\,R_\odot$ (Howard et al., 2019; Stenborg et al., 2024), and a largely dust-free zone interior to $\approx 5\,R_\odot$ (Howard et al., 2019; Stenborg et al., 2021, 2022).

At the same time, in-situ measurements from STEREO, Wind, PSP, and SolO have established consistent β-meteoroid flux densities in the range 4–10×10^{-5} m^{-2} s^{-1} at 1 au (Zaslavsky et al., 2012; Malaspina et al., 2015), with a radial dependence close to r^{-2} inside 1 au, and have resolved the bound dust population close to PSP's perihelion (Szalay et al., 2021; Zaslavsky et al., 2021; Kočiščák et al., 2024). Interplanetary nanodust were detected in-situ for the first time and their highly variable dynamics has been explored. The interstellar dust flux was identified for the first time in radio and plasma waves data, benefiting from the magnetic focusing configuration in place during the first years of the STEREO mission (Zaslavsky et al., 2012; Belheouane et al., 2012), and then identified with Wind/Waves (Malaspina et al., 2014). This discovery enabled monitoring the ISD flux over almost 30 years, revealing solar-cycle modulation of the interstellar dust flux, and a solar rotation modulation is likely linked to CME and SIR passages (Baalmann et al., 2024). Long term monitoring of dust impacts also made it possible to identify stream-like flux enhancements in the bound meteoroid and β-meteoroid populations, and possible signatures of interactions of these grains with solar wind transients as CMEs and SIRs.

https://doi.org/10.5194/egusphere-2026-4440
Preprint. Discussion started: 17 August 2026

5.3 Relevance for interstellar dust and debris disk studies

Observations of interstellar dust (ISD) in situ by spacecraft complement astronomical measurements by providing direct grain-size and mass determinations. Observations of large ISD grains in the heliosphere provide a basis for studies of ISD formation and dynamics in the surrounding interstellar medium. New in-situ compositional measurements with IMAP can exploit ISD fluxes derived from Wind and STEREO (and possibly in the future PSP, and Solar Orbiter) to separate the interstellar component in the IMAP dust measurements that just started (Horányi et al., 2025a; Szalay et al., 2026b). With robust statistics and observational records spanning more than 20 years, the derived ISD fluxes can trace time-dependent heliospheric structure in a manner analogous to constraints from Galactic cosmic rays. Improved understanding of dust detection via antenna measurements now permits these data to be used to derive an ISD mass distribution. Nonetheless, these studies would benefit substantially from velocity-resolved, large-area detectors; coordinated, multi-point long-term measurements; and co-located antennas and dedicated dust instruments for cross-calibration, as suggested by e.g. Sterken et al. (2023).

Understanding the interactions of the ISD flow with the heliosphere and the entry conditions serves as an example for the conditions of astrospheres (Sterken et al., 2022) and the circumstellar debris disks of theses systems. Planetary debris disks are optically thin, gas-poor dust disks around main sequence starts that are containing planetesimals and possibly planets. Most of them are identified by infrared/submillimetre excesses in the spectral brightness curves and considered analogues of the early solar system as their their dust clouds are denser than the zodiacal cloud. The notable difference is that the debris disks are usually observed at several 10 au from the stars in a region that is more comparable to the Kuiper belt (Poppe, 2016). The outer heliosphere is analogous to planetary debris disks, and measurements by the New Horizons mission have yielded new insights into its dust cloud (Poppe, 2016). The observations have continued (Bernardoni et al., 2022) and enable studies of dust trajectories and destruction processes specific to the outer heliosphere (Corbett et al., 2025).

Nonetheless, the dust interactions observed up close in the inner heliosphere also play a role in debris disks and comparisons can be made (Mann et al., 2006). One example is the role of β-meteoroids , which have been measured in the inner heliosphere in recent years: in debris disks these particles trigger collisions in the outer disk; and these collisions are a possible source of the observed gas components in the beta Pictoris system (Czechowski and Mann, 2007). Aside from radiation pressure, also the stellar and solar wind direct momentum transfer work in a similar way (Minato et al., 2006). The parameters of dust–dust collisions in astrophysics and space physics are highly uncertain because the relevant conditions can only be reproduced in the laboratory to a limited extent. Detailed analyses of dust mass distributions in the inner heliosphere, based on Parker Solar Probe (PSP) and Solar Orbiter (SolO) observations (Zaslavsky et al., 2021; Kočiščák, 2024; Szalay et al., 2024) and moreover the combination with models of collisional evolution (Szalay et al., 2021; Pokorný and Brown, 2016; Pokorný et al., 2024), can therefore provide inputs for constraining the dust collisions in the debris disks.

The dynamics of nanodust in the inner heliosphere (e.g. Czechowski and Mann, 2010), and in particular their magnetic trapping, is also relevant for dust around other stars. An example are dust particles that remain near stars despite strong radiation pressure. The existence of such dust particles has been proposed to explain the observed emission brightness in some systems (Su et al., 2013) and explained with the pile up of nanograins (Rieke et al., 2016). The discussion of the astronomical

https://doi.org/10.5194/egusphere-2026-4440
Preprint. Discussion started: 17 August 2026

observations motivated further theoretical investigations into the conditions for dust pile-up in the coronae of other stars, and these studies showed that the pile-up critically depends on a number of initial conditions (Stamm et al., 2019; Czechowski and Mann, 2021).

5.4 Near-term prospects and upcoming missions

Looking ahead, an anticipated near-term development is the exploitation of Solar Orbiter's high-inclination phase, currently underway, during which the spacecraft will reach heliographic latitudes exceeding 30°. These out-of-ecliptic in-situ observations will for the first time systematically probe the latitudinal structure of the inner Zodiacal cloud in-situ. The continued deepening of PSP's perihelion passages, combined with improved waveform processing, will further constrain the structure and mass flux of dust populations in the sub-20 $R_\odot$ region.

Currently, the heliospheric magnetic field is entering a new focusing phase with a maximum dust flux expected between ca. 2029 and 2035, presenting an excellent opportunity to continue monitoring the nanodust and ISD fluxes using long-term missions as Wind and STEREO and different types of instruments. In addition, the PSP and SolO may provide valuable insights into dust dynamics closer to the Sun and out of the ecliptic. This characterization of the interstellar dust (ISD) flux, relative to interplanetary dust components made from the ongoing antennas, can be combined with the in-situ mass spectrometry measurements anticipated from IMAP (Horányi et al., 2025b) and DESTINY+ (Arai et al., 2026; Simolka et al., 2024) in the near-future. All of these observations will not only advance our understanding of how solar activity modulates ISD and nanodust transport, but may also uncover new properties of the dust population itself.

5.4.1 Upcoming space missions

The measurement techniques validated in the inner heliosphere are directly exportable to several upcoming or proposed missions, which are expected to make significant contributions to dust science in the coming decade. Below we briefly outline those most relevant to the themes of this review.

IMAP (Interstellar Mapping and Acceleration Probe, NASA, launched 2025) is stationed at the Sun–Earth L1 point and carries the IDEX (Interstellar Dust EXperiment) instrument, a time-of-flight mass analyzer specifically designed to characterise the flux, mass distribution and composition of interstellar dust grains (McComas et al., 2018; McComas et al., 2025; Horányi et al., 2025b; Szalay et al., 2026b). Its extended L1 time series will complement and extend the Wind dataset to compositional measurements.

PUNCH (Polarimeter to UNify the Corona and Heliosphere, NASA, launched 2025) is a constellation of four small satellites providing continuous wide-field polarimetric imaging of the solar corona and inner heliosphere. Its capability to image the F-corona and to separate the weakly polarized dust-scattered light from the more strongly polarized electron-scattered K-corona is directly relevant to Zodiacal cloud structural studies. PUNCH images the entire inner heliosphere out to 47° from the Sun,

https://doi.org/10.5194/egusphere-2026-4440
Preprint. Discussion started: 17 August 2026

once every 32 minutes, in polarized light. (DeForest et al., 2026).

Vigil (ESA, planned launch ∼2031) will be placed at the Sun–Earth L5 Lagrange point, providing solar wind monitoring from a vantage 60° behind the Earth (Palomba and Luntama, 2022). Its remote-sensing suite, in particular its wide-angle visible-light imaging system will offer a complementary viewing geometry for Zodiacal cloud imaging.

Comet Interceptor (ESA/JAXA, planned launch ∼2029) is designed to fly by a dynamically new comet or a potential interstellar object on a hyperbolic trajectory (Snodgrass and Jones, 2019). Its Dust, Fields and Plasma (DFP) instrument suite (Rothkaehl et al., 2024) will study cometary dust properties in-situ, directly informing our understanding of one of the primary source populations of the Zodiacal cloud. Together with the DFP/DISC dust impact sensor, the DFP/COMPLIMENT instrument will make use of its electric field antenna to provide dust fluxes in the sub micrometer size range. Dust flux models are being developed to support mission planning with a flexible tool to predict the dust environment (Haslebacher et al., 2025) which will depend on the final target selection.

DESTINY$^+$ (Demonstration and Experiment of Space Technology for INterplanetary voYage, Phaethon fLyby and dUst Science, JAXA, planned launch ∼2028) will perform a flyby of asteroid (3200) Phaethon, the parent body of the Geminid meteor stream, after a flyby of asteroid (99942) Apophis and before flybys of other near-Earth asteroids. The onboard Destiny$^+$ Dust Analyser (DDA), a high-resolution impact-ionisation dust analyser, will measure the chemical composition, mass, velocity, and charge of asteroid-associated dust during asteroid flybys, and those of interplanetary and interstellar dust during the cruise phase (Arai et al., 2026; Simolka et al., 2024).

Author contributions. AZ and IM are co-first authors of this review. They planned and outlined the manuscript and coordinated the writing, they contributed equally to this work as senior authors. All authors participated in the writing and the discussion of the work.

Competing interests. At least one of the (co-)authors is a member of the editorial board of Annales Geophysicae.

Acknowledgements. This work is dedicated to the memory of our co-author and colleague Volker Bothmer, who sadly passed away during the preparation of this manuscript. Volker was a leading figure in solar wind and dust imaging, and a long-time, dedicated supporter of the Solar Orbiter and Parker Solar Probe missions. He is deeply missed by all who had the privilege of working with him.

This review grew out of the workshop *Exploring the Zodiacal Cloud with PSP and SolO: Results and Prospects*, held on 21–25 October 2024 at the Observatoire de Paris, Meudon. We thank all participants for the stimulating discussions that shaped the scope of this work.

https://doi.org/10.5194/egusphere-2026-4440
Preprint. Discussion started: 17 August 2026

VJS and AP received funding from the European Union's Horizon 2020 research and innovation programme under grant agreement Nr. 851544 – ASTRODUST. SA received funding from the European Union's Horizon Europe research and innovation program under the Marie Skodowska-Curie grant agreement No. 101150536, for the project 'FLAME'.
Coauthors ZS and AMS were funded by NASA's Heliophysics Guest Investigators—Open (HGIO) program, grant 80NSSC22K0753.
IM's work is funded by the Research Council of Norway, project 353378.

https://doi.org/10.5194/egusphere-2026-4440
Preprint. Discussion started: 17 August 2026

References

Abramov, V. I., Bandura, D. R., Ivanov, V. P., and Sysoev, A. A.: Energy and angular characteristics of ions emitted in the impact of accelerated dust particles on a target, Sov. Tech. Phys. Lett., 17, 194–195, 1991.

Alexashov, D. B., Katushkina, O. A., Izmodenov, V. V., and Akaev, P. S.: Interstellar dust distribution outside the heliopause: deflection at the heliospheric interface, MNRAS, 458, 2553–2564, https://doi.org/10.1093/mnras/stw514, 2016.

Altobelli, N., Postberg, F., Fiege, K., Trieloff, M., Kimura, H., Sterken, V. J., Hsu, H. W., Hillier, J., Khawaja, N., Moragas-Klostermeyer, G., Blum, J., Burton, M., Srama, R., Kempf, S., and Gruen, E.: Flux and composition of interstellar dust at Saturn from Cassini's Cosmic Dust Analyzer, Science, 352, 312–318, https://doi.org/10.1126/science.aac6397, 2016.

Andersson, B.-G., Lazarian, A., and Vaillancourt, J. E.: Interstellar Dust Grain Alignment, ARA&A, 53, 501–539, https://doi.org/10.1146/annurev-astro-082214-122414, 2015.

Andersson, L., Weber, T. D., Malaspina, D., Crary, F., Ergun, R. E., Delory, G. T., Fowler, C. M., Morooka, M. W., McEnulty, T., Eriksson, A. I., Andrews, D. J., Horanyi, M., Collette, A., Yelle, R., and Jakosky, B. M.: Dust observations at orbital altitudes surrounding Mars, Science, 350, aad0398, https://doi.org/10.1126/science.aad0398, 2015.

Angarita, Y., Versteeg, M., Haverkorn, M., Rodrigues, C., Magalhães, A., Santos-Lima, R., and Kawabata, K. S.: Interstellar polarization survey. III. Relation between optical polarization and reddening in the general interstellar medium, The Astronomical Journal, 166, 34, 2023.

Anghel, S.: Machine Learning in meteor science: Challenges and future directions, Icarus, p. 117185, https://doi.org/https://doi.org/10.1016/j.icarus.2026.117185, 2026.

Anghel, S., Drolshagen, E., Ott, T., Birlan, M., Colas, F., Nedelcu, D. A., Koschny, D., Zanda, B., Bouley, S., Jeanne, S., Malgoyre, A., Blanpain, C., Gattacceca, J., Jorda, L., Lecubin, J., Rault, J. L., Vaubaillon, J., Vernazza, P., Hueso, R., Peña-Asensio, E., Ribas, S. J., Rimola, A., Sánchez-Lavega, A., Tapia, M., Trigo-Rodriguez, J. M., Cauhape, P., Davadan, C., Dupouy, P., Herpin, M., Rousseu, D., and Tregon, B.: Energy signature of ton TNT-class impacts: analysis of the 2018 December 22 fireball over Western Pyrenees, Monthly Notices of the Royal Astronomical Society, 508, 5716–5733, https://doi.org/10.1093/mnras/stab2968, 2021.

Anghel, S., Nedelcu, D. A., Birlan, M., and Boaca, I.: Single-station meteor detection filtering using machine learning on MOROI data, Monthly Notices of the Royal Astronomical Society, 518, 2810–2824, https://doi.org/10.1093/mnras/stac3229, 2023.

Arai, T., Kobayashi, M., Ishibashi, K., Kimura, H., Okamoto, T., Okudaira, O., Yoshida, F., Wada, K., Morota, T., Srama, R., Krüger, H., Marshall, S., Imamura, H., Takashima, T., and Destiny+ Team: Current Status of DESTINY+ Flyby Mission to (99942) Apophis and (3200) Phaethon, in: 57th Lunar and Planetary Science Conference, vol. 3160 of *LPI Contributions*, p. 2016, 2026.

Aubier, M. G., Meyer-Vernet, N., and Pedersen, B. M.: Shot noise from grain and particle impacts in Saturn's ring plane, Geophys. Res. Lett., 10, 5–8, https://doi.org/10.1029/GL010i001p00005, 1983.

Auer, A. A. and Sitte, K.: Detection technique for micrometeoroids using impact ionization, Earth and Planetary Science Letters, 4, 178–183, https://api.semanticscholar.org/CorpusID:121569767, 1968.

Auer, S.: Instrumentation, in: Interplanetary Dust, edited by Grün, E., Gustafson, B., Dermott, S., and Fechtig., H., pp. 387–438, Springer, 2001a.

Auer, S.: Instrumentation, pp. 385–444, Springer Berlin Heidelberg, Berlin, Heidelberg, ISBN 978-3-642-56428-4, https://doi.org/10.1007/978-3-642-56428-4_9, 2001b.

https://doi.org/10.5194/egusphere-2026-4440
Preprint. Discussion started: 17 August 2026

Baalmann, L. R., Hunziker, S., Péronne, A., Kirchner, J. W., Glassmeier, K. H., Malaspina, D. M., Wilson, III, L. B., Strähl, C., Chadda, S., and Sterken, V. J.: A solar rotation signature in cosmic dust: Frequency analysis of dust particle impacts on the Wind spacecraft, A&A, 689, A329, https://doi.org/10.1051/0004-6361/202450069, 2024.

Baalmann, L. R., Janisch, T., Hunziker, S., Strub, P., Krüger, H., Hofstetter, K., Sieber, M., and Sterken, V. J.: Interstellar dust measured in situ by Ulysses: New aspects of the particle size distribution and its modulation by the heliosheath, A&A, 698, A138, https://doi.org/10.1051/0004-6361/202453532, 2025.

Bale, S. D., Ullrich, R., Goetz, K., Alster, N., Cecconi, B., Dekkali, M., Lingner, N. R., Macher, W., Manning, R. E., McCauley, J., Monson, S. J., Oswald, T. H., and Pulupa, M.: The Electric Antennas for the STEREO/WAVES Experiment, Space Sci. Rev., 136, 529–547, https://doi.org/10.1007/s11214-007-9251-x, 2008.

Bale, S. D., Goetz, K., Harvey, P. R., Turin, P., Bonnell, J. W., Dudok de Wit, T., Ergun, R. E., MacDowall, R. J., Pulupa, M., André, M., Bolton, M., Bougeret, J. L., Bowen, T. A., Burgess, D., Cattell, C. A., Chandran, B. D. G., Chaston, C. C., Chen, C. H. K., Choi, M. K., Connerney, J. E. P., Cranmer, S., Diaz-Aguado, M., Donakowski, W., Drake, J. F., Farrell, W. M., Fergeau, P., Fermin, J., Fischer, J., Fox, N., Glaser, D., Goldstein, M., Gordon, D., Hanson, E., Harris, S. E., Hayes, L. M., Hinze, J. J., Hollweg, J. V., Horbury, T. S., Howard, R. A., Hoxie, V., Jannet, G., Karlsson, M., Kasper, J. C., Kellogg, P. J., Kien, M., Klimchuk, J. A., Krasnoselskikh, V. V., Krucker, S., Lynch, J. J., Maksimovic, M., Malaspina, D. M., Marker, S., Martin, P., Martinez-Oliveros, J., McCauley, J., McComas, D. J., McDonald, T., Meyer-Vernet, N., Moncuquet, M., Monson, S. J., Mozer, F. S., Murphy, S. D., Odom, J., Oliverson, R., Olson, J., Parker, E. N., Pankow, D., Phan, T., Quataert, E., Quinn, T., Ruplin, S. W., Salem, C., Seitz, D., Sheppard, D. A., Siy, A., Stevens, K., Summers, D., Szabo, A., Timofeeva, M., Vaivads, A., Velli, M., Yehle, A., Werthimer, D., and Wygant, J. R.: The FIELDS Instrument Suite for Solar Probe Plus. Measuring the Coronal Plasma and Magnetic Field, Plasma Waves and Turbulence, and Radio Signatures of Solar Transients, Space Science Reviews, 204, 49–82, 2016.

Battams, K., Knight, M. M., Kelley, M. S. P., Gallagher, B. M., Howard, R. A., and Stenborg, G.: Parker Solar Probe Observations of a Dust Trail in the Orbit of (3200) Phaethon, ApJS, 246, 64, https://doi.org/10.3847/1538-4365/ab6c68, 2020.

Battams, K., Gutarra-Leon, A. J., Gallagher, B. M., Knight, M. M., Stenborg, G., Tanner, S., Linton, M. G., Szalay, J. R., Kelley, M. S., and Howard, R. A.: Continued PSP/WISPR observations of a Phaethon-related dust trail, The Astrophysical Journal, 936, 81, 2022.

Battams, K., Ryabova, G. O., Gutarra-Leon, A. J., Szalay, J. R., Gallagher, B. M., and Cukier, W.: A Comparison of Geminid Models with the PSP/WISPR-observed Phaethon Dust Trail, ApJ, 985, 133, https://doi.org/10.3847/1538-4357/adc801, 2025.

Belheouane, S.: Nanoparticules dans le milieu interplanétaire : observations spatiales et théorie, Phd thesis, Université Pierre et Marie Curie, available at https://theses.hal.science/tel-01086185v1, 2014.

Belheouane, S., Zaslavsky, A., Meyer-Vernet, N., Issautier, K., Mann, I., and Maksimovic, M.: Detection of Interstellar Dust with STEREO/WAVES at 1 AU, Sol. Phys., 281, 501–506, https://doi.org/10.1007/s11207-012-9995-7, 2012.

Berg, O. E. and Grün, E.: Evidence of hyperbolic cosmic dust particles., Space Research XIII, pp. 1047–1055, 1973.

Bernardoni, E., Horányi, M., Doner, A., Piquette, M., Szalay, J. R., Poppe, A. R., James, D., Hunziker, S., Sterken, V., Strub, P., et al.: Student dust counter status report: The first 50 AU, The Planetary Science Journal, 3, 69, 2022.

Bertaux, J. L. and Blamont, J. E.: Possible evidence for penetration of interstellar dust into the Solar System, Nature, 262, 263–266, https://doi.org/10.1038/262263a0, 1976.

Biermann, L.: Solar corpuscular radiation and the interplanetary gas, The Observatory, 77, 109–110, 1957.

https://doi.org/10.5194/egusphere-2026-4440
Preprint. Discussion started: 17 August 2026

Bougeret, J. L., Kaiser, M. L., Kellogg, P. J., Manning, R., Goetz, K., Monson, S. J., Monge, N., Friel, L., Meetre, C. A., Perche, C., Sitruk, L., and Hoang, S.: Waves: The Radio and Plasma Wave Investigation on the Wind Spacecraft, Space Sci. Rev., 71, 231–263, https://doi.org/10.1007/BF00751331, 1995.

Bougeret, J. L., Goetz, K., Kaiser, M. L., Bale, S. D., Kellogg, P. J., Maksimovic, M., Monge, N., Monson, S. J., Astier, P. L., Davy, S., Dekkali, M., Hinze, J. J., Manning, R. E., Aguilar-Rodriguez, E., Bonnin, X., Briand, C., Cairns, I. H., Cattell, C. A., Cecconi, B., Eastwood, J., Ergun, R. E., Fainberg, J., Hoang, S., Huttunen, K. E. J., Krucker, S., Lecacheux, A., MacDowall, R. J., Macher, W., Mangeney, A., Meetre, C. A., Moussas, X., Nguyen, Q. N., Oswald, T. H., Pulupa, M., Reiner, M. J., Robinson, P. A., Rucker, H., Salem, C., Santolik, O., Silvis, J. M., Ullrich, R., Zarka, P., and Zouganelis, I.: S/WAVES: The Radio and Plasma Wave Investigation on the STEREO Mission, Space Sci. Rev., 136, 487–528, https://doi.org/10.1007/s11214-007-9298-8, 2008.

Brown, P., Spalding, R. E., ReVelle, D. O., Tagliaferri, E., and Worden, S. P.: The flux of small near-Earth objects colliding with the Earth, Nature, 420, 294–296, https://doi.org/10.1038/nature01238, 2002.

Burchell, M. J., Cole, M. J., and Ratcliff, P. R.: Light Flash and Ionization from Hypervelocity Impacts on Ice, Icarus, 122, 359–365, https://doi.org/https://doi.org/10.1006/icar.1996.0129, 1996.

Burns, J. A., Lamy, P. L., and Soter, S.: Radiation forces on small particles in the solar system, Icarus, 40, 1–48, https://doi.org/10.1016/0019-1035(79)90050-2, 1979.

Carrillo-Sanchez, J. D., Nesvorny, D., Pokorný, P., Janches, D., and Plane, J. M. C.: Sources of cosmic dust in the Earth's atmosphere, Geophysical Research Letters, 43, 11,979–11,986, 2016.

Carrillo-Sánchez, J. D., Gómez-Martín, J. C., Bones, D. L., Nesvorný, D., Pokorný, P., Benna, M., Flynn, G. J., and Plane, J. M. C.: Cosmic dust fluxes in the atmospheres of Earth, Mars, and Venus, Icarus, 335, 113395, https://doi.org/10.1016/j.icarus.2019.113395, 2020.

Chadda, S., Malaspina, D. M., Baalmann, L. R., Sterken, V. J., Hunziker, S., and Sternovsky, Z.: A solar rotation signature in cosmic dust observed in STEREO spacecraft data, A&A, 692, A257, https://doi.org/10.1051/0004-6361/202451950, 2024.

Colas, F., Zanda, B., Bouley, S., Jeanne, S., Malgoyre, A., Birlan, M., Blanpain, C., Gattacceca, J., Jorda, L., Lecubin, J., Marmo, C., Rault, J. L., Vaubaillon, J., Vernazza, P., Yohia, C., Gardiol, D., Nedelcu, A., Poppe, B., Rowe, J., Forcier, M., Koschny, D., Trigo-Rodriguez, J. M., Lamy, H., Behrend, R., Ferrière, L., Barghini, D., Buzzoni, A., Carbognani, A., Di Carlo, M., Di Martino, M., Knapic, C., Londero, E., Pratesi, G., Rasetti, S., Riva, W., Stirpe, G. M., Valsecchi, G. B., Volpicelli, C. A., Zorba, S., Coward, D., Drolshagen, E., Drolshagen, G., Hernandez, O., Jehin, E., Jobin, M., King, A., Nitschelm, C., Ott, T., Sanchez-Lavega, A., Toni, A., Abraham, P., Affaticati, F., Albani, M., Andreis, A., Andrieu, T., Anghel, S., Antaluca, E., Antier, K., Appéré, T., Armand, A., Ascione, G., Audureau, Y., Auxepaules, G., Avoscan, T., Baba Aissa, D., Bacci, P., Bădescu, O., Baldini, R., Baldo, R., Balestrero, A., Baratoux, D., Barbotin, E., Bardy, M., Basso, S., Bautista, O., Bayle, L. D., Beck, P., Bellitto, R., Belluso, R., Benna, C., Benammi, M., Beneteau, E., Benkhaldoun, Z., Bergamini, P., Bernardi, F., Bertaina, M. E., Bessin, P., Betti, L., Bettonvil, F., Bihel, D., Birnbaum, C., Blagoi, O., Blouri, E., Boacă, I., Boată, R., Bobiet, B., Bonino, R., Boros, K., Bouchet, E., Borgeot, V., Bouchez, E., Boust, D., Boudon, V., Bouman, T., Bourget, P., Brandenburg, S., Bramond, P., Braun, E., Bussi, A., Cacault, P., Caillier, B., Calegaro, A., Camargo, J., Caminade, S., Campana, A. P. C., Campbell-Burns, P., Canal-Domingo, R., Carell, O., Carreau, S., Cascone, E., Cattaneo, C., Cauhape, P., Cavier, P., Celestin, S., Cellino, A., Champenois, M., Chennaoui Aoudjehane, H., Chevrier, S., Cholvy, P., Chomier, L., Christou, A., Cricchio, D., Coadou, P., Cocaign, J. Y., Cochard, F., Cointin, S., Colombi, E., Colque Saavedra, J. P., Corp, L., Costa, M., Costard, F., Cottier, M., Cournoyer, P., Coustal, E., Cremonese, G., Cristea, O., Cuzon, J. C., D'Agostino, G., Daiffallah, K., Dănescu, C., Dardon, A., Dasse, T., Davadan, C., Debs, V., Defaix, J. P., Deleflie, F., D'Elia, M., De Luca, P., De Maria, P., Deverchère, P., Devillepoix, H., Dias, A., Di Dato, A., Di Luca, R., Dominici, F. M., Drouard, A., Dumont, J. L., Dupouy, P., Duvignac, L., Egal, A., Erasmus, N., Esseiva, N., Ebel, A., Eisengarten, B., Federici, F., Feral, S., Ferrant, G.,

https://doi.org/10.5194/egusphere-2026-4440
Preprint. Discussion started: 17 August 2026

Ferreol, E., Finitzer, P., Foucault, A., Francois, P., Frîncu, M., Froger, J. L., Gaborit, F., Gagliarducci, V., Galard, J., Gardavot, A., Garmier, M., Garnung, M., Gautier, B., Gendre, B., Gerard, D., Gerardi, A., Godet, J. P., Grandchamps, A., Grouiez, B., Groult, S., Guidetti, D., Giuli, G., and Hello, Y.: FRIPON: a worldwide network to track incoming meteoroids, A&A, 644, A53, https://doi.org/10.1051/0004-6361/202038649, 2020.

Collette, A., Drake, K., Mocker, A., Sternovsky, Z., Munsat, T., and Horányi, M.: Time-resolved temperature measurements in hypervelocity dust impact, Planetary and Space Science, pp. –, https://doi.org/10.1016/j.pss.2013.02.007, 2013.

Collette, A., Grün, E., Malaspina, D. M., and Sternovsky, Z.: Micrometeoroid impact charge yield for common spacecraft materials, Journal of Geophysical Research-Space Physics, 119, 6019–6026, 2014.

Collette, A., Meyer, G., Malaspina, D., and Sternovsky, Z.: Laboratory investigation of antenna signals from dust impacts on spacecraft, Journal of Geophysical Research: Space Physics, 120, 5298 – 5305, https://doi.org/10.1002/2015ja021198, 2015.

Collette, A., Malaspina, D. M., and Sternovsky, Z.: Characteristic temperatures of hypervelocity dust impact plasmas, Journal of Geophysical Research: Space Physics, 121, 8182 – 8187, https://doi.org/10.1002/2015ja022220, 2016.

Corbett, T., Doner, A., Horányi, M., Brandt, P., Grundy, W., Lisse, C. M., Parker, J., Peltier, L., Poppe, A. R., Singer, K. N., et al.: Production, Transport, and Destruction of Dust in the Kuiper Belt: The Effects of Refractory and Volatile Grain Compositions, The Astrophysical Journal Letters, 979, L50, 2025.

Cukier, W. Z. and Szalay, J. R.: Formation, Structure, and Detectability of the Geminids Meteoroid Stream, The Planetary Science Journal, 4, 109, https://doi.org/10.3847/psj/acd538, 2023.

Czechowski, A. and Mann, I.: Local interstellar cloud grains outside the heliopause, A&A, 410, 165–173, https://doi.org/10.1051/0004-6361:20031254, 2003a.

Czechowski, A. and Mann, I.: Penetration of interstellar dust grains into the heliosphere, Journal of Geophysical Research (Space Physics), 108, 8038, https://doi.org/10.1029/2003JA009917, 2003b.

Czechowski, A. and Mann, I.: Collisional vaporization of dust and production of gas in the β Pictoris dust disk, The Astrophysical Journal, 660, 1541–1555, 2007.

Czechowski, A. and Mann, I.: Formation and Acceleration of Nano Dust in the Inner Heliosphere, ApJ, 714, 89–99, https://doi.org/10.1088/0004-637X/714/1/89, 2010.

Czechowski, A. and Mann, I.: Nanodust Dynamics in Interplanetary Space, in: Nanodust in the Solar System: Discoveries and Interpretations, edited by Mann, I., Meyer-Vernet, N., and Czechowski, A., vol. 385 of *Astrophysics and Space Science Library*, p. 47, https://doi.org/10.1007/978-3-642-27543-2_4, 2012.

Czechowski, A. and Mann, I.: Dynamics of nanodust in the vicinity of a stellar corona: Effect of plasma corotation, Astronomy & Astrophysics, 652, A131, 2021.

DeForest, C. E., Gibson, S. E., Killough, R., Waltham, N. R., Beasley, M. N., Colaninno, R. C., Laurent, G. T., Seaton, D. B., Hughes, J. M., Guhathakurta, M., et al.: Polarimeter to Unify the Corona and Heliosphere (PUNCH), Solar Physics, 301, 16, 2026.

Devillepoix, H. A. R., Cupák, M., Bland, P. A., Sansom, E. K., Towner, M. C., Howie, R. M., Hartig, B. A. D., Jansen-Sturgeon, T., Shober, P. M., Anderson, S. L., and et al.: A Global Fireball Observatory, Planet. Space Sci., 191, 105036, https://doi.org/10.1016/j.pss.2020.105036, 2020.

Dietzel, H., Neukum, G., and Rauser, P.: Micrometeoroid simulation studies on metal targets, Journal of Geophysical Research (1896-1977), 77, 1375–1395, https://doi.org/https://doi.org/10.1029/JB077i008p01375, _eprint: https://agupubs.onlinelibrary.wiley.com/doi/pdf/10.1029/JB077i008p01375, 1972.

Draine, B. T.: Dust in Diffuse Interstellar Clouds, in: The First Symposium on the Infrared Cirrus and Diffuse Interstellar Clouds, edited by Cutri, R. M. and Latter, W. B., vol. 58 of *Astronomical Society of the Pacific Conference Series*, pp. 227–+, 1994.

Drapatz, S. and Michel, K. W.: Theory of shock-wave ionization upon high-velocity impact of micrometeorites., Zeitschrift Naturforschung Teil A, 29, 870–879, https://doi.org/10.1515/zna-1974-0606, 1974.

Dudok de Wit, T., Krasnoselskikh, V. V., Agapitov, O., Froment, C., Larosa, A., Bale, S. D., Bowen, T., Goetz, K., Harvey, P., Jannet, G., Kretzschmar, M., MacDowall, R. J., Malaspina, D., Martin, P., Page, B., Pulupa, M., and Revillet, C.: First Results From the SCM Search-Coil Magnetometer on Parker Solar Probe, Journal of Geophysical Research (Space Physics), 127, e30018, https://doi.org/10.1029/2021JA030018, 2022.

Eckart, L. M., Hillier, J. K., Postberg, F., Marchi, S., and Sternovsky, Z.: Linking meteorites to their asteroid parent bodies: The capabilities of dust analyzer instruments during asteroid flybys, Meteoritics & Planetary Science, 58, 1449–1468, https://doi.org/10.1111/maps.14060, 2023.

Eichhorn, G.: Measurements of the light flash produced by high velocity particle impact, Planetary and Space Science, 23, 1519–1525, https://doi.org/https://doi.org/10.1016/0032-0633(75)90005-7, 1975.

Eichhorn, G.: Analysis of the hypervelocity impact process from impact flash measurements, Planetary and Space Science, 24, 771–781, https://doi.org/https://doi.org/10.1016/0032-0633(76)90114-8, 1976.

Ens, T. A., Brown, P. G., Edwards, W. N., and Silber, E. A.: Infrasound production by bolides: A global statistical study, Journal of Atmospheric and Solar-Terrestrial Physics, 80, 208–229, https://doi.org/10.1016/j.jastp.2012.01.018, 2012.

Eyles, C. J., Harrison, R. A., Davis, C. J., Waltham, N. R., Shaughnessy, B. M., Mapson-Menard, H. C. A., Bewsher, D., Crothers, S. R., Davies, J. A., Simnett, G. M., Howard, R. A., Moses, J. D., Newmark, J. S., Socker, D. G., Halain, J. P., Defise, J. M., Mazy, E., and Rochus, P.: The Heliospheric Imagers Onboard the STEREO Mission, Sol. Phys., 254, 387–445, https://doi.org/10.1007/s11207-008-9299-0, 2009.

Farrell, W. M., Halekas, J. S., Horányi, M., Killen, R. M., Grava, C., Szalay, J. R., Benna, M., Clark, P. E., Collier, M. R., Colaprete, A., et al.: The dust, atmosphere, and plasma at the Moon, Reviews in Mineralogy and Geochemistry, 89, 563–609, 2023.

Fiege, K., Trieloff, M., Hillier, J. K., Guglielmino, M., Postberg, F., Srama, R., Kempf, S., and Blum, J.: Calibration of relative sensitivity factors for impact ionization detectors with high-velocity silicate microparticles, Icarus, 241, 336–345, https://doi.org/10.1016/j.icarus.2014.07.015, 2014.

Fielding, L. A., Hillier, J. K., Burchell, M. J., and Armes, S. P.: Space science applications for conducting polymer particles: synthetic mimics for cosmic dust and micrometeorites, Chem. Commun., 51, 16 886–16 899, https://doi.org/10.1039/C5CC07405C, publisher: The Royal Society of Chemistry, 2015.

Fletcher, A., Close, S., and Mathias, D.: Simulating plasma production from hypervelocity impacts, Phys. Plasmas, 22, 093 504, 2015.

Fox, N., Velli, M. C., Bale, S. D., Decker, R., Driesman, A., Howard, R. A., Kasper, J. C., Kinnison, J., Kusterer, M., Lario, D., Lockwood, M. K., McComas, D. J., Raouafi, N. E., and Szabo, A.: The Solar Probe Plus Mission: Humanity's First Visit to Our Star, Space Science Reviews, 204, 7–48, 2016.

Friichtenicht, J. F.: Two-Million-Volt Electrostatic Accelerator for Hypervelocity Research, Review of Scientific Instruments, 33, 209–212, https://doi.org/10.1063/1.1746548, 1962.

Frisch, P., Dorschner, J., Geiss, J., Greenberg, J., Grün, E., Landgraf, M., Hoppe, P., Jones, A., Kraetschmer, W., Linde, T., Morfill, G., Reach, W., Slavin, J., Svestka, J., Witt, A., and Zank, G.: Dust in the Local Interstellar Wind, in: Bulletin of the American Astronomical Society, vol. 31, pp. 661–+, 1998.

Frisch, P. C., Dorschner, J. M., Geiss, J., Greenberg, J. M., Grün, E., Landgraf, M., Hoppe, P., Jones, A. P., Krätschmer, W., Linde, T. J., Morfill, G. E., Reach, W., Slavin, J. D., Svestka, J., Witt, A. N., and Zank, G. P.: Dust in the Local Interstellar Wind, ApJ, 525, 492–516, https://doi.org/10.1086/307869, 1999.

Galindo, Y. and Lorena, A. C.: Deep transfer learning for meteor detection, in: Anais do XV Encontro Nacional de Inteligência Artificial e Computacional, pp. 528–537, SBC, KS 66202, 2018.

Godenko, E. A. and Izmodenov, V. V.: The unexpected role of heliospheric boundaries in facilitating interstellar dust penetration at 1-5 AU, A&A, 687, L4, https://doi.org/10.1051/0004-6361/202450257, 2024.

Goldsworthy, B. J., Burchell, M. J., Cole, M. J., Green, S. F., Leese, M. R., McBride, N., McDonnell, J. A. M., Müller, M., Grün, E., Srama, R., Armes, S. P., and Khan, M. A.: Laboratory calibration of the cassini cosmic dust analyser (CDA) using new, low density projectiles, Advances in Space Research, 29, 1139–1144, https://doi.org/https://doi.org/10.1016/S0273-1177(02)00129-1, 2002.

Goldsworthy, B. J., Burchell, M. J., Cole, M. J., Armes, S. P., Khan, M. A., Lascelles, S. F., Green, S. F., McDonnell, J. A. M., Srama, R., and Bigger, S. W.: Time of flight mass spectra of ions in plasmas produced by hypervelocity impacts of organic and mineralogical microparticles on a cosmic dust analyser, A&A, 409, 1151–1167, https://doi.org/10.1051/0004-6361:20031087, 2003.

Grün, E., Zook, H., Fechtig, H., and Giese, R.: Collisional balance of the meteoritic complex, Icarus, 62, 244–272, 1985.

Grün, E., Zook, H. A., Fechtig, H., and Giese, R. H.: Collisional balance of the meteoritic complex, Icarus, 62, 244–272, https://doi.org/10.1016/0019-1035(85)90121-6, 1985.

Grün, E., Fechtig, H., Kissel, J., Linkert, D., Maas, D., McDonnell, J. A. M., Morfill, G. E., Schwehm, G., Zook, H. A., and Giese, R. H.: The Ulyssses dust experiment, A&AS, 92, 411–423, 1992.

Grün, E., Zook, H., Baguhl, M., Balogh, A., Bame, S., Fechtig, H., Forsyth, R., Hanner, M., Horányi, M., Kissel, J., Lindblad, B.-A., Linkert, D., Linkert, G., Mann, I., McDonnel, J., Morfill, G., Phillips, J., Polanskey, C., Schwehm, G., Siddique, N., Staubach, P., Svestka, J., and Taylor, A.: Discovery of Jovian dust streams and interstellar grains by the Ulysses spacecraft, Nature, 362, 428–430, 1993.

Grün, E., Zook, H. A., Baguhl, M., Balogh, A., Bame, S. J., Fechtig, H., Forsyth, R., Hanner, M. S., Horanyi, M., Kissel, J., Lindblad, B. A., Linkert, D., Linkert, G., Mann, I., McDonnell, J. A. M., Morfill, G. E., Phillips, J. L., Polanskey, C., Schwehm, G., Siddique, N., Staubach, P., Svestka, J., and Taylor, A.: Discovery of Jovian dust streams and interstellar grains by the Ulysses spacecraft, Nature, 362, 428–430, https://doi.org/10.1038/362428a0, 1993.

Grün, E., Gustafson, B., Mann, I., Baguhl, M., Morfill, G. E., Staubach, P., Taylor, A., and Zook, H. A.: Interstellar dust in the heliosphere, A&A, 286, 915–924, 1994.

Grün, E., Staubach, P., Baguhl, M., Hamilton, D. P., Zook, H. A., Dermott, S., Gustafson, B. A., FECHTIG, H., Kissel, J., Linkert, D., Linkert, G., Srama, R., Hanner, M. S., Polanskey, C., Horanyi, M., Lindblad, B. A., Mann, I., McDonnell, J. A. M., Morfill, G. E., and Schwehm, G.: South-North and Radial Traverses through the Interplanetary Dust Cloud, Icarus, 129, 270–288, 1997.

Gural, P. S.: Advances in the meteor image processing chain using fast algorithms, deep learning, and empirical fitting, Planetary and Space Science, 182, 104847, https://doi.org/10.1016/j.pss.2020.104847, 2020.

Gurnett, D., Grün, E., Gallagher, D., Kurth, W., and Scarf, F.: Micron-sized particles detected near Saturn by the Voyager plasma wave instrument, Icarus, 53, 236–254, https://doi.org/10.1016/0019-1035(83)90145-8, 1983.

Gurnett, D. A., Kurth, W. S., and Scarf, F. L.: Plasma-Waves Near Saturn - Initial Results From Voyager-1, Science, 212, 235 – 239, http://adsabs.harvard.edu/abs/1981iowa.reptQ....G, 1981.

https://doi.org/10.5194/egusphere-2026-4440
Preprint. Discussion started: 17 August 2026

Gurnett, D. A., Kurth, W. S., Scarf, F. L., Burns, J. A., Cuzzi, J. N., and Grün, E.: Micron-sized particle impacts detected near Uranus by the Voyager 2 Plasma Wave Instrument, Journal of Geophysical Research: Space Physics, 92, 14 959–14 968, https://doi.org/10.1029/JA092iA13p14959, 1987.

Gurnett, D. A., Kurth, W. S., Granroth, L. J., Allendorf, S. C., and Poynter, R. L.: Micron-size particles detected near Neptune by the Voyager 2 plasma wave instrument, J. Geophys. Res., 96, 19 177–19 186, https://doi.org/10.1029/91JA01270, 1991.

Gurnett, D. A., Kurth, W. S., Kirchner, D. L., Hospodarsky, G. B., Averkamp, T. F., Zarka, P., Lecacheux, A., MANNING, R., Roux, A., Canu, P., Cornilleau-Wehrlin, N., Galopeau, P., Meyer, A., Bostrom, R., Gustafsson, G., Wahlund, J. E., Ahlen, L., Rucker, H. O., Ladreiter, H. P., Macher, W., Woolliscroft, L., Alleyne, H., Kaiser, M. L., Desch, M. D., Farrell, W. M., Harvey, C. C., Louarn, P., Kellogg, P. J., Goetz, K., and Pedersen, A.: The Cassini radio and plasma wave investigation, Space Science Reviews, 114, 395 – 463, http://gateway.webofknowledge.com/gateway/Gateway.cgi?GWVersion=2&SrcAuth=mekentosj&SrcApp=Papers&DestLinkType=FullRecord&DestApp=WOS&KeyUT=000227472300007, 2004.

Habbal, S. R., Arndt, M. B., Nayfeh, M. H., Arnaud, J., Johnson, J., Hegwer, S., Woo, R., Ene, A., and Habbal, F.: On the detection of the signature of silicon nanoparticle dust grains in coronal holes, The Astrophysical Journal Letters, 592, L87–L90, 2003.

Hahn, J. M., Zook, H. A., Cooper, B., and Sunkara, B.: Clementine Observations of the Zodiacal Light and the Dust Content of the Inner Solar System, Icarus, 158, 360–378, https://doi.org/10.1006/icar.2002.6881, 2002.

Hajra, R. and Sunny, J. V.: Corotating Interaction Regions during Solar Cycle 24: A Study on Characteristics and Geoeffectiveness, Sol. Phys., 297, 30, https://doi.org/10.1007/s11207-022-01962-1, 2022.

Haslebacher, N., Thomas, N., Mokhtari, O., Marschall, R., Cipriani, F., Arpa, R., Johansson, F. L., and Reynier, P.: The cometary model of dust environments (ComMoDE) N. Haslebacher et al., CEAS Space Journal, pp. 1–15, 2025.

Hayes, A. P., Vourlidas, A., and Howard, R. A.: Deriving the Electron Density of the Solar Corona from the Inversion of Total Brightness Measurements, ApJ, 548, 1081–1086, https://doi.org/10.1086/319029, 2001.

Hervig, M. E., Malaspina, D., Sterken, V., Wilson, L. B., Hunziker, S., and Bailey, S. M.: Decadal and Annual Variations in Meteoric Flux From Ulysses, Wind, and SOFIE Observations, Journal of Geophysical Research (Space Physics), 127, e2022JA030749, https://doi.org/10.1029/2022JA030749, 2022.

Hillier, J. K.: Impact ionisation mass spectrometry of polypyrrole-coated pyrrhotite microparticles.

Hillier, J. K.: Impact ionisation mass spectrometry of platinum-coated olivine and magnesite-dominated cosmic dust analogues, 2018.

Hillier, J. K., McBride, N., Green, S. F., Kempf, S., and Srama, R.: Modelling CDA mass spectra, Planetary and Space Science, 54, 1007–1013, https://doi.org/https://doi.org/10.1016/j.pss.2006.05.013, 2006.

Hillier, J. K., Sestak, S., Green, S. F., Postberg, F., Srama, R., and Trieloff, M.: The production of platinum-coated silicate nanoparticle aggregates for use in hypervelocity impact experiments, Planetary and Space Science, 57, 2081–2086, https://doi.org/https://doi.org/10.1016/j.pss.2009.09.019, 2009.

Hillier, J. K., Postberg, F., Sestak, S., Srama, R., Kempf, S., Trieloff, M., Sternovsky, Z., and Green, S. F.: Impact ionization mass spectra of anorthite cosmic dust analogue particles, J. Geophys. Res., 117, E09 002, 2012.

Hiltner, W.: On the Presence of Polarization in the Continuous Radiation of Stars. II., ApJ, 109, 471–+, 1949.

Hornung, K. and Drapatz, S.: Residual ionization after impact of large dust particles, in: The Comet Halley Probe. Plasma Environment, edited by Longdon, N., pp. 23–37, European space agency, Paris, 1981.

Hornung, K. and Kissel, J.: On shock wave impact ionization of dust particles, A&A, 291, 324–336, 1994.

https://doi.org/10.5194/egusphere-2026-4440
Preprint. Discussion started: 17 August 2026

Hornung, K. and Michel, K. W.: Equation-of-State Data of Solids from Shock Vaporization, The Journal of Chemical Physics, 56, 2072–2078, https://doi.org/10.1063/1.1677500, 1972.

Hornung, K., Malama, Y. G., and Thoma, K.: Modeling of the very high velocity impact process with respect to in-situ ionization measurements, Advances in Space Research, 17, 77–86, https://doi.org/https://doi.org/10.1016/0273-1177(95)00762-4, 1996.

Horányi, M., Sternovsky, Z., Lankton, M., Dumont, C., Gagnard, S., Gathright, D., Grün, E., Hansen, D., James, D., Kempf, S., Lamprecht, B., Srama, R., Szalay, J. R., and Wright, G.: The Lunar Dust Experiment (LDEX) Onboard the Lunar Atmosphere and Dust Environment Explorer (LADEE) Mission, Space Science Reviews, 185, 93–113, https://doi.org/10.1007/s11214-014-0118-7, 2014.

Horányi, M., Tucker, S., Sternovsky, Z., Tyagi, K., Knappmiller, S., Ayari, E., Mikula, R., Szalay, J. R., Kempf, S., Bollendonk, C., Gurnee, R., Fisher, M., McCann, D., Coakley, L., Gurst, S., Davis, K., Bramer, S., Miller, M., Neher, J., Newcomb, G., Oberg, S., Sayler, J., Wade, S., Deaton, T., Doner, A., Fontanese, J., Grün, E., Miller, C., Wing, R., Holguin, L., Fowle, M., Hellickson, T., Rhode, A., Brennan, N., Hansen, D., O'Connor, D., Kostovny, A., Shaver, S., Looney, K., Turner, N. J., Hillier, J., Postberg, F., Srama, R., Christian, E., Gkioulidou, M., McComas, D. J., and Schwadron, N. A.: Interstellar Dust Experiment (IDEX) Onboard NASA's Interstellar Mapping And Acceleration Probe (IMAP), Space Science Reviews, 221, 102, https://doi.org/10.1007/s11214-025-01230-1, 2025a.

Horányi, M., Tucker, S., Sternovsky, Z., Tyagi, K., Knappmiller, S., Ayari, E., Mikula, R., Szalay, J. R., Kempf, S., Bollendonk, C., Gurnee, R., Fisher, M., McCann, D., Coakley, L., Gurst, S., Davis, K., Bramer, S., Miller, M., Neher, J., Newcomb, G., Oberg, S., Sayler, J., Wade, S., Deaton, T., Doner, A., Fontanese, J., Grün, E., Miller, C., Wing, R., Holguin, L., Fowle, M., Hellickson, T., Rhode, A., Brennan, N., Hansen, D., O'Connor, D., Kostovny, A., Shaver, S., Looney, K., Turner, N. J., Hillier, J., Postberg, F., Srama, R., Christian, E., Gkioulidou, M., McComas, D. J., and Schwadron, N. A.: Interstellar Dust Experiment (IDEX) Onboard NASA's Interstellar Mapping And Acceleration Probe (IMAP), Space Science Reviews, 221, 102, https://doi.org/10.1007/s11214-025-01230-1, 2025b.

Howard, R. A., Sheeley, Jr., N. R., Michels, D. J., and Koomen, M. J.: Coronal mass ejections: 1979-1981, J. Geophys. Res., 90, 8173–8192, https://doi.org/10.1029/JA090iA09p08173, 1985.

Howard, R. A., Moses, J. D., Vourlidas, A., Newmark, J. S., Socker, D. G., Plunkett, S. P., Korendyke, C. M., Cook, J. W., Hurley, A., Davila, J. M., Thompson, W. T., St Cyr, O. C., Mentzell, E., Mehalick, K., Lemen, J. R., Wuelser, J. P., Duncan, D. W., Tarbell, T. D., Wolfson, C. J., Moore, A., Harrison, R. A., Waltham, N. R., Lang, J., Davis, C. J., Eyles, C. J., Mapson-Menard, H., Simnett, G. M., Halain, J. P., Defise, J. M., Mazy, E., Rochus, P., Mercier, R., Ravet, M. F., Delmotte, F., Auchere, F., Delaboudiniere, J. P., Bothmer, V., Deutsch, W., Wang, D., Rich, N., Cooper, S., Stephens, V., Maahs, G., Baugh, R., McMullin, D., and Carter, T.: Sun Earth Connection Coronal and Heliospheric Investigation (SECCHI), Space Sci. Rev., 136, 67–115, https://doi.org/10.1007/s11214-008-9341-4, 2008.

Howard, R. A., Vourlidas, A., Bothmer, V., Colaninno, R. C., DeForest, C. E., Gallagher, B., Hall, J. R., Hess, P., Higginson, A. K., Korendyke, C. M., Kouloumvakos, A., Lamy, P. L., Liewer, P. C., Linker, J., Linton, M., Penteado, P., Plunkett, S. P., Poirier, N., Raouafi, N. E., Rich, N., Rochus, P., Rouillard, A. P., Socker, D. G., Stenborg, G., Thernisien, A. F., and Viall, N. M.: Near-Sun observations of an F-corona decrease and K-corona fine structure, Nature, 576, 232–236, https://doi.org/10.1038/s41586-019-1807-x, 2019.

Howard, R. A., Vourlidas, A., Colaninno, R. C., Korendyke, C. M., Plunkett, S. P., Carter, M. T., Wang, D., Rich, N., Lynch, S., Thurn, A., Socker, D. G., Thernisien, A. F., Chua, D., Linton, M. G., Koss, S., Tun-Beltran, S., Dennison, H., Stenborg, G., McMullin, D. R., Hunt, T., Baugh, R., Clifford, G., Keller, D., Janesick, J. R., Tower, J., Grygon, M., Farkas, R., Hagood, R., Eisenhauer, K., Uhl, A., Yerushalmi, S., Smith, L., Liewer, P. C., Velli, M. C., Linker, J., Bothmer, V., Rochus, P., Halain, J. P., Lamy, P. L., Auchère, F., Harrison, R. A., Rouillard, A., Patsourakos, S., St. Cyr, O. C., Gilbert, H., Maldonado, H., Mariano, C., and Cerullo, J.: The Solar Orbiter Heliospheric Imager (SoloHI), A&A, 642, A13, https://doi.org/10.1051/0004-6361/201935202, 2020.

https://doi.org/10.5194/egusphere-2026-4440
Preprint. Discussion started: 17 August 2026

Hunziker, S., Moragas-Klostermeyer, G., Hillier, J. K., Fielding, L. A., Hornung, K., Lovett, J. R., Armes, S. P., Fontanese, J., James, D., Hsu, H. W., Herrmann, I., Fechler, N., Poch, O., Pommerol, A., Srama, R., Malaspina, D., and Sterken, V. J.: Impact ionization dust detection with compact, hollow and fluffy dust analogs, Planet. Space Sci., 220, 105536, https://doi.org/10.1016/j.pss.2022.105536, 2022.

Ijaz, S., Vaverka, J., Šafránková, J., and Němeček, Z.: Study of Dust Impact Signals around Mars Using MAVEN/LPW Observations, ApJ, 970, 175, https://doi.org/10.3847/1538-4357/ad5670, 2024.

Ise, R. and Cagle, E. H.: The Apollo Telescope Mount on Skylab., Acta Astronautica, 1, 1315–1329, https://doi.org/10.1016/0094-5765(74)90078-2, 1974.

Ishimoto, H. and Mann, I.: Modeling the particle mass distribution within 1 AU of the Sun, Planetary and Space Science, 47, 225–232, 1998.

Janches, D., Close, S., Hormaechea, J. L., Swarnalingam, N., Murphy, A., O'Connor, D., Vandepeer, B., Fuller, B., Fritts, D. C., and Brunini, C.: THE SOUTHERN ARGENTINA AGILE METEOR RADAR ORBITAL SYSTEM (SAAMER-OS): AN INITIAL SPORADIC METEOROID ORBITAL SURVEY IN THE SOUTHERN SKY, The Astrophysical Journal, 809, 1–16, 2015.

Jannet, G., Dudok de Wit, T., Krasnoselskikh, V., Kretzschmar, M., Fergeau, P., Bergerard-Timofeeva, M., Agrapart, C., Brochot, J. Y., Chalumeau, G., Martin, P., Revillet, C., Bale, S. D., Maksimovic, M., Bowen, T. A., Brysbaert, C., Goetz, K., Guilhem, E., Harvey, P. R., Leray, V., and Lorfèvre, E.: Measurement of Magnetic Field Fluctuations in the Parker Solar Probe and Solar Orbiter Missions, Journal of Geophysical Research (Space Physics), 126, e28543, https://doi.org/10.1029/2020JA028543, 2021.

Jenniskens, P., Gural, P. S., Dynneson, L., Grigsby, B. J., Newman, K. E., Borden, M., Koop, M., and Holman, D.: CAMS: Cameras for Allsky Meteor Surveillance to establish minor meteor showers, Icarus, 216, 40–61, 2011.

Jian, L.: Stream Interaction Regions (SIRs) from *Wind* and ACE Data during 1995 – 2009, https://izw1.caltech.edu/ACE/ASC/DATA/level3/SIR_List_1995_2009_Jian.pdf, 2021.

Jian, L., Russell, C. T., Luhmann, J. G., and Skoug, R. M.: Properties of Stream Interactions at One AU During 1995 – 2004, Sol. Phys., 239, 337–392, https://doi.org/10.1007/s11207-006-0132-3, 2006.

Jones, G. H., Morrill, J. S., Hammer, D., Lisse, C. M., Farnham, T. L., and Lawrence, G. R.: Comet C/2002 V1 (NEAT) - Evidence of solar wind effects on a comet's ion and dust tails at 0.1 AU., in: AAS/Division for Planetary Sciences Meeting Abstracts #36, vol. 36 of *AAS/Division for Planetary Sciences Meeting Abstracts*, p. 21.02, 2004.

Jones, G. H., Morrill, J. S., Battams, K., Owens, M. J., Howard, R. A., and Stenborg, G. A.: Comet C/2006 P1 (McNaught): Observations by STEREO and SOHO, in: European Planetary Science Congress 2008, p. 832, 2008.

Juhász, A. and Horányi, M.: Dynamics and distribution of nano-dust particles in the inner solar system, Geophys. Res. Lett., 40, 2500–2504, https://doi.org/10.1002/grl.50535, 2013.

Kaiser, M. L., Kucera, T. A., Davila, J. M., St. Cyr, O. C., Guhathakurta, M., and Christian, E.: The STEREO Mission: An Introduction, Space Sci. Rev., 136, 5–16, https://doi.org/10.1007/s11214-007-9277-0, 2008.

Kellogg, P. J.: Note on the Pantellini et al. process for dust impact signals on spacecraft, Journal of Geophysical Research (Space Physics), 122, 63–70, https://doi.org/10.1002/2016JA023073, 2017.

Kellogg, P. J., Goetz, K., and Monson, S. J.: Are STEREO Single Hits Dust Impacts?, Journal of Geophysical Research (Space Physics), 123, 7211–7219, https://doi.org/10.1029/2018JA025554, 2018.

Kempf, S., Srama, R., Horányi, M., Burton, M., Helfert, S., Moragas-Klostermeyer, G., Roy, M., and Grün, E.: High-velocity streams of dust originating from Saturn, Nature, 433, 289–291, 2005.

Kempf, S., Tucker, S., Altobelli, N., Briois, C., Cable, M. L., Grün, E., Gudipati, M. S., Henderson, B. L., Hsu, H.-W., Hand, K., Horanyi, M., Postberg, F., Schmidt, J., Srama, R., Sternovsky, Z., Tobie, G., Zolotov, M. Y., Belting, C., Bortfeldt, S., Bouwman, J., Brennan, N., Bryant, K., Cassidy, T., Crotser, D., Curtin, A., DeVito, E., Ebuen, D., Faber, N., Fisher, M., Fontanese, J., Fowle, M., Frank, W., Gurst, S., Haselschwardt, S., Hoxie, V., Hubbell, K., James, D., Kien, M., Knappmiller, S., Kohnert, R., Lampe, A., Lankton, M., Lev-Tov, S., McGinn, C., Miller, M., Newcomb, G., Oberg, S., O'Brien, L., Pilewskie, K., Polson, S., Scarffe-Barrett, V., Summers, D., Wade, S., Ware, A., Yehle, A., Wuerthner, C., Garcia Arteaga, A., Oaida, B., Eberl, C., Fitton, P., Goode, W., Levin, Z., Lowry, G., Stanley, J., Tracy, A., Ulibarri, Z., Williams, E., Yoke, C., Southworth, B. S., Hillier, J. K., Khawaja, N., Klenner, F., Napoleoni, M., Simolka, J., and Sioeng, J.: SUDA: A SUrface Dust Analyser for Compositional Mapping of the Galilean Moon Europa, Space Science Reviews, 221, 10, https://doi.org/10.1007/s11214-025-01134-0, 2025.

Kimura, H. and Mann, I.: Brightness of the solar F-corona, Earth, Planets and Space, 50, 493–499, https://doi.org/10.1186/BF03352140, 1998a.

Kimura, H. and Mann, I.: Radiation pressure cross section for fluffy aggregates., Journal of Quantitative Spectroscopy and Radiative Transfer, 60, 425–438, 1998b.

Kimura, H. and Mann, I.: The Electric Charging of Interstellar Dust in the Solar System and Consequences for Its Dynamics, ApJ, 499, 454–462, 1998.

Kimura, H., Mann, I., and Jessberger, E. K.: Composition, structure, and size distribution of dust in the local interstellar cloud, The Astrophysical Journal, 583, 314–321, 2003a.

Kimura, H., Mann, I., and Jessberger, E. K.: Elemental abundances and mass densities of dust and gas in the local interstellar cloud, The Astrophysical Journal, 582, 846–858, 2003b.

Kissel, J. and Krueger, F. R.: Ion formation by impact of fast dust particles and comparison with related techniques, Applied Physics A, 42, 69–85, https://doi.org/10.1007/BF00618161, 1987.

Knabe, W. and Krueger, F. R.: Ion Formation from Alkali Iodide Solids by Swift Dust Particle Impact, Zeitschrift für Naturforschung A, 37, https://doi.org/10.1515/zna-1982-1203, 1982.

Knight, M. M., A'Hearn, M. F., Biesecker, D. A., Faury, G., Hamilton, D. P., Lamy, P., and Llebaria, A.: Photometric Study of the Kreutz Comets Observed by SOHO from 1996 to 2005, AJ, 139, 926–949, https://doi.org/10.1088/0004-6256/139/3/926, 2010.

Kobayashi, H., Watanabe, S.-i., Kimura, H., and Yamamoto, T.: Dust ring formation due to sublimation of dust grains drifting radially inward by the Poynting-Robertson drag: An analytical model, Icarus, 201, 395–405, https://doi.org/10.1016/j.icarus.2009.01.002, 2009.

Kočiščák, S., Theodorsen, A., and Mann, I.: The distribution of the near-solar bound dust grains detected with Parker Solar Probe, Astronomy & Astrophysics, 692, A68, 2024.

Kolokolova, L., Kimura, H., and Mann, I.: Characterization of dust particles using photopolarimetric data: example of cometary dust, in: Photopolarimetry in remote sensing, pp. 431–454, Springer, 2006.

Koseki, M.: EDMOND and SonotaCo net, eMeteorNews, 4, 220–224, 2019.

Koutchmy, S. and Lamy, P. L.: The F-Corona and the Circum-Solar Dust Evidences and Properties (ir), in: IAU Colloq. 85: Properties and Interactions of Interplanetary Dust, edited by Giese, R. H. and Lamy, P., p. 63, https://doi.org/10.1007/978-94-009-5464-9_14, 1985.

Kočiščák, S., Kvammen, A., Mann, I., Sørbye, S. H., Theodorsen, A., and Zaslavsky, A.: Modeling Solar Orbiter dust detection rates in the inner heliosphere as a Poisson process, A&A, 670, A140, https://doi.org/10.1051/0004-6361/202245165, 2023.

Kočiščák, S., Kvammen, A., Mann, I., Meyer-Vernet, N., Píša, D., Souček, J., Theodorsen, A., Vaverka, J., and Zaslavsky, A.: Impact Ionization Double Peaks Analyzed In High Temporal Resolution On Solar Orbiter, Annales Geophysicae, 42, 191–212, https://doi.org/10.5194/angeo-42-191-2024, 2024.

https://doi.org/10.5194/egusphere-2026-4440
Preprint. Discussion started: 17 August 2026

Kočiščák, S.: Understanding Inner Solar System Dust Environment Through In-Situ Measurements (PhD thesis), UiT Norges arktiske universitet, 2024.

Kočiščák, S., Fredriksen, A., DeLuca, M., Pavlů, J., and Sternovsky, Z.: Effective Temperatures of Olivine Dust Impact Plasmas, IEEE Transactions on Plasma Science, 48, 4298–4304, https://doi.org/10.1109/TPS.2020.3033578, 2020.

Krüger, H., Strub, P., Grün, E., and Sterken, V. J.: Sixteen Years of Ulysses Interstellar Dust Measurements in the Solar System. I. Mass Distribution and Gas-to-dust Mass Ratio, ApJ, 812, 139, https://doi.org/10.1088/0004-637X/812/2/139, 2015.

Krüger, H., Strub, P., Sommer, M., Altobelli, N., Kimura, H., Lohse, A.-K., Grün, E., and Srama, R.: Helios spacecraft data revisited: detection of cometary meteoroid trails by following in situ dust impacts, Astronomy and Astrophysics, 643, A96, 2020.

Krüger, H., Strub, P., and Grün, E.: Ulysses spacecraft in situ detections of cometary dust trails, Philosophical Transactions A, 382, 20230 200, 2024.

Kvammen, A., Wickstrøm, K., Kociscak, S., Vaverka, J., Nouzak, L., Zaslavsky, A., Rackovic Babic, K., Gjelsvik, A., Pisa, D., Soucek, J., and Mann, I.: Machine learning detection of dust impact signals observed by the Solar Orbiter, Annales Geophysicae, 41, 69–86, https://doi.org/10.5194/angeo-41-69-2023, 2023.

Landgraf, M.: Modeling the motion and distribution of interstellar dust inside the heliosphere, J. Geophys. Res., 105, 10 303–10 316, https://doi.org/10.1029/1999JA900243, 2000.

Le Chat, G., Zaslavsky, A., Meyer-Vernet, N., Issautier, K., Belheouane, S., Pantellini, F., Maksimovic, M., Zouganelis, I., Bale, S. D., and Kasper, J. C.: Interplanetary Nanodust Detection by the Solar Terrestrial Relations Observatory/WAVES Low Frequency Receiver, Sol. Phys., 286, 549–559, https://doi.org/10.1007/s11207-013-0268-x, 2013.

Le Chat, G., Issautier, K., Zaslavsky, A., Pantellini, F., Meyer-Vernet, N., Belheouane, S., and Maksimovic, M.: Effect of the Interplanetary Medium on Nanodust Observations by the Solar Terrestrial Relations Observatory, Sol. Phys., 290, 933–942, https://doi.org/10.1007/s11207-015-0651-x, 2015.

Lee, N., Close, S., Lauben, D., Linscott, I., Goel, A., Johnson, T., Yee, J., Fletcher, A., Srama, R., Bugiel, S., Mocker, A., Colestock, P., and GREEN, S.: Measurements of freely-expanding plasma from hypervelocity impacts, International Journal of Impact Engineering, 44, 40 – 49, https://doi.org/10.1016/j.ijimpeng.2012.01.002, 2012.

Leinert, C. and Blanck, B.: Stability and Symmetry of Zodiacal Light Polarization in the Antisolar Hemisphere, A&A, 105, 364, 1982.

Leinert, C., Link, H., Pitz, E., and Giese, R. H.: Interpretation of a rocket photometry of the inner zodiacal light., A&A, 47, 221–230, 1976.

Leinert, C., Hanner, M., and Pitz, E.: On the spatial distribution of interplanetary dust near 1 AU., A&A, 63, 183–187, 1978.

Leinert, C., Hanner, M., Richter, I., and Pitz, E.: The plane of symmetry of interplanetary dust in the inner solar system., A&A, 82, 328–336, 1980.

Leinert, C., Richter, I., Pitz, E., and Planck, B.: The zodiacal light from 1.0 to 0.3 A.U. as observed by the HELIOS space probes, A&A, 103, 177–188, 1981.

Leinert, C., Richter, I., Pitz, E., and Hanner, M.: HELIOS zodiacal light measurements - a tabulated summary., A&A, 110, 355–357, 1982.

Li, A. and Mann, I.: Nanodust in the interstellar medium in comparison to the solar system, in: Nanodust in the Solar System: Discoveries and Interpretations, pp. 5–30, Springer, 2012.

Linde, T. and Gombosi, T.: Interstellar dust filtration at the heliospheric interface, J. Geophys. Res., 105, 10 411–10 418, http://adsabs.harvard.edu/cgi-bin/nph-bib_query?bibcode=2000JGR...10510411L{&}db_key=AST, 2000.

Linsky, J., Redfield, S., Ryder, D., and Moebius, E.: Inhomogeneity in the local ISM and its relation to the heliosphere, Space Science Reviews, 218, 16, 2022.

https://doi.org/10.5194/egusphere-2026-4440
Preprint. Discussion started: 17 August 2026

Linsky, J. L. and Redfield, S.: Creating a new paradigm for the local interstellar medium–A perspective, Frontiers in Astronomy and Space Sciences, 10, 1119 589, 2023.

Lisse, C. M., Farnham, T. L., Fernandez, Y. R., Lawrence, G. R., Jones, G. H., Morill, J. S., Andrews, M. D., and Hammer, D.: SOHO Observations of Comet C/2002 V1 NEAT, in: AAS/Division for Planetary Sciences Meeting Abstracts #35, vol. 35 of *AAS/Division for Planetary Sciences Meeting Abstracts*, p. 47.09, 2003.

Love, S. G. and Brownlee, D. E.: A Direct Measurement of the Terrestrial Mass Accretion Rate of Cosmic Dust, Science, 262, 550, 1993.

MacQueen, R. M., Gosling, J. T., Hildner, E., Munro, R. H., Poland, A. I., and Ross, C. L.: The High Altitude Observatory white light coronagraph, in: Instrumentation in Astronomy II, edited by Menzel, D. H., Larmore, L., and Crawford, D., vol. 44 of *Society of Photo-Optical Instrumentation Engineers (SPIE) Conference Series*, pp. 207–212, https://doi.org/10.1117/12.953943, 1974.

Maksimovic, M., Bale, S. D., Chust, T., Khotyaintsev, Y., Krasnoselskikh, V., Kretzschmar, M., Plettemeier, D., Rucker, H. O., Souček, J., Steller, M., Štverák, Š., Trávníček, P., Vaivads, A., Chaintreuil, S., Dekkali, M., Alexandrova, O., Astier, P.-A., Barbary, G., Bérard, D., Bonnin, X., Boughedada, K., Cecconi, B., Chapron, F., Chariet, M., Collin, C., de Conchy, Y., Dias, D., Guéguen, L., Lamy, L., Leray, V., Lion, S., Malac-Allain, L. R., Matteini, L., Nguyen, Q. N., Pantellini, F., Parisot, J., Plasson, P., Thijs, S., Vecchio, A., Fratter, I., Bellouard, E., Lorfèvre, E., Danto, P., Julien, S., Guilhem, E., Fiachetti, C., Sanisidro, J., Laffaye, C., Gonzalez, F., Pontet, B., Quéruel, N., Jannet, G., Fergeau, P., Brochot, J.-Y., Cassam-Chenai, G., Dudok de Wit, T., Timofeeva, M., Vincent, T., Agrapart, C., Delory, G. T., Turin, P., Jeandet, A., Leroy, P., Pellion, J.-C., Bouzid, V., Katra, B., Piberne, R., Recart, W., Santolík, O., Kolmašová, I., Krupař, V., Krupařová, O., Píša, D., Uhlíř, L., Lán, R., Baše, J., Ahlèn, L., André, M., Bylander, L., Cripps, V., Cully, C., Eriksson, A., Jansson, S.-E., Johansson, E. P. G., Karlsson, T., Puccio, W., Břínek, J., Öttacher, H., Panchenko, M., Berthomier, M., Goetz, K., Hellinger, P., Horbury, T. S., Issautier, K., Kontar, E., Krucker, S., Le Contel, O., Louarn, P., Martinović, M., Owen, C. J., Retino, A., Rodríguez-Pacheco, J., Sahraoui, F., Wimmer-Schweingruber, R. F., Zaslavsky, A., and Zouganelis, I.: The Solar Orbiter Radio and Plasma Waves (RPW) instrument, A&A, 642, A12, https://doi.org/10.1051/0004-6361/201936214, 2020.

Malaspina, D. M. and Wilson, L. B.: A database of interplanetary and interstellar dust detected by the Wind spacecraft, Journal of Geophysical Research (Space Physics), 121, 9369–9377, https://doi.org/10.1002/2016JA023209, 2016.

Malaspina, D. M., Horányi, M., Zaslavsky, A., Goetz, K., Wilson, L. B., and Kersten, K.: Interplanetary and interstellar dust observed by the Wind/WAVES electric field instrument, Geophysical Research Letters, 41, 266–272, https://doi.org/10.1002/2013GL058786, 2014.

Malaspina, D. M., O'Brien, L. E., Thayer, F., Sternovsky, Z., and Collette, A.: Revisiting STEREO interplanetary and interstellar dust flux and mass estimates, Journal of Geophysical Research: Space Physics, 120, 6085 – 6100, https://doi.org/10.1002/2015ja021352, 2015.

Malaspina, D. M., Ergun, R. E., Bolton, M., Kien, M., Summers, D., Stevens, K., Yehle, A., Karlsson, M., Hoxie, V. C., Bale, S. D., and Goetz, K.: The Digital Fields Board for the FIELDS instrument suite on the Solar Probe Plus mission: Analog and digital signal processing, Journal of Geophysical Research-Space Physics, 121, 5088–5096, 2016.

Malaspina, D. M., Szalay, J. R., Pokorný, P., Page, B., Bale, S. D., Bonnell, J. W., de Wit, T. D., Goetz, K., Goodrich, K., Harvey, P. R., MacDowall, R. J., and Pulupa, M.: Observations of Inner Heliospheric Dust Variability, 2020.

Malaspina, D. M., Stenborg, G., Mehoke, D., Al-Ghazwi, A., Shen, M. M., Hsu, H.-W., Iyer, K., Bale, S. D., and Dudok de Wit, T.: Clouds of Spacecraft Debris Liberated by Hypervelocity Dust Impacts on Parker Solar Probe, ApJ, 925, 27, https://doi.org/10.3847/1538-4357/ac3bbb, 2022.

Malaspina, D. M., Toma, A., Szalay, J. R., Pulupa, M., Pokorný, P., Bale, S. D., and Goetz, K.: A Dust Detection Database for the Inner Heliosphere Using the Parker Solar Probe Spacecraft, The Astrophysical Journal Supplement Series, 266, 21, https://doi.org/10.3847/1538-4365/acca75, 2023.

https://doi.org/10.5194/egusphere-2026-4440
Preprint. Discussion started: 17 August 2026

Malaspina, D. M., Szalay, J. R., Mazurkiewicz, A., Lee-Bellows, D., and Landis, M. E.: A Search for Meteoroid Streams and Their Sources in the Near-Sun Zodiacal Dust Cloud, ApJ, 992, 76, https://doi.org/10.3847/1538-4357/ae0184, 2025.

Mann, I.: Interstellar Dust in the Solar System, ARA&A, 48, 173–203, https://doi.org/10.1146/annurev-astro-081309-130846, 2010.

Mann, I. and Czechowski, A.: Dust destruction and ion formation in the inner solar system, The Astrophysical Journal Letters, 621, L73–L76, 2005.

Mann, I. and Czechowski, A.: Dust observations from Parker Solar Probe: Dust ejection from the inner Solar System, Astronomy and Astrophysics, pp. 1–9, 2020.

Mann, I. and Czechowski, A.: Dust observations from Parker Solar Probe: dust ejection from the inner Solar System, A&A, 650, A29, https://doi.org/10.1051/0004-6361/202039362, 2021.

Mann, I. and Kimura, H.: Interstellar dust properties derived from mass density, mass distribution, and flux rates in the heliosphere, Journal of Geophysical Research, 105, 10 317–10 328, https://doi.org/10.1029/1999JA900404, 2000.

Mann, I. and Murad, E.: On the existence of silicon nanodust near the sun, The Astrophysical Journal Letters, 624, L125–L128, 2005.

Mann, I., Krivov, A., and Kimura, H.: Dust Cloud near the Sun, Icarus, 146, 568–582, https://doi.org/10.1006/icar.2000.6419, 2000.

Mann, I., Kimura, H., Biesecker, D. A., Tsurutani, B. T., Grün, E., McKibben, R. B., Liou, J.-C., MacQueen, R. M., Mukai, T., Guhathakurta, M., and Lamy, P.: Dust Near The Sun, Space Science Reviews, 110, 269–305, 2004.

Mann, I., Köhler, M., Kimura, H., Cechowski, A., and Minato, T.: Dust in the solar system and in extra-solar planetary systems, The Astronomy and Astrophysics Review, 13, 159–228, 2006.

Mann, I., Murad, E., and Czechowski, A.: Nanoparticles in the inner solar system, Planetary and Space Science, 55, 1000–1009, https://doi.org/10.1016/j.pss.2006.11.015, 2007.

Mann, I., Meyer-Vernet, N., and Czechowski, A.: Dust in the planetary system: Dust interactions in space plasmas of the solar system, Physics reports, 536, 1–39, 2014.

Mann, I., Nouzák, L., Vaverka, J., Antonsen, T., Fredriksen, A., Issautier, K., Malaspina, D., Meyer-Vernet, N., Pavlů, J., Sternovsky, Z., Stude, J., Ye, S., and Zaslavsky, A.: Dust observations with antenna measurements and its prospects for observations with Parker Solar Probe and Solar Orbiter, Annales Geophysicae, 37, 1121 – 1140, https://doi.org/10.5194/angeo-37-1121-2019, 2019.

May, B. H.: A survey of radial velocities in the zodiacal dust cloud, Ph.D. thesis, Imperial College, London, 2008.

McBride, N. and McDonnell, J. a. m.: Meteoroid impacts on spacecraft:. sporadics, streams, and the 1999 Leonids, Planet. Space Sci., 47, 1005–1013, https://doi.org/10.1016/S0032-0633(99)00023-9, 1999.

McComas, D., Christian, E. R., Schwadron, N. A., Fox, N., Westlake, J., Allegrini, F., Baker, D., Biesecker, D., Bzowski, M., Clark, G., et al.: Interstellar mapping and acceleration probe (IMAP): A new NASA mission, Space science reviews, 214, 1–54, 2018.

McComas, D. J., Christian, E. R., Schwadron, N. A., Gkioulidou, M., Allegrini, F., Baker, D. N., Bzowski, M., Clark, G., Cohen, C. M. S., Cohen, I., Collura, C., Cully, M. J., Dalla, S., Desai, M. I., Driesman, A., Eng, D., Fox, N. J., Funsten, H. O., Fuselier, S. A., Galli, A., Giacalone, J., Hahn, J., Hegarty, K. P., Horbury, T., Horanyi, M., Kistler, L. M., Kubiak, M. A., Kubota, S., Livi, S., Lugaz, N., Lee, C. O., Luhmann, J., Matthaeus, W., Mitchell, D. G., Mitchell, J. G., Moebius, E., Pope, S., Provornikova, E., Rankin, J. S., Reisenfeld, D. B., Reno, C., Richardson, J. D., Russell, C. T., Shaw-Lecerf, M. M., Scherrer, J., Skoug, R. M., Shen, M. M., Spence, H. E., Sternovsky, Z., Strumik, M., Szalay, J. R., Tapley, M., Tokumaru, M., Turner, D. L., Weidner, S., Westlake, J., Wurz, P., and Zank, G. P.: Interstellar Mapping And Acceleration Probe: The NASA IMAP Mission, Space Science Reviews, 221, 100, https://doi.org/10.1007/s11214-025-01224-z, 2025.

Meyer-Vernet, N.: Basics of the Solar Wind, https://doi.org/10.1017/CBO9780511535765, 2007.

https://doi.org/10.5194/egusphere-2026-4440
Preprint. Discussion started: 17 August 2026

Meyer-Vernet, N.: Will Nanodust Reappear in STEREO/WAVES Data?, Research Notes of the American Astronomical Society, 9, 17, https://doi.org/10.3847/2515-5172/adaf25, 2025.

Meyer-Vernet, N. and Perche, C.: Tool kit for antennae and thermal noise near the plasma frequency, J. Geophys. Res., 94, 2405–2415, https://doi.org/10.1029/JA094iA03p02405, 1989.

Meyer-Vernet, N., Aubier, M. G., and Pedersen, B. M.: Voyager 2 at Uranus: Grain impacts in the ring plane, Geophys. Res. Lett., 13, 617–620, https://doi.org/10.1029/GL013i007p00617, 1986a.

Meyer-Vernet, N., Couturier, P., Hoang, S., Perche, C., Steinberg, J. L., Fainberg, J., and Meetre, C.: Plasma Diagnosis from Thermal Noise and Limits on Dust Flux or Mass in Comet Giacobini-Zinner, Science, 232, 370–374, https://doi.org/10.1126/science.232.4748.370, 1986b.

Meyer-Vernet, N., Lecacheux, A., and Pedersen, B. M.: Constraints on Saturn's E Ring from the Voyager 1 Radio Astronomy Instrument, Icarus, 123, 113–128, https://doi.org/10.1006/icar.1996.0145, 1996.

Meyer-Vernet, N., Maksimovic, M., Czechowski, A., Mann, I., Zouganelis, I., Goetz, K., Kaiser, M. L., St. Cyr, O. C., Bougeret, J. L., and Bale, S. D.: Dust Detection by the Wave Instrument on STEREO: Nanoparticles Picked up by the Solar Wind?, Sol. Phys., 256, 463–474, https://doi.org/10.1007/s11207-009-9349-2, 2009.

Meyer-Vernet, N., Moncuquet, M., Issautier, K., and Lecacheux, A.: The importance of monopole antennas for dust observations: Why Wind/WAVES does not detect nanodust, Geophys. Res. Lett., 41, 2716–2720, https://doi.org/10.1002/2014GL059988, 2014.

Meyer-Vernet, N., Mann, I., Le Chat, G., Schippers, P., Belheouane, S., Issautier, K., Lecacheux, A., Maksimovic, M., Pantellini, F., and Zaslavsky, A.: The physics and detection of nanodust in the solar system, Plasma Physics and Controlled Fusion, 57, 014015, https://doi.org/10.1088/0741-3335/57/1/014015, 2015.

Meyer-Vernet, N., Lecacheux, A., Kaiser, M. L., and Gurnett, D. A.: Detecting nanoparticles at radio frequencies: Jovian dust stream impacts on Cassini/RPWS, Geophysical Research Letters, 36, 2008GL036 752, https://doi.org/10.1029/2008GL036752, 2009.

Meyer-Vernet, N., Moncuquet, M., Issautier, K., and Schippers, P.: Frequency range of dust detection in space with radio and plasma wave receivers: Theory and application to interplanetary nanodust impacts on Cassini, Journal of Geophysical Research: Space Physics, 122, 8–22, https://doi.org/10.1002/2016JA023081, 2017.

Mikula, R., Sternovsky, Z., Armes, S. P., Ayari, E., Bouwman, J., Chan, D. H. H., Fontanese, J., Horanyi, M., Hillier, J. K., Kempf, S., Khawaja, N., Kupihár, Z., Postberg, F., and Srama, R.: Impact Ionization Mass Spectra of Polypyrrole-Coated Anthracene Microparticles: A Useful Mimic for Cosmic Polycyclic Aromatic Hydrocarbon Dust, ACS Earth and Space Chemistry, 8, 586–605, https://doi.org/10.1021/acsearthspacechem.3c00353, 2024.

Minato, T., Köhler, M., Kimura, H., Mann, I., and Yamamoto, T.: Momentum transfer to interplanetary dust from the solar wind, Astronomy & Astrophysics, 424, L13–L16, 2004.

Minato, T., Köhler, M., Kimura, H., Mann, I., and Yamamoto, T.: Momentum transfer to fluffy dust aggregates from stellar winds, Astronomy & Astrophysics, 452, 701–707, 2006.

Miyachi, T., Fujii, M., Hasebe, N. J., and Miyajima, M.: Measurement of temperature after hypervelocity collision of microparticles in the range from 10 to 40 km/s, Appl. Phys. Lett., 93, 174 107, 2008.

Mocker, A., Bugiel, S., Auer, S., Baust, G., Colette, A., Drake, K., Fiege, K., Grün, E., Heckmann, F., Helfert, S., Hillier, J., Kempf, S., Matt, G., Mellert, T., Munsat, T., Otto, K., Postberg, F., Röser, H.-P., Shu, A., Sternovsky, Z., and Srama, R.: A 2 MV Van de Graaff accelerator as a tool for planetary and impact physics research, Review of Scientific Instruments, 82, 095 111, https://doi.org/10.1063/1.3637461, 2011.

Mocker, A., Hornung, K., Grün, E., Kempf, S., Collette, A., Drake, K., Horányi, M., Munsat, T., O'Brien, L., Sternovsky, Z., and Srama, R.: On the application of a linear time-of-flight mass spectrometer for the investigation of hypervelocity impacts of micron and sub-micron sized dust particles, Planetary and Space Science, 89, 47–57, https://doi.org/https://doi.org/10.1016/j.pss.2013.07.013, 2013.

Moorhead, A. V., Pokorný, P., Holden, M. A., and Kosmann, W.: Modeling the Meteoroid Environment Far from the Ecliptic Plane, PSJ, 7, 28, https://doi.org/10.3847/PSJ/ae27cb, 2026.

Morfill, G. E. and Grün, E.: The motion of charged dust particles in interplanetary space - II. Interstellar grains, Planet. Space Sci., 27, 1283–1292, https://doi.org/10.1016/0032-0633(79)90106-5, 1979.

Morfill, G. E., Gruen, E., and Leinert, C.: The Interaction of Solid Particles with the Interplanetary Medium, in: The Sun and the Heliosphere in Three Dimensions, edited by Marsden, R. G. and Fisk, L. A., vol. 123, p. 455, https://doi.org/10.1007/978-94-009-4612-5_49, 1986.

Müller, D., Zouganelis, I., St. Cyr, O. C., and Gilbert, H. R.: The Solar Orbiter Mission - Exploring the Sun-Heliosphere Connection, A&A, this volume, 2019.

Nedelcu, D. A., Birlan, M., Turcu, V., Boaca, I., Badescu, O., Gornea, A., Sonka, A. B., Blagoi, O., Danescu, C., and Paraschiv, P.: Meteorites Orbits Reconstruction by Optical Imaging (MOROI) Network, Romanian Astronomical Journal, 28, 57–65, 2018.

Nesvorny, D., Janches, D., Vokrouhlický, D., Pokorný, P., Bottke, W. F., and Jenniskens, P.: DYNAMICAL MODEL FOR THE ZODIACAL CLOUD AND SPORADIC METEORS, The Astrophysical Journal, 743, 129, 2011.

Nesvorný, D., Jenniskens, P., Levison, H. F., Bottke, W. F., Vokrouhlický, D., and Gounelle, M.: Cometary origin of the zodiacal cloud and carbonaceous micrometeorites, The Astrophysical Journal, 713, 816–836, 2010.

Nieves-Chinchilla, T., Vourlidas, A., Raymond, J. C., Linton, M. G., Al-haddad, N., Savani, N. P., Szabo, A., and Hidalgo, M. A.: Understanding the Internal Magnetic Field Configurations of ICMEs Using More than 20 Years of Wind Observations, Sol. Phys., 293, 25, https://doi.org/10.1007/s11207-018-1247-z, 2018.

Northrop, T. G.: Adiabatic Charged-Particle Motion, Reviews of Geophysics and Space Physics, 1, 283–304, https://doi.org/10.1029/RG001i003p00283, 1963.

Nouzák, L., Hsu, S., Malaspina, D., Thayer, F. M., Ye, S. Y., Pavlů, J., Němeček, Z., Šafránková, J., and Sternovsky, Z.: Laboratory modeling of dust impact detection by the Cassini spacecraft, Planetary and Space Science, 156, 85 – 91, https://doi.org/10.1016/j.pss.2017.11.014, 2018.

Nouzák, L., Sternovsky, Z., Horányi, M., Hsu, S., Pavlů, J., Shen, M.-H., and Ye, S.-Y.: Magnetic Field Effect on Antenna Signals Induced by Dust Particle Impacts, Journal of Geophysical Research: Space Physics, 125, e2019JA027 245, https://doi.org/https://doi.org/10.1029/2019JA027245, _eprint: https://agupubs.onlinelibrary.wiley.com/doi/pdf/10.1029/2019JA027245, 2020.

Nouzák, L., Edwards, K., Fontanese, J., Munsat, T., Pavlů, J., and Sternovsky, Z.: Laboratory measurements of the expansion characteristics of dust impact plasmas, Icarus, p. 116586, https://doi.org/10.1016/j.icarus.2025.116586, 2025.

Nozette, S., Rustan, P., Pleasance, L. P., Horan, D. M., Regeon, P., Shoemaker, E. M., Spudis, P. D., Acton, C. H., Baker, D. N., Blamont, J. E., Buratti, B. J., Corson, M. P., Davies, M. E., Duxbury, T. C., Eliason, E. M., Jakosky, B. M., and Kordas, J. F.: The Clementine Mission to the Moon - Scientific Overview, Science, 266, 1835, 1994.

Oberc, P.: Small-Scale Dust Structures in Halley's Coma: Evidence from the Vega-2 Electric Field Records, Icarus, 140, 156–172, https://doi.org/10.1006/icar.1999.6096, 1999.

https://doi.org/10.5194/egusphere-2026-4440
Preprint. Discussion started: 17 August 2026

O'Brien, L., Auer, S., Gemer, A., Grün, E., Horanyi, M., Juhasz, A., Kempf, S., Malaspina, D., Mocker, A., Moebius, E., Srama, R., and Sternovsky, Z.: Development of the nano-dust analyzer (NDA) for detection and compositional analysis of nanometer-size dust particles originating in the inner heliosphere, Review of Scientific Instruments, 85, 035113, https://doi.org/10.1063/1.4868506, 2014.

O'Shea, E., Sternovsky, Z., and Malaspina, D. M.: Interpreting Dust Impact Signals Detected by the STEREO Spacecraft, Journal of Geophysical Research (Space Physics), 122, 11,864–11,873, https://doi.org/10.1002/2017JA024786, 2017.

Over, J.: "", Proc. Kon. Neder. Akad. v. Wetensch. B, 61, 74, 1958.

O'Neill, T. J., Zucker, C., Goodman, A. A., and Edenhofer, G.: The Local Bubble is a local chimney: a new model from 3D dust mapping, The Astrophysical Journal, 973, 136, 2024.

Page, B., Bale, S. D., Bonnell, J. W., Goetz, K., Goodrich, K., Harvey, P. R., Larsen, R., MacDowall, R. J., Malaspina, D. M., Pokorný, P., Pulupa, M., and Szalay, J. R.: Examining Dust Directionality with the Parker Solar Probe FIELDS Instrument, ApJS, 246, 51, https://doi.org/10.3847/1538-4365/ab5f6a, 2020.

Palomba, M. and Luntama, J.-P.: Vigil: ESA space weather mission in L5, in: 44th COSPAR Scientific Assembly, vol. 44, p. 3544, 2022.

Pantellini, F., Belheouane, S., Meyer-Vernet, N., and Zaslavsky, A.: Nano dust impacts on spacecraft and boom antenna charging, Ap&SS, 341, 309–314, https://doi.org/10.1007/s10509-012-1108-4, 2012a.

Pantellini, F., Landi, S., Zaslavsky, A., and Meyer-Vernet, N.: On the unconstrained expansion of a spherical plasma cloud turning collisionless: case of a cloud generated by a nanometre dust grain impact on an uncharged target in space, Plasma Physics and Controlled Fusion, 54, 045005, https://doi.org/10.1088/0741-3335/54/4/045005, 2012b.

Pantellini, F., Le Chat, G., Belheouane, S., Meyer-Vernet, N., and Zaslavsky, A.: On the detection of nano dust using spacecraft based boom antennas, in: Solar Wind 13, edited by Zank, G. P., Borovsky, J., Bruno, R., Cirtain, J., Cranmer, S., Elliott, H., Giacalone, J., Gonzalez, W., Li, G., Marsch, E., Moebius, E., Pogorelov, N., Spann, J., and Verkhoglyadova, O., vol. 1539 of *American Institute of Physics Conference Series*, pp. 414–417, AIP, https://doi.org/10.1063/1.4811073, 2013.

Paouris, E., Vourlidas, A., Kouloumvakos, A., Papaioannou, A., Jagarlamudi, V. K., and Horbury, T.: The Space Weather Context of the First Extreme Event of Solar Cycle 25, on 2022 September 5, ApJ, 956, 58, https://doi.org/10.3847/1538-4357/acf30f, 2023.

Pedersen, B. M., Meyer-Vernet, N., Aubier, M. G., and Zarka, P.: Dust distribution around Neptune: Grain impacts near the ring plane measured by the Voyager planetary radio astronomy experiment, J. Geophys. Res., 96, 19 187–19 196, https://doi.org/10.1029/91JA01601, 1991.

Peterson, A. W.: Thermal Radiation from Interplanetary Dust., ApJ, 138, 1218, https://doi.org/10.1086/147718, 1963.

Plane, J. M., Flynn, G. J., Määttänen, A., Moores, J. E., Poppe, A. R., Carrillo-Sanchez, J. D., and Listowski, C.: Impacts of cosmic dust on planetary atmospheres and surfaces, Space Science Reviews, 214, 23, 2018.

Pokorný, P. and Brown, P. G.: A reproducible method to determine the meteoroid mass index, Astronomy & Astrophysics, 592, A150, https://doi.org/10.1051/0004-6361/201628134, 2016.

Pokorný, P., Moorhead, A. V., Kuchner, M. J., Szalay, J. R., and Malaspina, D. M.: How Long-lived Grains Dominate the Shape of the Zodiacal Cloud, The Planetary Science Journal, 5, 82, https://doi.org/10.3847/PSJ/ad2de8, 2024.

Poppe, A. and Lee, C.: The effects of solar wind structure on nanodust dynamics in the inner heliosphere, Journal of Geophysical Research: Space Physics, 125, e2020JA028 463, 2020.

Poppe, A. and Lee, C.: The effects of solar cycle variability on nanodust dynamics in the inner heliosphere: Predictions for future STEREO A/WAVES measurements, Journal of Geophysical Research: Space Physics, 127, e2022JA030 317, 2022.

Poppe, A. R.: An improved model for interplanetary dust fluxes in the outer Solar System, Icarus, 264, 369–386, 2016.

Poppe, A. R., James, D., and Horányi, M.: Interplanetary dust particle environments: A new model for the inner solar system, Journal of Geophysical Research: Planets, 116, 2011.

Porsche, H.: HELIOS mission: Mission objectives, mission verification, selected results, in: Solar System and its Exploration, edited by Burke, W. R., vol. 164 of *ESA Special Publication*, pp. 43–50, 1981.

Porubcan, V. and Jopek, T.: Meteor Data Center, http://www.astro.amu.edu.pl/~jopek/MDC2007/index.php, accessed: 2015-04-23, 2015.

Pulupa, M., Bale, S. D., Bonnell, J. W., Bowen, T. A., Dudok de Wit, T., Goetz, K., Harvey, P. R., Kasper, J. C., Kellogg, P. J., Malaspina, D. M., Maksimovic, M., MacDowall, R. J., Moncuquet, M., Page, B., Salem, C., and Szalay, J. R.: The Solar Probe Plus Radio Frequency Spectrometer: Measurement requirements, analog design, and digital signal processing, Journal of Geophysical Research: Space Physics, 122, 2836–2854, https://doi.org/10.1002/2016JA023345, 2017.

Pusack, A., Malaspina, D. M., Szalay, J. R., Bale, S. D., Goetz, K., and MacDowall, R. J.: Dust directionality and interplanetary dust populations detected by Parker Solar Probe, PSJ, 2021.

Péronne, A.: Dust impacts on the Wind satellite: variation with the passage of CMEs and SIRs, Presentation at the PSP-SolO workshop, presented at the PSP-SolO workshop, Meudon, France, 2024.

Rackovic Babic, K.: In-situ dust detection using radio antennas of different spacecraft - space observation and modeling, Ph.D. thesis, Université PSL - Observatoire de Paris, https://theses.fr/2022UPSLO015?domaine=personnes, 2022.

Rackovic Babic, K., Zaslavsky, A., Issautier, K., Meyer-Vernet, N., and Onic, D.: An analytical model for dust impact voltage signals and its application to STEREO/WAVES data, A&A, 659, A15, https://doi.org/10.1051/0004-6361/202142508, 2022.

Ragot, B. R. and Kahler, S. W.: Interactions of Dust Grains with Coronal Mass Ejections and Solar Cycle Variations of the F-Coronal Brightness, ApJ, 594, 1049–1059, https://doi.org/10.1086/377076, 2003.

Raouafi, N. E., Matteini, L., Squire, J., Badman, S. T., Velli, M., Klein, K. G., Chen, C. H. K., Matthaeus, W. H., Szabo, A., Linton, M., Allen, R. C., Szalay, J. R., Bruno, R., Decker, R. B., Akhavan-Tafti, M., Agapitov, O. V., Bale, S. D., Bandyopadhyay, R., Battams, K., Berčič, L., Bourouaine, S., Bowen, T. A., Cattell, C., Chandran, B. D. G., Chhiber, R., Cohen, C. M. S., D'Amicis, R., Giacalone, J., Hess, P., Howard, R. A., Horbury, T. S., Jagarlamudi, V. K., Joyce, C. J., Kasper, J. C., Kinnison, J., Laker, R., Liewer, P., Malaspina, D. M., Mann, I., McComas, D. J., Niembro-Hernandez, T., Nieves-Chinchilla, T., Panasenco, O., Pokorný, P., Pusack, A., Pulupa, M., Perez, J. C., Riley, P., Rouillard, A. P., Shi, C., Stenborg, G., Tenerani, A., Verniero, J. L., Viall, N., Vourlidas, A., Wood, B. E., Woodham, L. D., and Woolley, T.: Parker Solar Probe: Four Years of Discoveries at Solar Cycle Minimum, Space Sci. Rev., 219, 8, https://doi.org/10.1007/s11214-023-00952-4, 2023.

Ratcliff, P., Burchell, M., Cole, M. J., Murphy, T. W., and Firooz, A.: Experimental measurements of hypervelocity impact plasma yield and energetics, Int. J. Impact Engng, 20, 663–674, 1997.

Ratcliff, P. R. and Allahdadi, F.: Characteristics of the plasma from A 94 kms^{-1} micro-particle impact, Advances in Space Research, 17, 87–91, https://doi.org/https://doi.org/10.1016/0273-1177(95)00763-5, 1996.

Redfield, S. and Linsky, J. L.: The structure of the local interstellar medium. IV. Dynamics, morphology, physical properties, and implications of cloud-cloud interactions, The Astrophysical Journal, 673, 283–314, 2008.

Rieke, G. H., Gáspár, A., and Ballering, N. P.: Magnetic grain trapping and the hot excesses around early-type stars, The Astrophysical Journal, 816, 50, 2016.

Rothkaehl, H., Andre, N., Auster, H.-U., Corte, V. D., Edberg, N. J. T., Galand, M., Henri, P., Keyser, J. D., Morawski, M., Nilsson, H., Prech, L., Volwerk, M., Goetz, C., Gunell, H., Lavraud, B., Rotundi, A., and Soucek, J.: Dust, Field and Plasma(DFP) instrument onboard

https://doi.org/10.5194/egusphere-2026-4440
Preprint. Discussion started: 17 August 2026

Comet Interceptor ESA mission as the tool for diagnostics of the comet and their environment, in: 45th COSPAR Scientific Assembly, vol. 45, p. 263, 2024.

Rowan-Robinson, M. and May, B.: An improved model for the infrared emission from the zodiacal dust cloud: cometary, asteroidal and interstellar dust, MNRAS, 429, 2894–2902, https://doi.org/10.1093/mnras/sts471, 2013.

Russell, H. N.: On Meteoric Matter Near the Stars, ApJ, 69, 49, https://doi.org/10.1086/143158, 1929.

Saito, K., Poland, A. I., and Munro, R. H.: A study of the background corona near solar minimum., Sol. Phys., 55, 121–134, https://doi.org/10.1007/BF00150879, 1977.

Scarf, F. L., Ferdinand, V., Coroniti, V., Kennel, C. F., Gurnett, D. A., Ip, W. H., and Smith, E. J.: Plasma Wave Observations at Comet Giacobini-Zinner, Science, 232, 377–381, https://doi.org/10.1126/science.232.4748.377, 1986.

Schippers, P., Meyer-Vernet, N., Lecacheux, A., Kurth, W. S., Mitchell, D. G., and André, N.: Nanodust detection near 1 AU from spectral analysis of Cassini/Radio and Plasma Wave Science data, Geophys. Res. Lett., 41, 5382–5388, https://doi.org/10.1002/2014GL060566, 2014.

Schippers, P., Meyer-Vernet, N., Lecacheux, A., Belheouane, S., Moncuquet, M., Kurth, W. S., Mann, I., Mitchell, D. G., and André, N.: Nanodust Detection between 1 and 5 AU Using Cassini Wave Measurements, ApJ, 806, 77, https://doi.org/10.1088/0004-637X/806/1/77, 2015.

Schwadron, N. and Gloeckler, G.: Pickup ions and cosmic rays from dust in the heliosphere, Space science reviews, 130, 283–291, 2007.

Schwadron, N. A., Geiss, J., Fisk, L. A., Gloeckler, G., Zurbuchen, T. H., and von Steiger, R.: Inner source distributions: Theoretical interpretation, implications, and evidence for inner source protons, Journal of Geophysical Research, 105, 7465–7472, 2000.

Shen, M. M., Sternovsky, Z., Garzelli, A., and Malaspina, D. M.: Electrostatic Model for Antenna Signal Generation From Dust Impacts, Journal of Geophysical Research: Space Physics, 126, e2021JA029 645, https://doi.org/10.1029/2021JA029645, 2021a.

Shen, M. M., Sternovsky, Z., Horányi, M., Hsu, H., and Malaspina, D. M.: Laboratory Study of Antenna Signals Generated by Dust Impacts on Spacecraft, Journal of Geophysical Research: Space Physics, 126, e2020JA028 965, https://doi.org/10.1029/2020JA028965, 2021b.

Shen, M. M., Sternovsky, Z., and Malaspina, D. M.: Variability of Antenna Signals From Dust Impacts, Journal of Geophysical Research: Space Physics, 128, https://doi.org/10.1029/2022ja030981, 2023.

Shen, M. M., Szalay, J. R., Pokorny, P., Mitchell, J. G., Hill, M., Mitchell, D. G., McComas, D. J., Christian, E. R., Cohen, C. M. S., Schwadron, N. A., Bale, S. D., and Malaspina, D. M.: Diverse dust populations in the near-Sun environment characterized by PSP/ISOIS, ApJ, 2025.

Shu, A., Collette, A., Drake, K., Grün, E., Horányi, M., Kempf, S., Mocker, A., Munsat, T., Northway, P., Srama, R., Sternovsky, Z., and Thomas, E.: 3 MV hypervelocity dust accelerator at the Colorado Center for Lunar Dust and Atmospheric Studies, Review of Scientific Instruments, 83, 075 108, https://doi.org/10.1063/1.4732820, 2012.

Simolka, J., Blanco, R., Ingerl, S., Krüger, H., Sommer, M., Srama, R., Strack, H., Wagner, C., Arai, T., Bauer, M., et al.: The DESTINY+ Dust Analyser—a dust telescope for analysing cosmic dust dynamics and composition, Philosophical Transactions A, 382, 20230 199, https://doi.org/10.1098/rsta.2023.0199, 2024.

Slavin, J. D., Frisch, P. C., Müller, H.-R., Heerikhuisen, J., Pogorelov, N. V., Reach, W. T., and Zank, G.: Trajectories and Distribution of Interstellar Dust Grains in the Heliosphere, ApJ, 760, 46, https://doi.org/10.1088/0004-637X/760/1/46, 2012.

Smith, A. M., Sternovsky, Z., Juhász, A., Malaspina, D., and Pokorný, P.: Updating the Electrostatic Model for Dust Impact Detection with Antenna Instruments, The Astrophysical Journal, 995, 100, https://doi.org/10.3847/1538-4357/ae1fe0, 2025.

Snodgrass, C. and Jones, G. H.: The European Space Agency's comet interceptor lies in wait, Nature communications, 10, 5418, 2019.

https://doi.org/10.5194/egusphere-2026-4440
Preprint. Discussion started: 17 August 2026

Soja, R. H., Grün, E., Strub, P., Sommer, M., Millinger, M., Vaubaillon, J., Alius, W., Camodeca, G., Hein, F., Laskar, J., Gastineau, M., Fienga, A., Schwarzkopf, G. J., Herzog, J., Gutsche, K., Skuppin, N., and Srama, R.: IMEM2: a meteoroid environment model for the inner solar system, Astronomy and Astrophysics, 628, A109–13, 2019.

Sommer, M.: Alpha-Meteoroids then and now: Unearthing an overlooked micrometeoroid population, Planetary and Space Science, 236, 105 751, https://doi.org/10.1016/j.pss.2023.105751, 2023.

SonotaCo: Ongoing Meteor Work, WGN, 37, 2009.

Soucek, J., Píša, D., Kolmasova, I., Uhlir, L., Lan, R., Santolík, O., Krupar, V., Kruparova, O., Baše, J., Maksimovic, M., et al.: Solar Orbiter radio and plasma waves–time domain sampler: in-flight performance and first results, Astronomy & Astrophysics, 656, A26, https://doi.org/10.1051/0004-6361/202140948, 2021.

Srama, R., Ahrens, T. J., Altobelli, N., Auer, S., Bradley, J. G., Burton, M., Dikarev, V. V., Economou, T., Fechtig, H., Görlich, M., Grande, M., Graps, A., Grün, E., Havnes, O., Helfert, S., Horanyi, M., Igenbergs, E., Jessberger, E. K., Johnson, T. V., Kempf, S., Krivov, A. V., Krüger, H., Mocker-Ahlreep, A., Moragas-Klostermeyer, G., Lamy, P., Landgraf, M., Linkert, D., Linkert, G., Lura, F., McDonnell, J. A. M., Möhlmann, D., Morfill, G. E., Müller, M., Roy, M., Schäfer, G., Schlotzhauer, G., Schwehm, G. H., Spahn, F., Stübig, M., Svestka, J., Tschernjawski, V., Tuzzolino, A. J., Wäsch, R., and Zook, H. A.: The Cassini Cosmic Dust Analyzer, Space Science Reviews, 114, 465–518, https://doi.org/10.1007/s11214-004-1435-z, 2004.

St. Cyr, O. C., Kaiser, M. L., Meyer-Vernet, N., Howard, R. A., Harrison, R. A., Bale, S. D., Thompson, W. T., Goetz, K., Maksimovic, M., Bougeret, J. L., Wang, D., and Crothers, S.: STEREO SECCHI and S/WAVES Observations of Spacecraft Debris Caused by Micron-Size Interplanetary Dust Impacts, Sol. Phys., 256, 475–488, https://doi.org/10.1007/s11207-009-9362-5, 2009.

St Cyr, O. C., Wilson, III, L. B., Rockcliffe, K., Mills, A., Nieves-Chinchilla, T., Adrian, M. L., and Malaspina, D.: Investigations of Wind/WAVES Dust Impacts, in: AGU Fall Meeting Abstracts, vol. 2017, pp. SH23D–2682, 2017.

Stamm, J., Czechowski, A., Mann, I., Baumann, C., and Myrvang, M.: Dust trajectory simulations around the Sun, Vega, and Fomalhaut, Astronomy & Astrophysics, 626, A107, 2019.

Stauffer, J. R., Stenborg, G., and Howard, R. A.: Measuring the Flattening of the Outer F-corona Using STEREO-A/HI-1 Images, ApJ, 864, 29, https://doi.org/10.3847/1538-4357/aad689, 2018.

Steel, D. I. and Elford, W. G.: Collisions in the solar system. III - Meteoroid survival times, Monthly Notices of the Royal Astronomical Society (ISSN 0035-8711), 218, 185–199, 1986.

Stenborg, G. and Howard, R. A.: The Evolution of the Surface of Symmetry of the Interplanetary Dust from 24° to 5° Elongation, ApJ, 848, 57, https://doi.org/10.3847/1538-4357/aa8ef0, 2017a.

Stenborg, G. and Howard, R. A.: A Heuristic Approach to Remove the Background Intensity on White-light Solar Images. I. STEREO/HI-1 Heliospheric Images, ApJ, 839, 68, https://doi.org/10.3847/1538-4357/aa6a12, 2017b.

Stenborg, G., Howard, R. A., and Stauffer, J. R.: Characterization of the White-light Brightness of the F-corona between 5° and 24° Elongation, ApJ, 862, 168, https://doi.org/10.3847/1538-4357/aacea3, 2018.

Stenborg, G., Howard, R. A., Hess, P., and Gallagher, B.: PSP/WISPR observations of dust density depletion near the Sun. I. Remote observations to 8 $R_\odot$ from an observer between 0.13 and 0.35 AU, A&A, 650, A28, https://doi.org/10.1051/0004-6361/202039284, 2021.

Stenborg, G., Howard, R. A., Vourlidas, A., and Gallagher, B.: PSP/WISPR Observations of Dust Density Depletion near the Sun. II. New Insights from within the Depletion Zone, ApJ, 932, 75, https://doi.org/10.3847/1538-4357/ac6b36, 2022.

Stenborg, G., Paouris, E., Howard, R. A., Vourlidas, A., and Hess, P.: Investigating Coronal Holes and CMEs as Sources of Brightness Depletion Detected in PSP/WISPR Images, ApJ, 949, 61, https://doi.org/10.3847/1538-4357/acd2cf, 2023.

https://doi.org/10.5194/egusphere-2026-4440
Preprint. Discussion started: 17 August 2026

Stenborg, G., Vourlidas, A., Paouris, E., and Howard, R. A.: Novel Insights on the Dust Distribution in the Zodiacal Dust Cloud from PSP/WISPR Observations at Large Elongations, ApJ, 972, 24, https://doi.org/10.3847/1538-4357/ad58b6, 2024.

Sterken, V. J., Altobelli, N., Kempf, S., Schwehm, G., Srama, R., and Grün, E.: The flow of interstellar dust into the solar system, A&A, 538, A102, https://doi.org/10.1051/0004-6361/201117119, 2012.

Sterken, V. J., Strub, P., von Steiger, R., and Frisch, P. C.: SIXTEEN YEARS OF ULYSSES INTERSTELLAR DUST MEASUREMENTS IN THE SOLAR SYSTEM. III. SIMULATIONS AND DATA UNVEIL NEW INSIGHTS INTO LOCAL INTERSTELLAR DUST, The Astrophysical Journal, 812, 1–24, 2015.

Sterken, V. J., Baalmann, L. R., Draine, B. T., Godenko, E., Herbst, K., Hsu, H.-W., Hunziker, S., Izmodenov, V., Lallement, R., and Slavin, J. D.: Dust in and Around the Heliosphere and Astrospheres, Space Sci. Rev., 218, 71, https://doi.org/10.1007/s11214-022-00939-7, 2022.

Sterken, V. J., Hunziker, S., Dialynas, K., Leitner, J., Sommer, M., Srama, R., Baalmann, L. R., Li, A., Herbst, K., Galli, A., Brandt, P., Riebe, M., Baggaley, W. J., Blanc, M., Czechowski, A., Effenberger, F., Fields, B., Frisch, P., Horanyi, M., Hsu, H. W., Khawaja, N., Krüger, H., Kurth, W. S., Ligterink, N. F. W., Linsky, J. L., Lisse, C., Malaspina, D., Miller, J. A., Opher, M., Poppe, A. R., Postberg, F., Provornikova, E., Redfield, S., Richardson, J., Rowan-Robinson, M., Scherer, K., Shen, M. M., Slavin, J. D., Sternovsky, Z., Stober, G., Strub, P., Szalay, J., and Trieloff, M.: Synergies between interstellar dust and heliospheric science with an interstellar probe, RAS Techniques and Instruments, 2, 532–547, https://doi.org/10.1093/rasti/rzad034, 2023.

Strub, P., Krüger, H., and Sterken, V. J.: Sixteen Years of Ulysses Interstellar Dust Measurements in the Solar System. II. Fluctuations in the Dust Flow from the Data, ApJ, 812, 140, https://doi.org/10.1088/0004-637X/812/2/140, 2015.

Strub, P., Sterken, V. J., Soja, R., Kruger, H., Grün, E., and Srama, R.: Heliospheric modulation of the interstellar dust flow on to Earth, Astronomy and Astrophysics, 621, A54–16, 2019.

Su, K. Y., Rieke, G. H., Malhotra, R., Stapelfeldt, K. R., Hughes, A. M., Bonsor, A., Wilner, D. J., Balog, Z., Watson, D. M., Werner, M. W., et al.: Asteroid belts in debris disk twins: Vega and Fomalhaut, The Astrophysical Journal, 763, 118, 2013.

Swaczyna, P., Schwadron, N. A., Möbius, E., Bzowski, M., Frisch, P. C., Linsky, J. L., McComas, D. J., Rahmanifard, F., Redfield, S., Winslow, R. M., et al.: Mixing interstellar clouds surrounding the Sun, The Astrophysical Journal Letters, 937, L32, 2022.

Szalay, J. R. and Horányi, M.: The Impact Ejecta Environment of Near Earth Asteroids, The Astrophysical Journal Letters, 830, L29, https://doi.org/10.3847/2041-8205/830/2/L29, 2016.

Szalay, J. R., Pokorný, P., Bale, S. D., Christian, E. R., Goetz, K., Goodrich, K., Hill, M. E., Kuchner, M., Larsen, R., Malaspina, D., McComas, D. J., Mitchell, D., Page, B., and Schwadron, N.: The Near-Sun Dust Environment: Initial Observations from Parker Solar Probe, ApJS, 246, 27, https://doi.org/10.3847/1538-4365/ab50c1, 2020.

Szalay, J. R., Pokorný, P., Malaspina, D. M., Pusack, A., Bale, S. D., Battams, K., Gasque, L. C., Goetz, K., Krüger, H., McComas, D. J., Schwadron, N. A., and Strub, P.: Collisional Evolution of the Inner Zodiacal Cloud, The Planetary Science Journal, 2, 185, https://doi.org/10.3847/PSJ/abf928, 2021.

Szalay, J. R., Pokorný, P., and Malaspina, D. M.: Size distribution of small grains in the inner zodiacal cloud, The Planetary Science Journal, 5, 266, https://doi.org/10.3847/PSJ/ad8b27, 2024.

Szalay, J. R., Pokorný, P., Malaspina, D. M., Poppe, A. R., Battams, K., and McComas, D. J.: Meteoroid Streams Sculpt the Inner Zodiacal Cloud, PSJ, 6, 221, https://doi.org/10.3847/PSJ/adfb6f, 2025.

Szalay, J. R., McComas, D. J., Rankin, J. S., Pokorný, P., Schwadron, N. A., and Malaspina, D. M.: Zodiacal Fluctuations Should Drive Inner-source Pickup Ion Variability, ApJ, 1001, 68, https://doi.org/10.3847/1538-4357/ae548f, 2026a.

https://doi.org/10.5194/egusphere-2026-4440
Preprint. Discussion started: 17 August 2026

Szalay, J. R., Provornikova, E., Ayari, E., Bzowski, M., Christian, E. R., Funsten, H. O., Galli, A., Gkioulidou, M., Horányi, M., Livi, S., McComas, D. J., Möbius, E., Ogasawara, K., Rahmanifard, F., Rankin, J. S., Reisenfeld, D. B., Schwadron, N. A., Sternovsky, Z., Swaczyna, P., Turner, D., Zank, G. P., and Zirnstein, E. J.: Direct Samples of Interstellar and Interplanetary Material with IMAP, Space Sci. Rev., 222, 36, https://doi.org/10.1007/s11214-026-01291-w, 2026b.

Thernisien, A.: Implementation of the Graduated Cylindrical Shell Model for the Three-dimensional Reconstruction of Coronal Mass Ejections, ApJS, 194, 33, https://doi.org/10.1088/0067-0049/194/2/33, 2011.

Thomas, E., Auer, S., Drake, K., Horányi, M., Munsat, T., and Shu, A.: FPGA cross-correlation filters for real-time dust detection and selection, Planetary and Space Science, 89, 71–76, https://doi.org/https://doi.org/10.1016/j.pss.2013.09.004, 2013.

Tsembelis, K., Burchell, M. J., Cole, M. J., and Margaritis, N.: Residual temperature measurements of light flash under hypervelocity impact, International Journal of Impact Engineering, 35, 1368–1373, https://doi.org/https://doi.org/10.1016/j.ijimpeng.2007.09.004, 2008.

Utterback, N. G. and Kissel, J.: Attogram Dust Cloud a Million Kilometers from Comet Halley, AJ, 100, 1315, https://doi.org/10.1086/115599, 1990.

Vaverka, J., Nakamura, T., Kero, J., Mann, I., De Spiegeleer, A., Hamrin, M., Norberg, C., Lindqvist, P., and Pellinen-Wannberg, A.: Comparison of Dust Impact and Solitary Wave Signatures Detected by Multiple Electric Field Antennas Onboard the MMS Spacecraft, Journal of Geophysical Research: Space Physics, 123, 6119–6129, https://doi.org/10.1029/2018JA025380, 2018.

Vaverka, J., Pavlů, J., Nouzák, L., Šafránková, J., Němeček, Z., Mann, I., Ye, S., and Lindqvist, P.: One-Year Analysis of Dust Impact-Like Events Onto the MMS Spacecraft, Journal of Geophysical Research: Space Physics, 124, 8179–8190, https://doi.org/10.1029/2019JA027035, 2019.

Vida, D., Gural, P. S., Brown, P. G., Campbell-Brown, M., and Wiegert, P.: Global Meteor Network, Planetary and Space Science, 182, 104 845, 2020.

Vida, D., Blaauw Erskine, R. C., Brown, P. G., Kambulow, J., Campbell-Brown, M., and Mazur, M. J.: Computing optical meteor flux using global meteor network data, MNRAS, 515, 2322–2339, https://doi.org/10.1093/mnras/stac1766, 2022.

Voelzke, M. R.: Disconnection Events Processes in Cometary Tails, Earth Moon and Planets, 97, 399–409, https://doi.org/10.1007/s11038-006-9073-y, 2005.

Vourlidas, A., Howard, R. A., Plunkett, S. P., Korendyke, C. M., Thernisien, A. F. R., Wang, D., Rich, N., Carter, M. T., Chua, D. H., Socker, D. G., Linton, M. G., Morrill, J. S., Lynch, S., Thurn, A., Van Duyne, P., Hagood, R., Clifford, G., Grey, P. J., Velli, M., Liewer, P. C., Hall, J. R., DeJong, E. M., Mikic, Z., Rochus, P., Mazy, E., Bothmer, V., and Rodmann, J.: The Wide-Field Imager for Solar Probe Plus (WISPR), Space Science Reviews, 204, 83–130, 2016.

Wehry, A. and Mann, I.: Identification of β-meteoroids from measurements of the dust detector onboard the ULYSSES spacecraft, A&A, 341, 296–303, 1999.

Weryk, R. J.: The Canadian Meteor Orbit Radar (CMOR): system overview and recent work, in: Proceedings of the International Meteor Conference, pp. 84–85, Dept. of Physics and Astronomy, University of Western Ontario, London, ON, N6A 3K7, Canada. weryk@meteor.uwo.ca, 2014.

Westphal, A. J., Stroud, R. M., Bechtel, H. A., Brenker, F. E., Butterworth, A. L., Flynn, G. J., Frank, D. R., Gainsforth, Z., Hillier, J. K., Postberg, F., et al.: Stardust mission: Dust collection and analysis, Science, 345, 786–791, 2014.

Whipple, F. L.: A Comet Model. II. Physical Relations for Comets and Meteors., Astrophysical Journal, 113, 464, 1951.

Wiegert, P. A., Vaubaillon, J., and Campbell-Brown, M.: A dynamical model of the sporadic meteoroid complex, Icarus, 201, 295–310, 2009.

Wilck, M. and Mann, I.: Radiation pressure forces on "typical" interplanetary dust grains, Planetary and Space Science, 44, 493–499, 1996.

https://doi.org/10.5194/egusphere-2026-4440
Preprint. Discussion started: 17 August 2026

Wilson, III, L. B., Salem, C. S., and Bonnell, J. W.: Spacecraft Floating Potential Measurements for the Wind Spacecraft, ApJS, 269, 52, https://doi.org/10.3847/1538-4365/ad0633, 2023.

Wimmer-Schweingruber, R. F. and Bochsler, P.: On the origin of inner-source pickup ions, Geophysical Research Letters, 30, 1077, 2003.

Witte, M.: Kinetic parameters of interstellar neutral helium. Review of results obtained during one solar cycle with the Ulysses/GAS-instrument, A&A, 426, 835–844, https://doi.org/10.1051/0004-6361:20035956, 2004.

Ye, S., Gurnett, D., and Kurth, W.: In-situ measurements of Saturn's dusty rings based on dust impact signals detected by Cassini RPWS, Icarus, 279, 51–61, https://doi.org/10.1016/j.icarus.2016.05.006, 2016.

Ye, S., Kurth, W. S., Hospodarsky, G. B., Persoon, A. M., Sulaiman, A. H., Gurnett, D. A., Morooka, M., Wahlund, J., Hsu, H., Sternovsky, Z., Wang, X., Horanyi, M., Seiß, M., and Srama, R.: Dust Observations by the Radio and Plasma Wave Science Instrument During Cassini's Grand Finale, Geophysical Research Letters, 45, https://doi.org/10.1029/2018GL078059, 2018.

Ye, S. Y., Averkamp, T. F., Kurth, W. S., Brennan, M., Bolton, S., Connerney, J. E. P., and Joergensen, J. L.: Juno Waves Detection of Dust Impacts Near Jupiter, Journal of Geophysical Research: Planets, 125, 200 – 13, https://doi.org/10.1029/2019je006367, 2020.

Zaslavsky, A.: Floating potential perturbations due to micrometeoroid impacts: Theory and application to S/WAVES data, Journal of Geophysical Research: Space Physics, 120, 855–867, https://doi.org/10.1002/2014JA020635, 2015.

Zaslavsky, A., Meyer-Vernet, N., Mann, I., Czechowski, A., Issautier, K., Le Chat, G., Pantellini, F., Goetz, K., Maksimovic, M., Bale, S. D., and Kasper, J. C.: Interplanetary dust detection by radio antennas: Mass calibration and fluxes measured by STEREO/WAVES, Journal of Geophysical Research: Space Physics, 117, 2011JA017 480, https://doi.org/10.1029/2011JA017480, 2012.

Zaslavsky, A., Mann, I., Soucek, J., Czechowski, A., Píša, D., Vaverka, J., Meyer-Vernet, N., Maksimovic, M., Lorfèvre, E., Issautier, K., Rackovic Babic, K., Bale, S. D., Morooka, M., Vecchio, A., Chust, T., Khotyaintsev, Y., Krasnoselskikh, V., Kretzschmar, M., Plettemeier, D., Steller, M., Štverák, Š., Trávníček, P., and Vaivads, A.: First dust measurements with the Solar Orbiter Radio and Plasma Wave instrument, A&A, 656, A30, https://doi.org/10.1051/0004-6361/202140969, 2021.

Zouganelis, I., Maksimovic, M., Meyer-Vernet, N., Bale, S. D., Eastwood, J. P., Zaslavsky, A., Dekkali, M., Goetz, K., and Kaiser, M. L.: Measurements of stray antenna capacitance in the STEREO/WAVES instrument: Comparison of the measured voltage spectrum with an antenna electron shot noise model, Radio Science, 45, RS1005, https://doi.org/10.1029/2009RS004194, 2010.

Zucker, C., Redfield, S., Starecheski, S., Konietzka, R., and Linsky, J. L.: The origin of the cluster of local interstellar clouds, The Astrophysical Journal, 986, 58, 2025.